Study of Nonlinear Phenomena in Switching DC/DC Converters

by

Herbert Ho-Ching Iu

Submitted in partial fulfillment of the

requirements for the degree of

Doctor of Philosophy

in the Department of Electronic and Information Engineering

The Hong Kong Polytechnic University

Hong Kong SAR, China

August 2000

Abstract

of the thesis entitled
"Study of Nonlinear Phenomena in Switching DC/DC Converters"
submitted by Herbert Ho-Ching Iu
for the degree of Doctor of Philosophy
at The Hong Kong Polytechnic University in August 2000

This thesis studies some nonlinear phenomena such as bifurcation and chaos in DC/DC switching converters. Five phases of investigations are described. The first phase reviews the existing tools for analyzing nonlinear systems that are helpful to the investigation of nonlinear phenomena in power electronic circuits. Some of these existing tools are employed to study the nonlinear behaviour of power electronic circuits in the subsequent phases. The second phase focuses on the analysis of bifurcation behaviour of parallel-connected DC/DC converters under a master-slave current sharing scheme. An iterative discrete-time map and its Jacobian are established to predict the onset of period-doubling or Neimark-Sacker bifurcation. Both parallel-connected buck converters and boost converters are studied. The third phase studies an autonomous free-running Ćuk converter under a hysteretic current-mode control. Hopf bifurcation is observed, for the first time, in this kind of autonomous power electronic circuits. The method of state-space averaging is employed to predict the occurrence of such bifurcation. Extensive simulations and experiments confirm the predicted results. A typical bifurcation sequence from stable fixed points to chaos, via limit cycles and quasi-periodic orbits, is demonstrated. The fourth phase investigates the possibility of synchronization of two chaotic autonomous free-running Ćuk converters. With a particular capacitor voltage as driving signal, synchronization is found possible. Averaged state equations and conditional Lyapunov exponents are used to predict the possibility of synchronization while computer simulations and PSPICE simulations provide the verification. The last phase gives suggestions for future research.

Acknowledgements

The road to a doctorate is seldom without its ups and downs. Luckily, I have always been blessed with wonderful guides and excellent companions. First of all, I am indebted to Prof. Michael Tse, my supervisor, for his guidance and support throughout the course of this project. His enthusiasm and encouragement have made undertaking this project a pleasure. During the three years working in his group, I have been given the opportunity to pursue my own scientific interests while learning to explore complexity in electronic circuits and systems. It has indeed been a very precious experience for me.

I would like to thank Dr. Y.M. Lai for his constructive comments and suggestions throughout my study. Also, I wish to thank Mr. V. Pjevalica for his kind assistance in performing the experimental tests.

I will be forever grateful to my colleagues in the Circuit Development Laboratory who have imparted direct assistance on me during the course of my study. In particular, I would like to convey my heartfelt thanks to Dr. William Chan, Mr. Michael Wu, Mr. J. Feng, Mr. Martin Cheung and Mr. George Lam for their incessant support and inspiration. It has been a very enjoyable experience working with them.

I gratefully acknowledge the Research Committee of The Hong Kong Polytechnic University for its financial support during the entire period of my candidature.

Last, but not least, I must thank my parents, my sister and my friends for their love and care over the years.

Contents

List of Figures

List of Tables

Chapter 1

Introduction

1.1 Motivation

Almost all systems are nonlinear in real life. Nonlinearity arises either from interaction of the various parts of a system or from some inherent properties of the constituent components. The study of nonlinear systems leads to better understanding or new discovery in the real world. Unlike linear systems, most nonlinear systems are difficult to solve analytically. The essential difference is that linear systems can be broken down into parts, and each part can be solved separately and finally recombined to get the answer. This idea allows a drastic simplification of complex problems and underlies such methods as normal modes, Laplace transforms, superposition arguments, and Fourier analysis. However, for nonlinear problems, every problem is a unique problem and each must be treated separately. There can hardly be any generalization. This makes the study of nonlinear systems challenging and interesting.

Nonlinear systems can be found in a wide variety of disciplines such as meteorology, physics, biology, economics, mathematics and engineering. In particular, power electronic circuits, which find practical applications in our daily life, are nonlinear systems. By studying the nonlinear phenomena in these systems, useful information about their dynamics can be obtained. Moreover, possible applications exploiting the nonlinear behaviour of these systems may be identified.

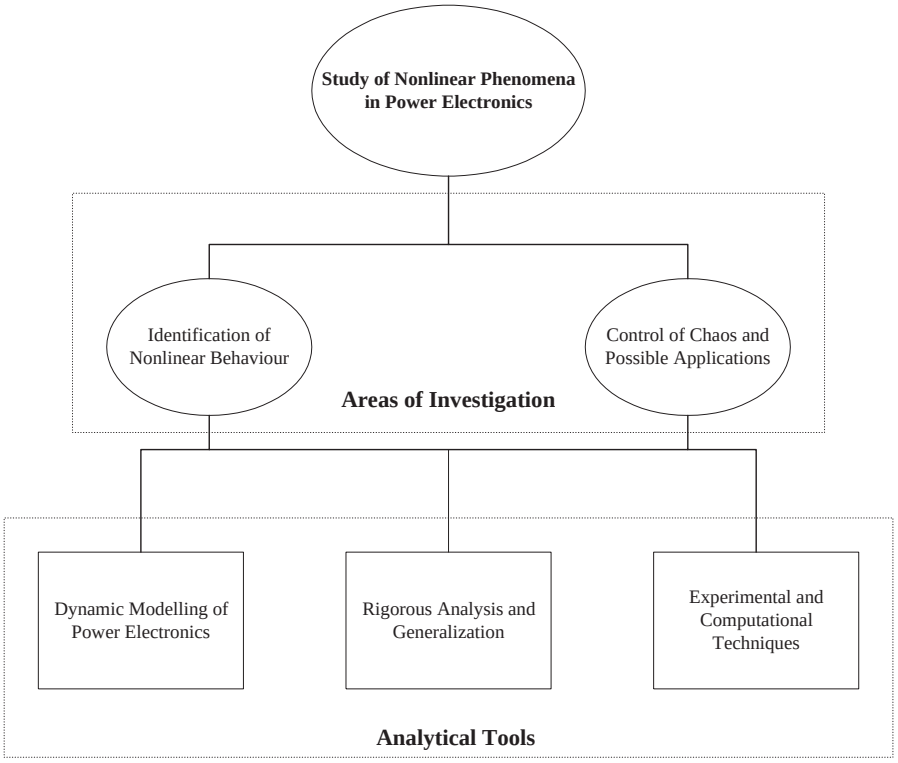

Figure 1.1: Study of nonlinear phenomena in power electronics

Power electronics is a field spawned by many real-life applications in industrial, commercial and aerospace environments [1]. At the same time, it is also a field rich in nonlinear dynamics [2]. As one of the most popular members in power electronic circuits, the DC/DC converter has found widespread applications for many decades. However, it had not been thoroughly analyzed and studied until the late 1970's. Advanced analytic and modeling work is still being actively pursued today. Nonlinear phenomena in DC/DC converters, though commonly found, have drawn attention only recently. Studying the nonlinear behaviour in DC/DC converters is not only interesting, but also very useful, as we will see in this thesis. Figure 1.1 summarizes the main areas of investigation and analytical tools for studying nonlinear phenomena in power electronics.

DC/DC converters can be described as piecewise switched circuits, which assume different topologies at different times. The number of involving topologies is usually fixed, and the toggling is done in a cyclic manner. The result is nonlinear time-varying operation, which requires the use of nonlinear methods for analysis and design. Over the past decades, researchers and engineers have put much

effort to devise linear methods for modeling and analysis. These methods arrive at linearized models that can fit in a frequency-domain analysis, but a certain degree of accuracy is often traded off in return.

One of the most popular approaches for modeling is the state-space averaging method [3]–[4]. In this method, an average is taken over the state equations of the different circuit configurations that have been involved within a cycle. The resulting "averaged" model is subsequently linearized to give a linear model. Hence, the nonlinear system is reduced to a simple linear, time-invariant system which can be conveniently analyzed. This technique is widely applied because of its ease of use. However, such models fall short of predicting the nonlinear phenomena that actually occur in DC/DC converters.

Recently, advances in computer technology have enhanced the development of nonlinear systems theory. Specifically, computer simulations provide fast indications of the possible behaviour exhibited by a given system which is otherwise too complex for manual analysis. Thus, by combining theoretical analysis and computer simulations, many new features can be revealed in nonlinear systems, and some well-known nonlinear phenomena can now be identified. The study of nonlinear dynamics in DC/DC converters offers an opportunity of rationalizing the commonly observed behaviour. Moreover, it can give new insights into the design of new control algorithms for DC/DC converters. Above all, many previously unused nonlinear operating regimes may be profitably exploited for useful engineering applications in the future.

1.2 Literature Review

In recent years, chaos and bifurcation phenomena in DC/DC converters have been seriously considered by the power electronics and the circuits and systems communities.

In 1984, Brockett and Wood [5] presented a paper mentioning chaos in a controlled buck DC/DC converter. In 1988, Hamill and Jefferies [6] reported the

first analysis of bifurcation and chaotic dynamics in DC/DC converters. They used difference equations and zigzag return maps to identify stable and unstable regions in a first order PWM voltage-mode controlled converter. In 1989, Deane and Hamill [7] identified a wide variety of power electronic circuits as potentially chaotic. Again in 1990, Deane and Hamill [8] examined the first order and second order voltage-mode controlled PWM buck converters. With the input voltage as the bifurcation parameter, the converter was shown to bifurcate from stable to subharmonic oscillations, then to chaos. Chaos was shown by determining boundary conditions on the circuit differential equations, by SPICE simulation and by experiments. Bifurcation diagrams, phase portraits, time-amplitude plots and Poincaré sections were used to illustrate the results.

In 1990, Krein and Bass [9] seriously pointed out the importance of nonlinear studies in power electronics circuits. Experimental observations were made regarding instabilities, namely unboundedness, chattering and chaos.

In 1992, Hamill *et al.* [10] reported an attempt to derive an implicit iterative map for a simple buck regulator operating in continuous conduction mode. The occurrence of period-doubling bifurcations, subharmonics and chaos has been demonstrated by numerical experiments on the implicit iterative map, as well as confirmed by SPICE simulations and laboratory measurements.

In 1994, period-doubling cascades were demonstrated by Tse [11] in a simple boost converter operating in discontinuous mode. This work attempted to model the boost converter, when operating in discontinuous mode, as a first-order iterative map, and to analytically locate the onset of period-doubling bifurcation. Simulations and laboratory measurements confirmed the findings. In the same year, Tse [12] also performed a similar study for a buck converter working in discontinuous mode. Formal theoretical study of the conditions for possible occurrence of period-doubling cascades in the discontinuous mode DC/DC converter was reported in 1997 by Chan and Tse [13].

Further work on the bifurcation behaviour of the buck converter was reported by Chakrabarty *et al.* [14]. This work studied in detail the bifurcation behaviour

under variation of a range of circuit parameters including storage inductance, load resistance and output capacitance. Also in 1996, Fossas and Olivar [15] reexamined Hamill *et al.*'s approach. A mathematical analysis of period-1 and period-2 orbits was presented and various regions of the chaotic attractor of the buck converter were identified.

In 1995, bifurcation phenomena and chaos were studied in a fourth-order Ćuk DC/DC converter under a current-programmed control scheme by Tse and Chan [16]. The system was represented by an implicit fourth-order iterative map, from which routes to chaos were identified numerically. Experimental verification of the circuit was performed in 1996 by Tse *et al.*[17].

Much of the early work had focussed on voltage-mode controlled PWM DC/DC converters. In fact, the current-programmed DC/DC control is a widely used control scheme for the boost and buck-boost converters. The bifurcation behaviour of DC/DC converters under current-programmed control has been studied by a number of researchers. In 1992, Deane [18] first reported on chaotic behaviour in a current-programmed boost converter. In 1995, Zafrany and Ben-Yaakov [19] also studied the dynamics of the same system. Chan and Tse [20]–[21] studied various routes to chaos and their dependence upon the choice of bifurcation parameters. Similar study of bifurcation bahaviour in a boost converter under current-mode control was reported by Banerjee *et al.* [22].

Bifurcation and chaos were theoretically examined by Banerjee *et al.* [23]–[25] in the light of "border collision bifurcation", which has later proven to be a common type of bifurcation in DC/DC converters.

As DC/DC converters are non-autonomous systems driven by fixed-period clock signals, one effective approach to study their dynamics is using appropriate discrete-time maps. Di Bernardo *et al.* [26]–[27] studied various sampling schemes and their application in the identification of bifurcation and chaos.

Apart from period-doubling bifurcation and border collision bifurcation, quasi-periodicity and chaos were also found in simple DC/DC converters. El Aroudi *et al.* [28]–[29] studied a boost converter and a buck-boost converter

under voltage-mode PWM control, in which quasi-periodic behaviour and chaos were observed.

When external clocks are absent and the system is "free-running", e.g., when a converter is under a hysteretic current-controlled scheme, the system is autonomous and does not have a fixed switching period. Tse *et al.* [30] studied a hysteretic current-controlled free-running Ćuk converter. As a fourth-order system, it has been shown to exhibit Hopf bifurcation and chaos.

In addition to identification of bifurcation and chaos, control of chaos in DC/DC converters is also a popular topic among researchers. In 1995, Poddar *et al.* [31]–[32] attempted to control chaos by targeting the unstable fixed points in every cycle. Batlle *et al.* [33] also made a similar study in 1996. In 1999, the same group of researchers [34] used time-delayed feedback to stabilize unstable periodic orbits in a PWM controlled buck converter.

1.3 Objectives

Recently, it has been shown that DC/DC converters can exhibit several types of nonlinear phenomena including bifurcation, quasi-periodicity and chaos, under both voltage-mode and control-mode control schemes. The major purpose of this thesis is to present a systematic study of some new and typical nonlinear phenomena in DC/DC converters. By using some well-established techniques in the analysis of nonlinear dynamics and chaos, several kinds of nonlinear phenomena are studied. First, extensive investigation is performed to identify bifurcation and chaos in parallel-connected DC/DC converters. An iterative discrete time map is developed to locate the onset of instability such as period-doubling bifurcation and Neimark-Sacker bifurcation. Second, a free-running hysteretic current-controlled Ćuk converter serves as a subject of investigation, in which Hopf bifurcation and chaos are observed. An averaged model is used to predict the instability while simulations and experiments confirm the findings. Third, the synchronization property of two autonomous free-running Ćuk converters is studied. Averaged state equations and conditional Lyapunov exponents are estab-

lished. Computer simulations and SPICE simulations show the synchronization scenarios. The organization of the thesis is summarized in the following section.

1.4 Outline of the Thesis

Chapter 2 outlines the basics of DC/DC converters. In this chapter, the basic operating principle of DC/DC converters is expounded. The usual control schemes of DC/DC converters are discussed. This serves as an introduction to the more advanced topics discussed in the subsequent chapters of this thesis.

Chapter 3 gives an overview of nonlinear dynamics, particularly bifurcation and chaos in DC/DC converters. This chapter also discusses some basic concepts about bifurcation and chaos. The notation and terminology to be used are stated. Specifically, various tools for analysis of bifurcation and chaos in nonlinear dynamical systems are reviewed.

Chapters 4 and 5 study some typical types of bifurcation exhibited by parallel-connected DC/DC converters under a master-slave current control. Paralleling power converter systems are becoming popular, but their nonlinear phenomena are rarely investigated. Computer simulations and experiments are performed to capture the bifurcation phenomena when some chosen parameters are varied. For parallel-connected buck converters, it is found that while variation of the voltage feedback gains lead to standard period-doubling bifurcation, variation of the current sharing ratio leads to border collision bifurcation. For parallel-connected boost converters, it is found that variation of the voltage feedback gains and the current sharing ratio lead to standard Neimark-Sacker bifurcation. Then, analysis is performed using an iterative discrete-time map and its Jacobian to explain the observations.

Chapter 6 considers an autonomous free-running Ćuk converter. Analysis of the describing nonlinear state equations shows the system loses stability via a supercritical Hopf bifurcation. The boundary of stability is derived and local trajectories of motion studied. Computer simulations of the system reveal a

typical bifurcation from a stable fixed point to chaos, via limit cycles and quasi-periodic orbits. Experimental measurements confirm the bifurcation scenarios.

Chapter 7 studies the synchronization property of chaotic free-running DC/DC Ćuk converters. This study includes the derivation of describing differential equations and conditional Lyapunov exponents (CLE's) of the synchronizing system based on the differential equations. It is found that all the CLE's are negative for certain chosen parameters, and hence synchronization is possible in this system. With the drive-response system connected, synchronization is demonstrated using both exact time-domain simulations and PSPICE simulations.

Chapter 8 gives some suggestions for future work and concludes the thesis by summarizing the phenomena and important results that have been established from studying nonlinear phenomena in DC/DC converters.

Chapter 2

Basics of DC/DC Switching Converters

2.1 Introduction

DC/DC switching power converters are power processing devices that utilize lossless components such as switches, inductors and capacitors to process DC power with minimum energy loss in response to some control signal which determines the input to output conversion function. As is common to all power electronic systems, the DC/DC converter is a multi-structural system with its circuit topology varied according to the states of the switches. The change of the circuit configuration from one to another is governed by the opening and closing of switches. This special property makes the circuit nonlinear. In this chapter, some common DC/DC converter topologies and control methods are reviewed. Also, some approaches of modelling and analysis are briefly described. It will be shown that DC/DC switching converters exhibit a range of nonlinear behaviour that may not be identified from conventional methods of analysis. In addition, a review of paralleling schemes for power supply modules will be given.

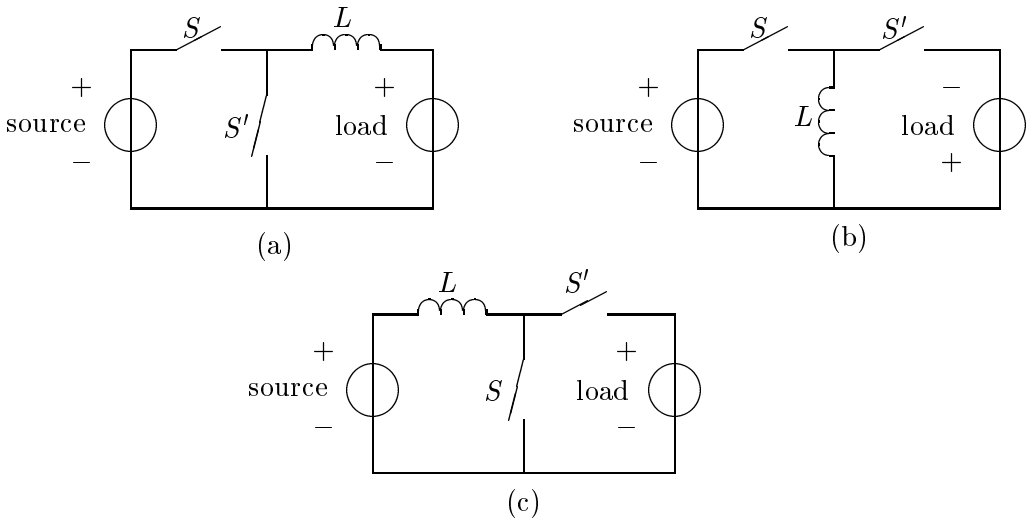

Figure 2.1: Simple DC/DC converters. (a) Buck; (b) buck-boost; (c) boost.

2.2 DC/DC Switching Converter Topologies

The most commonly used DC/DC converters are the buck, buck-boost and boost converters, as shown in Fig. 2.1, which represent the simplest topologies involving only one inductive storage element to transfer power from a voltage source to a voltage load. In common practice, one of the switches is realized as a diode and the voltage load is a parallel combination of a capacitor and a resistor. Practical forms of these circuits are shown in Fig. 2.2. These simplest DC/DC converter circuits are second-order since each of them includes an inductor and a capacitor. That is, for any given switching condition, two independent first-order differential equations are required to describe the complete behaviour of the converter.

Severns and Bloom [35] stated that all known DC/DC switching converters can be derived from a combination of buck and/or boost converters along with some form of transformation function. In 1977, Ćuk introduced a converter which is constructed by combining the buck and the boost converters, as shown in Fig. 2.3. This circuit is fourth-order and is commonly used today.

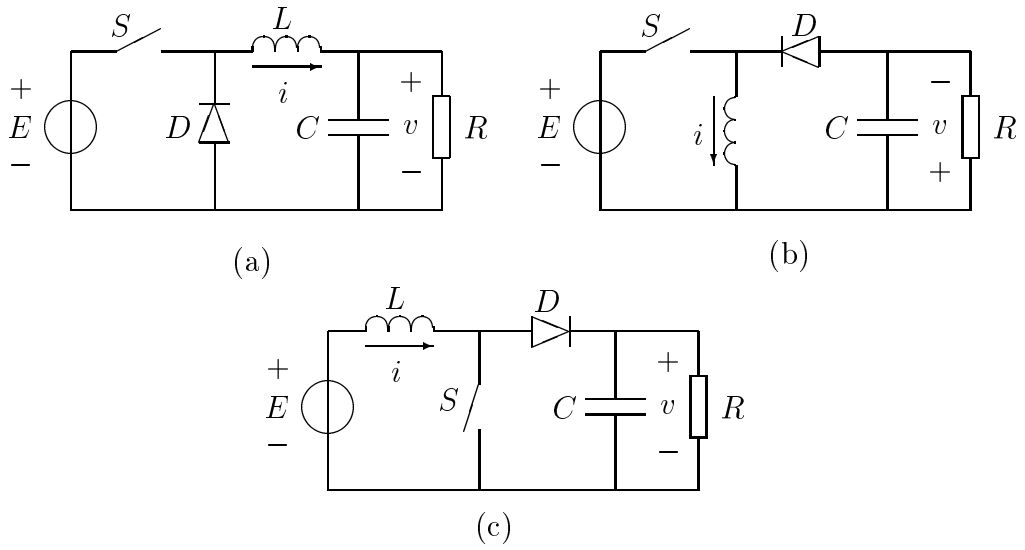

Figure 2.2: Practical forms of DC/DC converters. (a) Buck; (b) buck-boost; (c) boost.

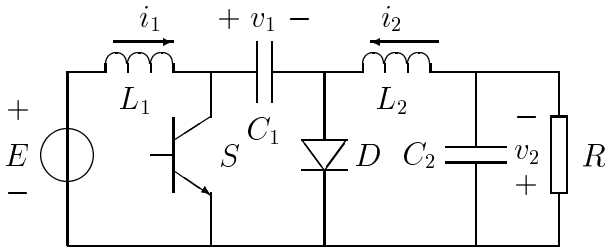

Figure 2.3: The Ćuk converter.

2.3 Modes of Operation of DC/DC Switching Converters

DC/DC converters can have different modes of operation depending on the sequence of the switch states. There are two typical modes of operation that can be identified in the buck, buck-boost and boost converters: (1) continuous mode (two-state mode); (2) discontinuous mode (three-state mode). When operating in continuous mode, two switch states exist. The buck, buck-boost, boost converters will work in this mode, provided that the inductive storage is sufficiently large. If the inductive storage is smaller than a critical value, the operation falls into a discontinuous mode. In this mode of operation, three switch states can be identified.

The mode of operation can be distinguished by inspecting the inductor current waveform. Let d be the duty ratio and T the switching period. Fig. 2.4(a) shows the inductor current waveform when the converter operates in continuous mode. dT is the duration in a cycle during which the diode is open and the switch is closed; $(1-d)T$ is the duration during which the diode is closed and the switch is open. In this case, the inductor current is always non-zero. Such a non-zero current condition requires sufficiently large inductance and sufficiently short switching period. However, if the inductance is relatively small or the switching period is relatively long, the inductor current waveform becomes the one shown in Fig. 2.4(b). In this case, the converter is said to operate in discontinuous mode. dT is the duration in a cycle during which the diode is open and the switch is closed; $d'T$ is the duration during which the diode is closed and the switch is open; $d''T$ is the duration during which both the diode and switch are open, and is equal to $(1-d-d')T$.

The state equation of the converter corresponding to each switch state can be written as

$$\dot{x} = A_j x(t) + B_j u(t) \tag{2.1}$$

where x is the vector of state variables, A_j and B_j are system matrices of the linear circuit concerned, and in the case of the simple DC/DC converters,

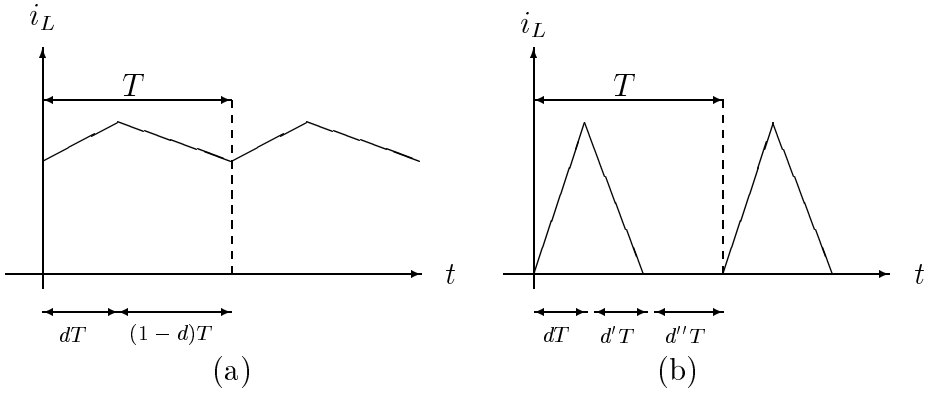

Figure 2.4: Inductor current waveform. (a)Continuous mode; (b)discontinuous mode.

- j=1 when the switch is closed and the diode is open, i.e., $0 < t < dT$.
- j=2 when the switch is open and the diode is closed, i.e., $dT < t < (1-d)T$ for continuous mode or $dT < t < (d + d')T$ for discontinuous mode.
- j=3 when the switch and the diode are open, i.e., $(d + d')T < t < T$ for discontinuous mode.

In the next section, piecewise switched models of the boost converter, the buck converter and the Ćuk converter will be derived. These models will be used for formulating the computer simulation programs used throughout this thesis.

2.4 The Boost Converter

In this section, the piecewise switched model of the boost converter is derived. The boost converter is a second-order circuit comprising an inductor, a switch, a diode, and a load resistance which is connected in parallel with a capacitor. Figure 2.2(c) shows the basic circuit. When operating in continuous mode, two switch states can be identified: (1) switch S on and diode D off; (2) switch S off and diode D on. The two switch states toggle periodically in the steady state. It is assumed that the circuit takes switch state 1 for $nT \leq t < (n+d)T$, and switch state 2 for $(n + d)T \leq t < (n + 1)T$, where n is an integer, d is the duty cycle and T is the switching period. When the converter is operating in discontinuous

mode, a third switch state corresponding to switch S off and diode D off can be identified.

As stated previously, the boost converter circuit is a multi-structural system that toggles its topology according to the states of the switches. The boost converter operating in continuous mode can thus be described by the following sequence of state equations:

$$\dot{x} = A_1 x + B_1 E \text{ for } nT \leq t < (n+d)T, \tag{2.2}$$

$$\dot{x} = A_2 x + B_2 E \text{ for } (n+d)T \leq t < (n+1)T, \tag{2.3}$$

where x denotes the state vector of the circuit, i.e., $x = [v \;\; i]^T$, and in particular, A's and B's in (2.2) and (2.3) are given by

$$A_1 = \begin{bmatrix} -\frac{1}{CR} & 0 \\ 0 & 0 \end{bmatrix}, B_1 = \begin{bmatrix} 0 \\ \frac{1}{L} \end{bmatrix} \tag{2.4}$$

when the switch is in state 1, and

$$A_2 = \begin{bmatrix} -\frac{1}{CR} & \frac{1}{C} \\ -\frac{1}{L} & 0 \end{bmatrix}, B_2 = \begin{bmatrix} 0 \\ \frac{1}{L} \end{bmatrix} \tag{2.5}$$

when the switch is in state 2.

When the converter is operating in discontinuous mode, an additional state has to be added in each period in addition to the two states in continuous mode. Its operation can be described by the following sequence of state equations:

$$\dot{x} = A_1 x + B_1 E \text{ for } nT \leq t < (n+d)T, \tag{2.6}$$

$$\dot{x} = A_2 x + B_2 E \text{ for } (n+d)T \leq t < (n+d+d')T, \tag{2.7}$$

$$\dot{x} = A_3 x + B_3 E \text{ for } (n+d+d')T \leq t < (n+1)T, \tag{2.8}$$

where A_3 and B_3 are

$$A_3 = \begin{bmatrix} -\frac{1}{CR} & 0 \\ 0 & 0 \end{bmatrix}, B_3 = \begin{bmatrix} 0 \\ 0 \end{bmatrix}. \tag{2.9}$$

2.5 The Buck Converter

The derivation of the piecewise switching model of the buck converter is essentially the same as that in the case of the boost converter. The buck converter is a second-order circuit comprising an inductor, a switch, a diode, a load resistance which is connected in parallel with a capacitor. Figure 2.2(a) shows the basic circuit.

The buck converter operating in continuous mode can be described by the following state equations:

$$\dot{x} = A_1 x + B_1 E \text{ for } nT \leq t < (n+d)T, \tag{2.10}$$

$$\dot{x} = A_2 x + B_2 E \text{ for } (n+d)T \leq t < (n+1)T, \tag{2.11}$$

where x denotes the state vector of the circuit, i.e., $x = [v \;\; i]^T$, and in particular, A's and B's in (2.10) and (2.11) are given by

$$A_1 = \begin{bmatrix} -\frac{1}{CR} & \frac{1}{C} \\ -\frac{1}{L} & 0 \end{bmatrix}, B_1 = \begin{bmatrix} 0 \\ \frac{1}{L} \end{bmatrix} \tag{2.12}$$

when the switch is in state 1, and

$$A_2 = \begin{bmatrix} -\frac{1}{CR} & \frac{1}{C} \\ -\frac{1}{L} & 0 \end{bmatrix}, B_2 = \begin{bmatrix} 0 \\ 0 \end{bmatrix} \tag{2.13}$$

when the switch is in state 2.

When the converter is operating in discontinuous mode, an additional state has to be added in each period in addition to the two states in continuous mode. Its operation can be described by the following sequence of state equations:

$$\dot{x} = A_1 x + B_1 E \text{ for } nT \leq t < (n+d)T, \tag{2.14}$$

$$\dot{x} = A_2 x + B_2 E \text{ for } (n+d)T \leq t < (n+d+d')T, \tag{2.15}$$

$$\dot{x} = A_3 x + B_3 E \text{ for } (n+d+d')T \leq t < (n+1)T, \tag{2.16}$$

where A_3 and B_3 are

$$A_3 = \begin{bmatrix} -\frac{1}{CR} & 0 \\ 0 & 0 \end{bmatrix}, B_3 = \begin{bmatrix} 0 \\ 0 \end{bmatrix}. \tag{2.17}$$

2.6 The Ćuk Converter

DC/DC converters with more than two storage elements are also commonly used in practice. The Ćuk converter is a typical higher-order circuit with four storage elements. In the following, the piecewise switched model of the Ćuk converter is derived, which will be used in the later parts of the thesis.

The Ćuk converter is a fourth-order circuit comprising two inductors, two capacitors, a switch, a diode, and a load resistance connected in parallel with one capacitor. Figure 2.3 shows the basic circuit. Similar to the buck, buck-boost, and boost converters, when operating in continuous mode, two switch states are identified. The circuit can work in discontinuous mode which can be either discontinuous-inductor-current or discontinuous-capacitor-voltage mode [36]. The converter can have four possible constituent linear circuit configurations.

When deriving the state equations for the Ćuk converter, all capacitor voltages and inductor currents are chosen as state variables, i.e.,

$$x = \begin{bmatrix} v_2 \\ v_1 \\ i_2 \\ i_1 \end{bmatrix}. \tag{2.18}$$

The system matrices corresponding to the form of state equation (2.1) are given as follows. As mentioned previously, the Ćuk converter operating in continuous mode has two switch states. In switch state 1, the switch is on and the diode is off. A_1 and B_1 are given by

$$A_1 = \begin{bmatrix} -\frac{1}{C_2 R} & 0 & \frac{1}{C_2} & 0 \\ 0 & 0 & -\frac{1}{C_1} & 0 \\ -\frac{1}{L_2} & \frac{1}{L_2} & 0 & 0 \\ 0 & 0 & 0 & 0 \end{bmatrix}, B_1 = \begin{bmatrix} 0 \\ 0 \\ 0 \\ \frac{1}{L_1} \end{bmatrix}. \tag{2.19}$$

In switch state 2, the diode is off and the diode is on. In this case, A_2 and B_2 are

given by

$$A_2 = \begin{bmatrix} -\frac{1}{C_2 R} & 0 & \frac{1}{C_2} & 0 \\ 0 & 0 & 0 & \frac{1}{C_1} \\ -\frac{1}{L_2} & 0 & 0 & 0 \\ 0 & -\frac{1}{L_1} & 0 & 0 \end{bmatrix}, B_2 = \begin{bmatrix} 0 \\ 0 \\ 0 \\ \frac{1}{L_1} \end{bmatrix}. \tag{2.20}$$

As stated before, there are two distinct types of discontinuous-mode operation. For discontinuous-inductor-current mode operation, it is characterized by the presence of a duration in which both the switch and the diode are open, i.e., $i_1 + i_2 = 0$. This happens when the inductances are relatively small, similar to the discontinuous-mode operation of the simple second-order converters studied previously. The system matrices corresponding to the additional duration are

$$A_3 = \begin{bmatrix} -\frac{1}{C_2 R} & 0 & \frac{1}{C_2} & 0 \\ 0 & 0 & 0 & \frac{1}{C_1} \\ -\frac{1}{L_1+L_2} & \frac{1}{L_1+L_2} & 0 & 0 \\ \frac{1}{L_1+L_2} & -\frac{1}{L_1+L_2} & 0 & 0 \end{bmatrix}, B_3 = \begin{bmatrix} 0 \\ 0 \\ -\frac{1}{L_1+L_2} \\ \frac{1}{L_1+L_2} \end{bmatrix}. \tag{2.21}$$

The discontinuous-capacitor-voltage mode is characterized by the presence of a duration in which the capacitor voltage, v_1, is zero. This happens when the capacitance of capacitor C_1 is relatively small, such that the value of v_1 drops to zero within the switch on-time, introducing a duration in which both the switch and diode are conducting. During this duration, the system matrices are given by

$$A_4 = \begin{bmatrix} -\frac{1}{C_2 R} & 0 & \frac{1}{C_2} & 0 \\ 0 & 0 & 0 & 0 \\ -\frac{1}{L_2} & 0 & 0 & 0 \\ 0 & 0 & 0 & 0 \end{bmatrix}, B_4 = \begin{bmatrix} 0 \\ 0 \\ 0 \\ \frac{1}{L_2} \end{bmatrix}. \tag{2.22}$$

2.7 Control of DC/DC Switching Converters

The most important application of a DC/DC converter is a high efficiency voltage or current regulator. The main objective of a voltage regulator is to produce output voltage which is independent of variations in the input voltage and the

load current. Regulators are indispensable components in power supply systems for a wide range of applications, like computers, automotives and aerospace applications. One approach to establishing regulation is to use a feedback network which compares the output voltage and a reference voltage to modify the converter control signal. The most popular control techniques include voltage-mode feedback control (duty cycle control) and current-programmed control (current-mode control) [37]–[41]. They will be discussed in the next subsection.

Other control methods reported in the literature include sliding mode control [42]–[43], charge control [44], one-cycle control [45], hysteretic control [46], boundary control [47], LQR optimal control [48]–[49], robust control [50]–[51], adaptive control [52]–[53], function control [54]–[55], Lyapunov-based control [56]–[57], nonlinear control [58]–[59], and other forms of digital control [60]–[61].

2.7.1 Voltage-mode Feedback Control Scheme

In voltage-mode feedback control, the output voltage is compared with a reference to generate a control signal which drives the pulse-width modulator via some typical feedback compensation configuration. In the following description, the buck converter is used as an example for illustration. The schematic diagram of a voltage-mode feedback controlled buck regulator is shown in Fig. 2.5. Voltage-mode feedback control uses a constant period saw-tooth signal as can be seen in Fig. 2.5. The output voltage, v, of the buck converter is compared with a control reference, V_{ref}. The switching signal as shown in Fig. 2.6 is generated by comparing the amplified error value and the saw-tooth signal. The switch is on when the positive input of the comparator is larger than the saw-tooth voltage, and is off otherwise.

2.7.2 Current-programmed Control Scheme

Current-programmed control, in its simplest form, consists of an inner current loop which samples the inductor current value and turns the switch off as soon as

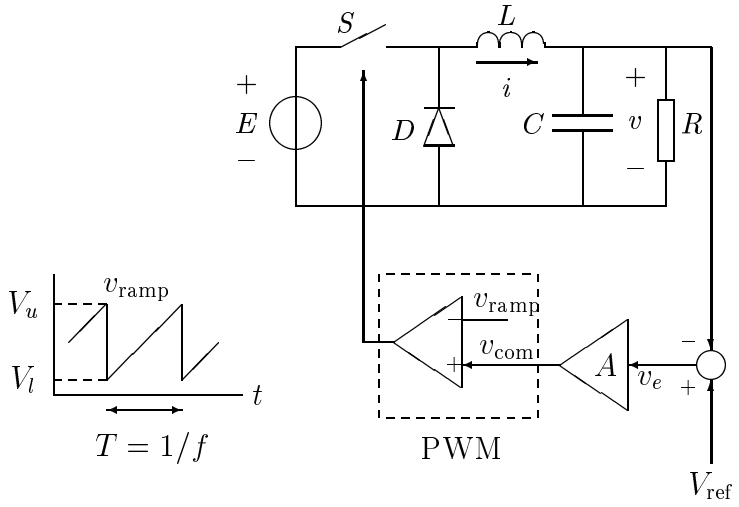

Figure 2.5: Schematic diagram of voltage-mode feedback controlled buck converter.

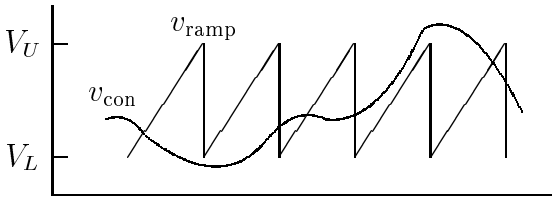

Comparator output (PWM signal)

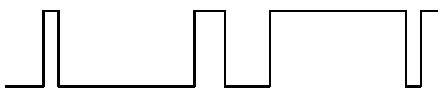

Figure 2.6: Pulse width modulation.

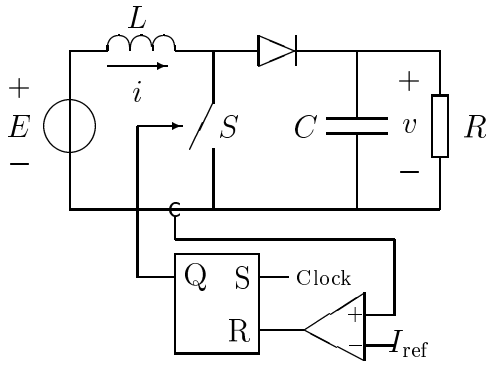

Figure 2.7: Schematic diagram of open-loop current-programmed boost converter.

the current reaches a certain value set by the outer voltage feedback loop. The switch will turn on at the next clock pulse. The method of current-programming achieves a faster response, and is now widely used for boost and buck-boost converters which suffer from an undesirable non-minimum phase response.

The boost converter is used for illustration. Figure 2.7 shows the schematic diagram of a current-programmed boost converter without voltage feedback. The inductor current is chosen as the programming variable which, by comparing with a reference current, i_{ref}, generates the on-off driving signal for switch S. Specifically, switch S is turned on at the beginning of the cycle, i.e., at $t = nT$. The inductor current increases while switch S is on. As i climbs to the value of i_{ref}, switch S is turned off, and remains off until the next cycle begins.

A typical waveform of the inductor current of the boost converter is shown in Fig. 2.8. It should be noted that although an inner current loop always exists, the circuit is regarded as an open-loop system when the value of i_{ref} is fixed, i.e., in the absence of an outer voltage feedback loop. In practice, however, an outer voltage feedback loop is usually included for the purpose of output regulation, which forces the value of i_{ref} to be a function of the output voltage v. In this case, the converter is said to be under a closed-loop current-programmed control.

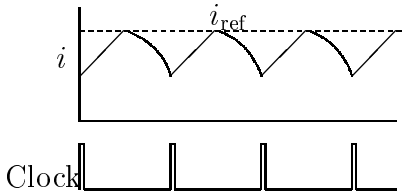

Figure 2.8: Waveforms of inductor current of open-loop current-programmed boost converter.

2.8 Conventional Approaches of Modelling and Analysis of DC/DC Switching Converters

Power electronic converters are nonlinear dynamical systems. The nonlinearities arise primarily due to switching, and the nonlinear property of power devices and passive components. Traditionally, there are two major approaches to modelling and analysis of the switching nonlinearity in DC/DC converters. The most widely used approach is a small-signal analysis based on linearization and state-space averaging or circuit averaging using the PWM switch model [62]–[64]. This approach however fails to predict the fast-scale dynamics and can capture only the slow-scale dynamics. The second approach is based on the sampled-data modelling technique [65]–[68]. It takes into account the sampling effect due to switching and can predict the boundary of the period-1 stability. However, it is rather difficult to use for analyzing chaotic dynamics.

2.8.1 State-space Averaging

The conventional way of modelling DC/DC converters is to take an average over a switching cycle, an approach first proposed by Wester and Middlebrook in 1972 [62]. Since conventional control theory requires a linear model, the averaged circuit is generally linearized about a suitable operating point. State-space averaging, developed by Ćuk and Middlebrook [3]–[4], operates on the state equations of the circuit. In 1990, Vorperian gave a method of treating the switch-diode combination in isolation from the converter circuit [63]–[64]. Ignoring the details, these methods have the same aim: to replace the nonlinear, time-varying dynam-

ical system with an averaged, linearized one. Clearly, some information about the dynamics of the system must be lost in the process.

In order to demonstrate the limitation of the conventional modelling technique, the state-space averaging approach for the buck converter is illustrated. In continuous conduction mode, switch S conducts for a fraction d of each cycle and diode D conducts for $1-d$. The averaged equations are found by multiplying (2.10) by d and (2.11) by $1-d$, and then summing:

$$\frac{di}{dt} = \frac{dE - v}{L}, \tag{2.23}$$

$$\frac{dv}{dt} = \frac{i - v/R}{C}. \tag{2.24}$$

The nonlinear time-varying buck converter model now becomes a nonlinear time-invariant model. Subsequently, the model can be linearized for control design. Such an approach is called small-signal analysis which has been widely used over the past decades to study the dynamics of DC/DC switching converters. Since the small-signal models are linear and hence easily applied to most practical design problems, the designers are tempted to use small-signal linearization technique in the design of closed-loop systems. Small-signal models generally provide enough information for designing the necessary feedback loop. However, due to the small-signal assumption, these models do not describe the behaviour of the converter adequately during large transients. Worse still, the small-signal models fail to give stability information of the regulator over the entire operating region.

Small-signal analysis is now applied to the state-space averaged model of the buck converter derived earlier. By giving a small perturbation, $i = I + \hat{i}$, $v = V + \hat{v}$ and $d = D + \hat{d}$, and substituting $dI/dt = 0$ and $dV/dt = 0$, the following expressions are obtained:

$$\frac{d\hat{i}}{dt} = \frac{(D + \hat{d})E - (V + \hat{v})}{L}, \tag{2.25}$$

$$\frac{d\hat{v}}{dt} = \frac{(I + \hat{i}) - (V + \hat{v})/R}{C}. \tag{2.26}$$

The steady-state solutions can be calculated by setting all perturbation terms to zero. The solutions are $V = DE$ and $I = V/R$. The system is linearized about this steady-state operating point. Expanding (2.25) and (2.26) and then neglecting second-order perturbation terms, the following equations are obtained:

$$\frac{d\hat{i}}{dt} = \frac{\hat{d}E - \hat{v}}{L}, \tag{2.27}$$

$$\frac{d\hat{v}}{dt} = \frac{\hat{i} - \hat{v}/R}{C}. \tag{2.28}$$

Equations (2.27) and (2.28) represent the small-signal behaviour of the buck converter. Applying Laplace transformation and eliminating $\hat{i}$ yield the control-to-output transfer function:

$$\frac{\hat{v}}{\hat{d}} = \frac{E}{1 + sL/R + s^2LC}. \tag{2.29}$$

Using a similar approach, the transfer function of the error amplifier and PWM is easily found as

$$\frac{\hat{d}}{\hat{v_e}} = \frac{A}{V_u - V_l}, \tag{2.30}$$

where A, V_u and V_l are defined in Figs. 2.5 and 2.6. Hence, the overall gain is

$$G_H(s) = \frac{\hat{v}}{\hat{v_e}} = \frac{AE}{V_u - V_l} \frac{1}{1 + sL/R + s^2LC}. \tag{2.31}$$

The stability of the closed-loop system can be analyzed by studying (2.31).

Despite the fact that small-signal models are very convenient for analysis, they have inherent inadequacy. They fail to identify nonlinear phenomena such as bifurcation and chaos. In the work of Hamill, Deane and Jefferies [10], it is shown that even though stable operation is concluded from small-signal analysis, the system can actually be unstable.

In Hamill *et al.*'s work, the buck converter is designed to accept an input voltage of 15V to 40V, and to produce a regulated output voltage close to 12V. The following parameter values apply: f_s=2.5kHz, A=8.4, V_u=8.2V, V_l=3.8V, V_{ref}=12V, L=20mH, C=47 μF and R=22 Ω. From (2.31), the phase margin of the system can be calculated. The phase margin varies from 10.2^o at the minimum input voltage of 15V, to 6.2^o at the maximum, 40V. Thus, according to the linear

model, the closed-loop converter is stable over the entire input voltage range. But analytical and experimental results reported in [10] showed that subharmonics and chaos occurred.

2.8.2 Sampled-data Modelling

Sampled-data models are naturally matched to power electronic converters: firstly, because of the cyclic way in which power converters are operated and controlled; secondly, because such models are well suited to the design of digital controllers which are used increasingly in power electronics. Like averaged models, sampled-data models allow us to focus on cycle-to-cycle behaviour ignoring details of the intra-cycle behaviour.

As mentioned previously, DC/DC converters are multi-structural systems. During one switching cycle, several circuit configurations can be identified. A state equation can be written for each of these configurations, and its solution can be obtained in terms of the respective transition matrices. The solution to each of these state equations can be "stacked" over a switching cycle, resulting in a total increment acquired during a cycle. The procedure gives a large-signal discrete-time nonlinear difference equation. For example, the discrete-time model of a boost converter working in continuous conduction mode can be written as

$$\begin{aligned} x(k+1) &= e^{A_2 d'(k)T} e^{A_1 d(k)T} x(k) + e^{A_2 d'(k)T} {A_1}^{-1} (e^{A_1 d(k)T} - 1) B_1 E \\ &\quad + {A_2}^{-1} (e^{A_2 d'(k)T} - 1) B_2 E, \end{aligned} \tag{2.32}$$

where $x(k)$ and $x(k+1)$ are the vectors of the state variables at the beginning of the current and next switching periods, respectively; $d(k)$ is the duty ratio and $d'(k) = 1 - d(k)$; $T > 0$ is the switching period; E is the input voltage; A_1, A_2, B_1, B_2 are the system matrices of the linear circuit concerned.

Equation (2.32) describes the dynamical behaviour of the system. However, it is complex and analysis cannot be done conveniently. The usual approach to analyze such a system is based on linear-ripple approximation, where the system state trajectories are approximated by piecewise-linear segments using $e^{AT} \approx$

$1 + AT$. Under this approximation, (2.32) is reduced to:

$$x(k+1) = [1 + A_1 d(k)T + A_2 d'(k)T]x(k) + d(k)TB_1E + d'(k)TB_2E. \quad (2.33)$$

Equation (2.33) defines an approximated large-signal discrete-time model. However, as shown in the work of Pavljašević and Maksimović [69], this approach may give erroneous results both quantitatively and qualitatively for some situations in a current-programmed converter. In their work, subharmonic oscillations under large parameter and large signal variations in a boost converter with current-programmed control are analyzed. The converter is operated with constant current reference without voltage feedback. The slope of compensation ramp m_c serves as a bifurcation parameter. Bifurcation analysis using the exact and approximated models are compared by varying the values of m_c. The approximated model predicts unstable subharmonic oscillations while the exact model implies stable subharmonic oscillations. The result of stable subharmonic oscillations is verified by computer simulations and experiments in [69].

The error reveals that the traditional approach is inadequate for the study of bifurcation and chaotic dynamics of nonlinear systems. The exact model gives a real scenario about the system's behaviour, but it is quite difficult to perform analysis with such a complex model. Thus, a better model that facilitates analysis and still retains the fundamental nonlinear properties of the system is needed.

2.9 Paralleling Methods for Power Supply Modules

Generally, the paralleling of power converter modules offers a number of advantages over a single, high-power, centralized power supply [70]–[76]. Paralleling of standardized converter modules is an approach that is used widely in distributed power systems. A desirable characteristic of a parallel supply system is that individual converters share the load current equally. Parallel modules are usually non-identical due to finite tolerances in the power stages and control parameters. It is possible that one or more units may have an excessive load current

when there is no specific current sharing scheme among the modules. This causes higher thermal stress on specific units and reduces the system reliability.

In order to achieve desirable characteristics when operating converter modules in parallel, a variety of approaches, with different levels of complexity and current-sharing performance, have been proposed, developed and analyzed in the past [70]–[76]. A successful selection of the paralleling scheme requires a firm understanding of merits and limitations of different paralleling schemes. The paralleling scheme must be selected by taking the complexity, cost, modularity, and reliability into consideration. Various interactions among converter modules should be incorporated into the control design and system integration to ensure stability, reliability and a good dynamic performance.

2.9.1 Classification of Paralleling Schemes

Paralleling methods are classified into two basic categories from the viewpoint of operating mechanism for current sharing, i.e., droop methods and active current sharing methods. Based on the droop features, the droop methods can be further categorized into a number of conducting schemes [75]–[76]. For active current-sharing methods, a conducting scheme consists of a specific control structure and a current-programming method. There are three basic control structures from the viewpoint of a current control strategy, namely, inner loop regulation, outer loop regulation and external controller structures. Also, there are a number of current-programming schemes among the paralleled modules. Figure 2.9 shows the classification graphically.

2.9.2 Droop Schemes

The droop method can be defined as one in which the output voltage droops as the load current is increased. Its operation mechanism is to program output impedance to achieve current sharing among converters. Generally speaking, the better the current sharing, the worse the voltage regulation is for the converters;

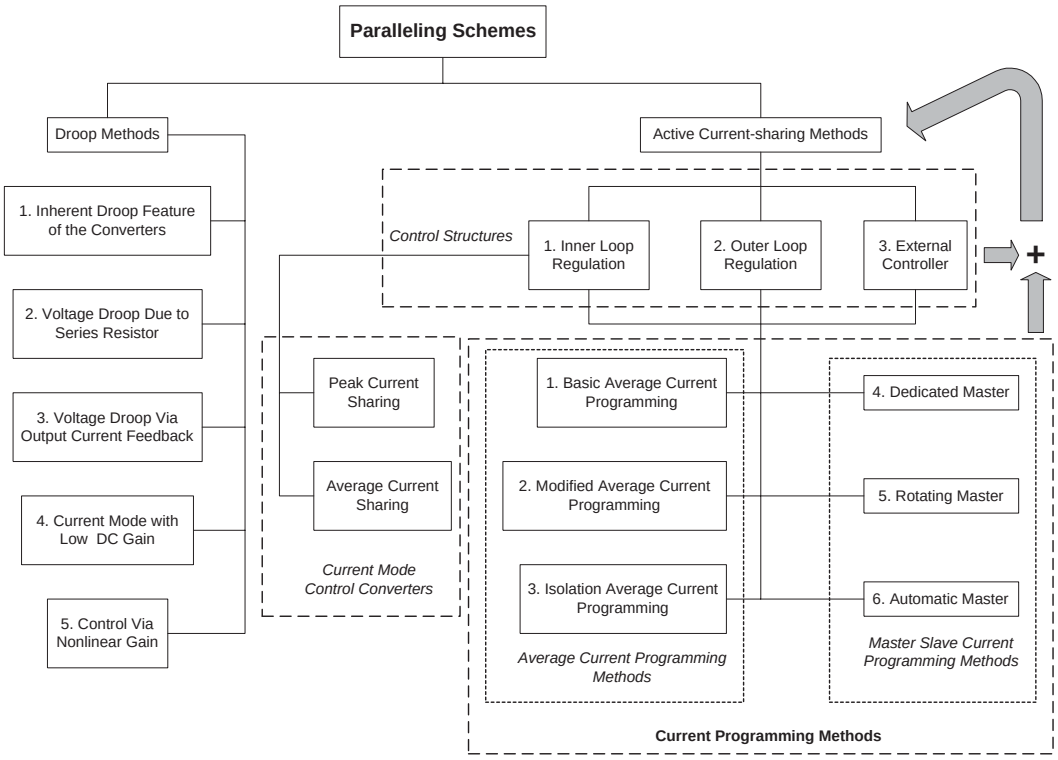

Figure 2.9: Classification diagram for paralleling methods.

so the reason conventional power supplies do not share current well is that they are designed to be good voltage sources with a low output resistance. In other words, a converter's current-sharing ability can be determined by its droop characteristic, i.e., the converter's output current versus output voltage.

The family of droop schemes needs no wire interconnections among control circuits of parallel converters, and so it is actually an open loop technique that individually programs the output impedance of each power supply. In practice, five possible droop schemes are used to parallel power supplies or power converters. They are

1. Inherent Droop Feature of the Converters;
2. Voltage Droop due to Series Resistor;
3. Voltage Droop via Output Current Feedback;
4. Current Mode with Low DC Gain; and
5. Control via Nonlinear Gain.

Advantages of the droop schemes are summarized as follows:

- Ease of implementation and expansion
- No wire connection among control circuits of converters
- High modularity and reliability

Disadvantages of the droop schemes are summarized as follows:

- Poor load regulation due to the need to achieve droop characteristics
- Poor current-sharing when compared with active current sharing schemes

2.9.3 Active Current-sharing Schemes

An active current-sharing scheme is a combination of a specific control structure and a current-programming scheme. Three control structures and six current-programming schemes can be classified. Their merits and limitations are summarized in the following.

A. Control Structures

1. Inner Loop Regulation
    - Merits – stable current-sharing; precise output voltage regulation.
    - Limitations - degradation of modularity of the system; poor fault-tolerance.
2. Outer Loop Regulation
    - Merits – good modularity and standardization for manufacturing; flexibility in system configuration, ease of expansion and maintenance of the system; excellent fault-tolerance against the failure of any single module.

- Limitations – possible instability in transient period; limited voltage-feedback gain.

3. External Controller

   - Merits – ease of implementation of interleaving; good current sharing and output voltage regulation; ease of implementation of failure monitoring; good chance to fully utilize an existing supervision system.
   - Limitations – increased interconnections among modules and external controller; degradation of modularity; degradation of reliability due to more interconnections and the complicated control.

B. Current-programming Schemes

1. Basic Average Current-programming
2. Modified Average Current-programming
3. Isolation Average Current-programming
4. Master-slave Current-programming with Dedicated Master
5. Master-slave Current-programming with Rotating Master
6. Master-slave Current-programming with Automatic Master

   The merits and limitations of the first three schemes are as follows:

   - Merits – relatively stable and precise current sharing; single interconnection sharing bus; noise immunity sharing control.
   - Limitations – relatively poor reliability; poor fault-tolerance.

   The merits and limitations of the last three schemes are as follows:

   - Merits – single interconnection sharing bus; good fault-tolerance; ease of expansion and modification of paralleling system.
   - Limitations – poor transient sharing performances; poor sharing control failure; noise sensitive sharing control.

The foregoing has provided a brief review of paralleling schemes for power supply modules. A more detailed classification and evaluation of paralleling methods for power supply modules can be found in a paper by Luo *et al.* [77].

In Chapters 4 and 5, we will investigate some systems of parallel-connected DC/DC converters under the master-slave current-sharing scheme. It will be shown that nonlinear behaviour is rich in such systems.

2.10 Summary

In this chapter, the basics of DC/DC converters are discussed. In particular, piecewise switched models of some commonly used DC/DC converters are established. These models will be used in the later parts of the thesis. Also, some conventional modelling and analysis methods are discussed and their limitations are summarized. Moreover, a classification of existing paralleling methods for power converter modules is given.

Chapter 3

An Overview of Analysis of Bifurcation and Chaos in DC/DC Switching Converters

3.1 Background

The study of dynamics began in the mid-1600s, when Newton invented differential equations, discovered his laws of motion and universal gravitation, and combined them to explain Kepler's laws of planetary motion. In the late 1800s, Poincaré developed a powerful geometric approach to analyze dynamical problems. That approach has flowered into the modern subject of dynamics, with applications reaching far beyond celestial mechanics.

The invention of high-speed computers in the 1950s was a watershed in the history of dynamics. The computer allows one to deal with equations in a way that was impossible before, and thereby to develop some insights about nonlinear systems. This led to Lorenz's discovery in 1963 of chaotic motion with a strange attractor [78]. He discovered the extreme sensitivity to perturbations of a simplified computer model of atmospheric convection.

Lorenz's work had little impact on nonlinear dynamics until 1970s, the booming years for chaos. In 1971, Ruelle and Takens proposed a new theory for the onset of turbulence in fluids, based on abstract consideration about strange

attractors [79]. In 1975, Li and Yorke first used the term "chaos" in their paper [80]. One year later, May found examples of chaos in iterated mappings arising from population biology, and wrote an influential article describing how simple nonlinear systems can have complex, chaotic behaviour [81]. Next came the most surprising discovery of all, due to the physicist Feigenbaum. He discovered that there are certain universal laws governing the transition from regular to chaotic behaviour [82]. His work established a link between chaos and phase transitions, and enticed a generation of physicists to the study of dynamics.

Although chaos stole the spotlight, there were two other major developments in dynamics in the 1970s. Mandelbrot codified and popularized fractals, produced magnificent computer graphics of them, and showed how they could be applied in a variety of subjects [83]. And in the emerging area of mathematical biology, Winfree applied the geometric methods of dynamics to biological oscillations, especially circadian rhythms and heart rhythms [84].

Chaotic effects in electronic circuits were first noted by Van der Pol in 1927 [85]. In 1983, Chua and Matsumoto synthesized the first autonomous chaotic electronic circuits [86], the double scroll oscillator, now known simply as *Chua's circuit*, which has been widely studied as the archetypal chaotic electronic circuit [87]. In the past decades, many people were working on dynamics, with contributions too numerous to list. Table 3.1 outlines this history.

The noun *chaos* and the adjective *chaotic* are used to describe the time behaviour of a *deterministic* system when the behaviour is aperiodic and is apparently random or noisy. Over the past few decades, a number of chaotic systems have been identified in a wide range of disciplines including solid state physics, fluid mechanics, plasma physics, cosmology, astrophysics, chemistry, biology, meteorology, acoustics, economics, social sciences, electrical engineering and pure mathematics. A collection of reprints of early important papers concerning bifurcation and chaos can be found in the books edited by Cvitanović [88] and Hao [89]. Also, reviews of chaos in nonlinear electronic circuits are found in the books by van Wyk and Steeb [90], Ogorzalek [91] and also Carroll and Pecora [92]. Nonlinear phenomena, though are commonly found in power electronics,

Dynamics - A Brief History		
1666	Newton	Invention of calculus, explanation of planetary motion
1700s		Flowering of calculus and classical mechanics
1800s		Analytical studies of planetary motion
1890s	Poincaré	Geometric approach
1920-1950		Nonlinear oscillators in physics and engineering, invention of radio, radar, laser
1920s-1960	Birkhoff	Complex behaviour in Hamiltonian mechanics
	Kolmogorov	
	Arnol'd	
	Moser	
1963	Lorenz	Strange attractor in simple model of convection
1970s	Ruelle and Takens	Turbulence and chaos
	May	Chaos in logistic map
	Feigenbaum	Universality and renormalization, connection between chaos and phase transitions
		Experimental studies of chaos
	Winfree	Nonlinear oscillators in biology
	Mandelbrot	Fractals
1980s		Widespread interest in chaos, fractals, oscillators, and their applications

Table 3.1: A brief history of dynamics

have only received formal treatments in very recent years [2], [93]–[94].

In this chapter, elementary bifurcation concepts, different routes to chaos, and common tools to quantify chaos are reviewed. Some of these concepts and tools will be used in the later part of this thesis. Also, the common procedures for analysis of power electronic circuits will be discussed.

3.2 Electronic Circuits as Dynamical Systems

A *system* is something having parts which may be perceived as a single entity. A *dynamical system* is one which changes with time; what changes is the state of the system. Mathematically, a dynamic system consists of a space of states (called the state space or phase space) and a rule, called the *dynamics*, for determining which state corresponds at a given future time to a given present state. A *deterministic* dynamical system is one whose state at any time is completely determined by its initial states and dynamics.

A deterministic dynamical system may have a *continuous* or *discrete* state space with *continuous-time* or *discrete-time* dynamics.

A lumped circuit containing resistive elements (resistors, voltage and current sources) and energy-storage elements (capacitors and inductors) may be modeled as a continuous-time deterministic dynamical system in $\Re^n$. The evolution of the state of the circuit is described by a system of ordinary differential equations called state equations.

Discrete-time deterministic dynamical systems occur in electronic engineering as models of switched-capacitor and digital filters, sampled phase-locked loops, and sigma-delta modulators. Discrete-time dynamical systems also arise when analyzing the stability of steady-state solutions of continuous-time systems. The evolution of a discrete-time dynamical system is described by a system of difference equations.

3.3 Continuous-time Dynamical System and Discrete-time Dynamical System

3.3.1 Continuous-time Dynamical System

Definition 3.1 [95] *A continuous-time deterministic dynamical system is defined*

by a system of ordinary differential equations of the form:

$$\dot{x}(t) = F(x(t), t), \tag{3.1}$$

where $x(t) \in \Re^n$ *is called the state,* $\dot{x}(t)$ *denotes the derivative of* $x(t)$*,* $x(t_0) = x_0$ *is called the initial condition, and the map* $F(.,.) : \Re^n \times \Re_+ \to \Re^n$ *is continuous almost everywhere on* $\Re^n \times \Re_+$ *and globally Lipschitz.*

For each $(x_0, t_0) \in \Re^n \times \Re_+$, there exists a continuous function $\phi(.; x_0, t_0) : \Re_+ \to \Re^n$ such that

$$\phi(t_0; x_0, t_0) = x_0 \tag{3.2}$$

and

$$\dot{\phi}(t; x_0, t_0) = F(\phi(t; x_0, t_0), t). \tag{3.3}$$

Furthermore, this function is unique. The function $\phi(.; x_0, t_0)$ is called the solution or trajectory through (x_0, t_0) of the dynamical system (3.1).

If the vector field of a continuous-time deterministic system depends only on the state and is independent of the time t, then the system is said to be *autonomous* and may be written as

$$\dot{x}(t) = F(x(t)). \tag{3.4}$$

3.3.2 Discrete-time Dynamical System

Definition 3.2 [95] *A discrete time deterministic dynamical system is defined by a system of difference equations of the form:*

$$x(k+1) = F(x(k), k) \tag{3.5}$$

where $x(k) \in \Re^n$ *is called the state,* $x(k_0) = x_0$ *is the initial condition, and* $F(.,.) : \Re^n \times Z_+ \to \Re^n$ *maps the current state* $x(k)$ *into the next state* $x(k+1)$*, where* $k_0 \in Z_+$*.*

For each $(x_0, k_0) \in \Re^n \times Z_+$, there exists a function $\phi(.; x_0, k_0) : Z_+ \to \Re^n$ such that

$$\phi(k_0; x_0, k_0) = x_0 \tag{3.6}$$

and

$$\phi(k+1; x_0, k_0) = F(\phi(k; x_0, t_0), k). \tag{3.7}$$

The function $\phi(.; x_0, k_0) : Z_+ \rightarrow \Re^n$ is called the solution or trajectory through (x_0, k_0) of the dynamical system (3.5).

The image $\phi(k; x_0, k_0) \in \Re^n | k \in Z_+$ of the trajectory through (x_0, k_0) is called an orbit through (x_0, k_0).

If the map $F(.,.)$ of a discrete-time dynamical system depends only on the state $x(k)$ and is independent of k, then the system is said to be autonomous and may be written simply as

$$x(k+1) = F(x(k)). \tag{3.8}$$

3.4 Equilibrium, Periodicity, Quasi-periodicity and Chaos

3.4.1 Equilibrium Point

The simplest steady-state behaviour of a dynamical system is an equilibrium point. An equilibrium point or stationary point of (3.1) is a state, x_Q, at which the vector field is zero. Thus $F(x_Q) = 0$ and $\phi_t(x_Q) = x_Q$; a trajectory starting from an equilibrium point remains indefinitely at that point.

In the state space, the limit set consists of a single nonwandering point x_Q. A point is a zero-dimensional object. Thus, an equilibrium point is said to have zero dimension.

In the time domain, an equilibrium point of a system is simply a constant solution or operating point.

An equilibrium point or fixed point of a discrete-time dynamical system is a point x_Q which satisfies $F(x_Q) = x_Q$.

3.4.2 Periodic Steady State

A state x is called periodic if there exists $T > 0$ such that $\phi_T(x) = x$. A periodic orbit which is not a stationary point is called a limit cycle.

A limit cycle Γ is an isolated periodic orbit of a dynamical system. The limit cycle trajectory visits every point on the simple closed curve Γ with period T. Indeed, $\phi_{t+T}(x) = \phi_t(x) \; \forall \; x \; \in \; \Gamma$. Thus, every point on the limit cycle Γ is a nonwandering point.

A limit cycle is said to have dimension one because a small piece of it looks like a one-dimensional object: an arc. The n components $x_i(t)$ of a limit cycle trajectory $x(t) = (x_1(t), x_2(t), \ldots, x_n(t))^T$ in $\Re^n$ are periodic time waveforms with period T.

3.4.3 Subharmonic Periodic Steady State

A subharmonic periodic solution or period-K orbit with $K \in Z_+$ of a discrete-time dynamic system is a set of K points, $\{x_1, x_2, \ldots, x_k\}$, which satisfy

$$x_2 = F(x_1), \quad x_3 = F(x_2), \quad \ldots, \quad x_K = F(x_{K-1}), \quad x_1 = F(x_K). \tag{3.9}$$

More compactly, we may write $x_i = F^K(x_i)$ where $F^K = F(F(\ldots(F(.))\ldots))$ denotes F being applied K times to the argument of the map; this is called the Kth iterate of F.

Subharmonic periodic solutions occur in systems which contain two or more competing frequencies, such as forced oscillators or sampled-data circuits. Subharmonic solutions also arise following period-doubling bifurcations, a concept to be further reviewed below.

3.4.4 Quasi-periodic Steady State

Quasi-periodicity is a complicated form of steady-state behaviour. In state space, this corresponds to a torus. While a small piece of a limit cycle in $\Re^3$ looks like

a tiny line segment, a small section of two-torus looks like a tiny planar surface; a two-torus has dimension two.

A quasi-periodic function is one that may be expressed as a countable sum of periodic functions with incommensurate frequencies, i.e., frequencies which are not rationally related. For example, $x(t) = \sin(t) + \sin(2\pi t)$ is a quasi-periodic signal. In the time domain, a quasi-periodic signal may look like an amplitude-modulated or phase-modulated waveform.

Quasi-periodic behaviour occurs in discrete-tine systems where two incommensurate frequencies are present. A periodically-forced or discrete-time dynamical system has a frequency associated with the period of forcing or sampling interval of the system; if a secondary frequency is introduced which is not rationally related to the period of the forcing or the sampling interval, then quasi-periodicity may occur.

3.4.5 Chaotic Steady State

Equilibrium, periodic, and quasi-periodic steady-state behaviours have been correctly identified and classified since the poineering days of engineering in the 1920s. By contrast, the existence of more exotic steady-state behaviour in electronic circuits has only been acknowledged in the past thirty years. While the notion of chaotic behaviour in dynamical systems has existed in the mathematical literature since the turn of the century, unusual behaviour were described as "strange" in the physical sciences as recently as the 1960s. Today, we classify *chaos* as (low-dimensional) nonwandering motion in deterministic dynamical systems which exhibits both "randomness" and "order".

From an experimentalist's point of view, chaos may be defined as bounded steady-state behaviour which is not an equilibrium point, not periodic, and not quasi-periodic.

Chaos is characterized by repeated stretching and folding of a bundle of trajectories in state space. Two trajectories started from almost identical ini-

tial conditions diverge and soon become uncorrelated; this is called "sensitive dependence on initial conditions" and gives rise to long-term unpredictability.

In the time domain, a chaotic trajectory is neither periodic nor quasi-periodic but looks "random". While an equilibrium point, a limit cycle, and a K-torus each has an integer dimension, the repeated stretching and folding of trajectories in a chaotic steady state gives the limit set a more complicated structure which, for three-dimensional continuous-time circuits, is something more than a surface but not quite a volume; it has a fractional dimension. A set which has a non-integer dimension is called a *fractal*.

3.5 Stability of Equilibrium Points

Qualitatively, an equilibrium point is said to be stable if trajectories starting close to it remain nearby for all future time, or unstable otherwise. Stability is generally a local concept for nonlinear systems, dealing with trajectories in a small neighbourhood of the equilibrium point of the underlying system.

To analyze the behaviour of the vector field in the vicinity of an equilibrium point, x_Q, writing $x = x_Q + \tilde{x}$ and substituting it into (3.4), one gets:

$$\dot{x_Q} + \dot{\tilde{x}} = F(x_Q + \tilde{x}), \tag{3.10}$$

$$F(x_Q) + \dot{\tilde{x}} \approx F(x_Q) + D_x F(x_Q)\tilde{x} \tag{3.11}$$

where only the first two terms of the Taylor series expansion of $F(x)$ about x_Q are kept. The *Jacobian* $D_x F(x)$ is the matrix consisting of partial derivatives of $F(x)$ with respect to x:

$$D_x F(x) = \begin{bmatrix} \frac{\partial F_1(x)}{\partial x_1} & \frac{\partial F_1(x)}{\partial x_2} & \cdots & \frac{\partial F_1(x)}{\partial x_n} \\ \frac{\partial F_2(x)}{\partial x_1} & \frac{\partial F_2(x)}{\partial x_2} & \cdots & \frac{\partial F_2(x)}{\partial x_n} \\ \vdots & \vdots & \ddots & \vdots \\ \frac{\partial F_n(x)}{\partial x_1} & \frac{\partial F_n(x)}{\partial x_2} & \cdots & \frac{\partial F_n(x)}{\partial x_n} \end{bmatrix}. \tag{3.12}$$

Subtracting $F(x_Q)$ from both sides of (3.11), a linear system is obtained:

$$\dot{\tilde{x}} = D_x F(x_Q)\tilde{x} \tag{3.13}$$

where the Jacobian is evaluated at x_Q. This linearization describes the behaviour of the system in the vicinity of x_Q; it is called the local behaviour.

3.6 Eigenvalues

If x_Q is an equilibrium point of the autonomous system (3.4), a complete description of its stability is contained in the eigenvalues of the linearization of (3.4) about x_Q. These are defined as the roots λ of its corresponding characteristic equation:

$$\det(\lambda \mathbf{1} - D_x F(x_Q)) = 0 \tag{3.14}$$

where $\mathbf{1}$ is the identity matrix.

If the real parts of all the eigenvalues of $D_x F(x_Q)$ are strictly negative, then the equilibrium point x_Q is asymptotically stable and is called a sink because all nearby trajectories converge towards it.

If any of the eigenvalues has a positive real part, the equilibrium point is unstable; if all the eigenvalues have positive real parts, the equilibrium point is called a source. An equilibrium point which has eigenvalues with both negative and positive real parts is called a saddle. A saddle is unstable.

An equilibrium point is said to be hyperbolic if all the eigenvalues of $D_x F(x_Q)$ have non-zero real parts. All hyberbolic equilibrium points are either unstable or asymptotically stable.

For discrete-time dynamical systems, the stability of a fixed point x_Q of the system

$$x_{k+1} = F(x_k) \tag{3.15}$$

is determined by the eigenvalues of $D_x F(x_Q)$ evaluated at x_Q. The equilibrium point is classified as stable if all the eigenvalues of $D_x F(x_Q)$ are strictly less than unity in modulus, and unstable if any has modulus greater than unity.

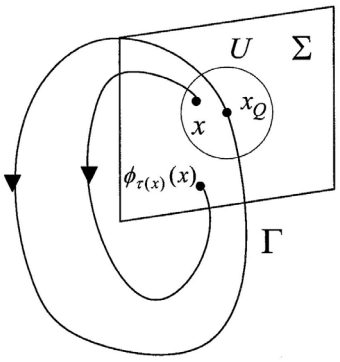

Figure 3.1: The Poinacré section.

3.7 Poincaré Section

A *Poincaré section* of an n-dimensional autonomous continuous-time dynamical system is an (n-1)-dimensional hyperplane, $\sum$, in the state space which is intersected transversally by the flow.

Let Γ be a closed orbit of the flow of a smooth vector field F, and let x_Q be a point of intersection of Γ with $\sum$. If T is the period of Γ and $x \in \sum$ is sufficiently close to x_Q, then trajectory $\phi_t(x)$ through x will return to $\sum$ after a time $\tau(x) \approx T$ and intersect the hyperplane at a point, $\phi_{\tau(x)}(x)$, as shown Fig. 3.1.

This construction implicitly defines a function (called a *Poincaré map*) $F : U \to \sum$, satisfying

$$F(x) = \phi_{\tau(x)}(x) \tag{3.16}$$

where U is a small region of $\sum$ containing x_Q. The corresponding discrete-time dynamical system

$$x_{k+1} = F(x_k) \tag{3.17}$$

has a fixed point at x_Q.

The stability of a limit cycle of the map F is determined by the eigenvalues of the linearization $D_xF(x_Q)$ of F at x_Q. If all the eigenvalues of $D_xF(x_Q)$ have modulus less than unity, the limit cycle is asymptotically stable; if any has modulus greater than unity, it is unstable.

Note that the stability of the limit cycle is independent of the position and

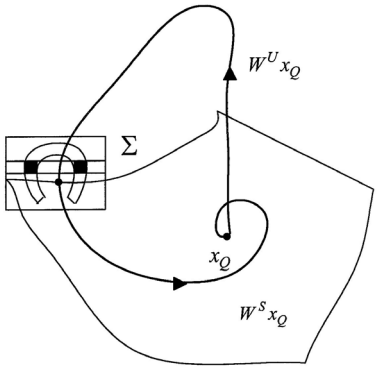

Figure 3.2: The homoclinic orbit.

orientation of the Poincaré plane, provided that the intersection is chosen to be transverse to the flow. For a non-autonomous system with periodic forcing, a natural choice for the hyperplane is at a fixed phase θ_0 of the forcing.

In the Poincaré section, a fixed point corresponds to a limit cycle. A period-K subharmonic of a non-autonomous system with periodic forcing appears as a period-K orbit of the corresponding map.

The Poincaré section of a quasi-periodic attractor consisting of two incommensurate frequencies looks like a closed curve – a transverse cut through a two-torus.

The Poincaré section of a chaotic attractor has a fractal structure.

3.8 Chaos in the Sense of Shil'nikov

Consider a flow ϕ in $\Re^3$ which has an equilibrium point at the origin with a real eigenvalue $\gamma > 0$ and a pair of complex conjugate eigenvalues $\sigma \pm j\omega$ with $\sigma < 0$ and $\omega \neq 0$. Assume that the flow has a homoclinic orbit Γ through the origin.

A Poincaré map for this system can be defined by taking a transverse section through the homoclinic orbit, as shown in Fig. 3.2, where W^S and W^U are the stable and unstable manifolds of the equilibrium point x_Q, respectively.

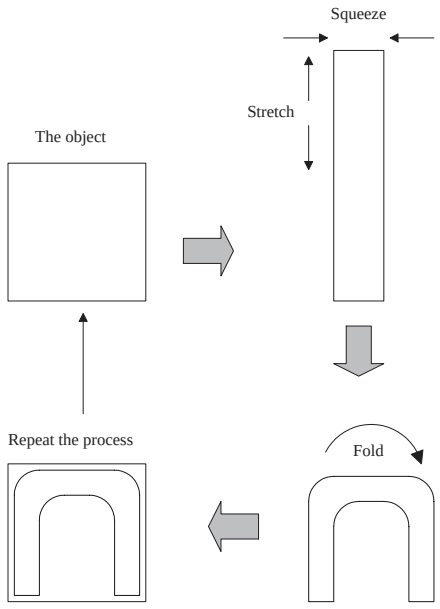

Figure 3.3: The horseshoe map.

Theorem 3.1 [95] *If* $|\sigma/\gamma| < 1$, *the flow* ϕ *can be perturbed to* ϕ' *such that* ϕ'*has a homoclinic orbit* Γ' *near* Γ *and the Poincaré map of* ϕ' *defined in a neighbourhood of* Γ' *has a countable number of horseshoes in its discrete dynamics.*

The characteristic horseshoe shape in the Poincaré map stretches and folds trajectories repeatedly. The resulting dynamics exhibit extreme sensitivity to initial conditions. The presence of horseshoes in the flow of a continuous-time system which satisfies the assumptions of Shil'nikov's theorem implies the existence of a countable number of unstable periodic orbits of arbitrarily long period as well as an uncountable number of complicated bounded nonperiodic chaotic solutions. This concept is further discussed next.

3.9 Horseshoes

In 1967, Smale showed that the stretching-and-folding property of chaotic systems could be captured by a transformation known as the horseshoe mapping [96]. To visualize this, consider a two-dimensional autonomous system. As shown in Fig. 3.3, take a square area in the state space. Stretch it in one direction and squeeze it in another. Then fold the expanding direction to shape it like a

horseshoe. Now take the area that contains this horseshoe shape and repeat the process. Repeated application of this mapping leads to a fine layered structure that is found in the strange attractors of chaotic systems.

3.10 Devaney's Definition of Chaos

There are many possible definitions of chaos in a dynamical system, among which Devaney's definition (for discrete-time systems) is a very popular one because it applies to a large number of important examples.

Theorem 3.2 [97] *Let V be a set. A map $f : V \to V$ is said to be chaotic on V if*

1. *f has sensitive dependence on initial conditions;*
2. *f is topological transitive;*
3. *f has infinitely many periodic points that together are dense in V.*

3.11 Lyapunov Exponents

One popular way to characterize a chaotic system is to quantify the rates of stretching and squeezing of its orbits in the state space. This is done by means of Lyapunov exponents. In the direction of stretching, two nearby trajectories diverge, while in the directions of squeezing, nearby trajectories converge. If we approximate this divergence and convergence by exponential functions, the rates of stretching and squeezing would be quantified by the exponents. These are the Lyapunov exponents. Since the exponents vary over the state space, one has to take the long time average exponential rates of divergence (or convergence) of nearby orbits.

The total number of Lyapunov exponents is equal to the degree of freedom of the system. If the system trajectories have at least one positive Lyapunov exponent, then those trajectories are either unstable or chaotic. If the trajectories are

bounded and have positive Lyapunov exponents, the system definitely includes chaotic behaviour. The larger the positive exponent, the shorter the time scale of system predictability. The estimation of the largest exponent therefore assumes a special importance.

Here, we only state the definitions of Lyapunov exponents for continuous-time and discrete-time nonlinear systems. More detailed descriptions of various algorithms for calculating Lyapunov exponents can be found in references [98]–[103].

3.11.1 Lyapunov Exponents for Continuous-time Nonlinear Systems

For a given continuous dynamical system in an n-dimensional phase space, we monitor the long-term evolution of an infinitesimal n-sphere of initial conditions. The sphere will evolve into an n-ellipsoid due to the locally deforming nature of the flow. The ith one-dimensional Lyapunov exponent can be defined in terms of the length of the ellipsoidal principal axis $l_i(t)$:

$$\lambda_i = \lim_{t\to\infty} \frac{1}{t} \ln \left| \frac{l_i(t)}{l_i(0)} \right|, \tag{3.18}$$

whenever the limit exists [98]–[99]. Thus, the Lyapunov exponents are related to the expanding or the contracting nature of the principle axes in phase space. A positive Lyapunov exponent describes an exponentially increasing separation of nearby trajectories in a certain direction. This property, in turn, leads to the sensitive dependence of the dynamics on initial conditions, which is a necessary but not sufficient condition for chaotic behaviour. Since the orientation of the ellipsoid changes continuously as it evolves, the directions associated with a given exponent vary in a complicated way through the attractor. We cannot therefore speak of a well defined direction associated with a given exponent.

For systems whose equations of motion are known explicitly, Benettin *et al.* [99] have proposed a straightforward technique for computing the complete Lyapunov spectrum. This method can be described in principle as follows. Let

an m-dimensional compact manifold $\mathcal{M}$ be the state space of a dynamical system. The system on $\mathcal{M}$ is a nonlinear differentiable map $\phi : \mathcal{M} \to \mathcal{M}$, which can be conveniently described by the following difference equation:

$$x(n) = \phi(x(n-1)) = \phi^n(x(0)). \tag{3.19}$$

Let $v(0)$ denote an initial perturbation of a generic point $x(0)$, and ε be a constant that is small enough. Consider the separation of trajectories of the unperturbed and perturbed points after n iterations:

$$\begin{aligned} \|\phi^n(x(0)) - \phi^n(x(0) + \varepsilon v(0))\| &= \|D\phi^n(x(0))v(0)\varepsilon\|\mathcal{O}(\varepsilon^2) && (3.20) \\ &= \left\| \left(\prod_{k=0}^{n-1} D\phi^n(x(k)) \right) v(0)\varepsilon \right\| + \mathcal{O}(\varepsilon^2), && (3.21) \end{aligned}$$

where $D\phi(x(k))$ is the Jacobian, that is, the $m \times m$ matrix of partial derivatives of ϕ evaluated at the point $x(k)$. Let the distinct eigenvalues $D\phi(x(k))$ be denoted by $\{d_i^k : k = 0, \ldots, n-1; i = 1, \ldots, m\}$. Then the Lyapunov exponents of the dynamical system are defined by

$$\lambda_i = \lim_{n \to \infty} \frac{1}{n} \sum_{k=0}^{n-1} \ln(d_i^k). \tag{3.22}$$

Unfortunately, this method cannot be applied directly to experimental data, since we do not usually know the underlying dynamical equations. For experimental data, one has to resort to (3.18).

3.11.2 Lyapunov Exponents for Discrete-time Nonlinear Systems

Consider any initial condition x_0, and let $\{x_k\}_{k=0}^{\infty}$ be the corresponding orbit of a p-dimensional, discrete-time map P. Let $m_1(k), m_2(k), \ldots, m_p(k)$ be the eigenvalues of $DP^k(x_0)$. The ith one-dimensional Lyapunov exponent of P with respect to x_0 can be defined by

$$\lambda_i = \lim_{k \to \infty} \frac{1}{k} \ln|m_i(k)|, \tag{3.23}$$

whenever the limit exists [103].

3.11.3 Lyapunov Spectra

The set $\{\lambda_i, i = 1, 2, \ldots, n\}$ is called the Lyapunov spectrum. An attractor has the property that the sum of its LEs is negative. The Lyapunov spectrum may be used to identify attractors, as summarized in Table 3.2.

Steady-state	Limit set	Spectrum	LEs	Dimension
Equilibrium point	fixed point	spike	$0 > \lambda_1 \geq \cdots \lambda_n$	0
Periodic	closed curve	fundamental plus integer harmonics	$\lambda_1 = 0,$ $0 > \lambda_2 \geq \cdots \lambda_n$	1
Quasi-periodic	K-torus	incommensurate frequencies	$\lambda_1 = \cdots = \lambda_K = 0,$ $0 > \lambda_{K+1} \geq \cdots \lambda_n$	K
Chaotic	fractal	broad spectrum	$\lambda_1 > 0,\ \sum_{i=1}^{n} \lambda_i < 0$	non-integer

Table 3.2: Classification of steady-state behaviour according to their limit sets, power spectra, Lyapunov exponents, and dimension.

3.12 Bifurcation Diagrams

A bifurcation diagram is a plot of the steady-state points of a system versus a control parameter. Typically, one chooses a state variable and plots this against a single control parameter. In discrete-time systems, one simply plots successive values of a state variable. In continuous-time systems, some type of discretization is needed, typically by means of a Poincaré section. A bifurcation diagram summarizes the state-space information so that the variation as a function of the parameter can be viewed. The transition from steady state to chaos can be observed.

3.13 Types of Bifurcation for Continuous-time Dynamical Systems

Bifurcation refers to a qualitative change in the dynamics which occurs as a system parameter is changed. The parameter value at which bifurcation occurs is called a *bifurcation point.*

For two-dimensional continuous-time dynamical systems, there are two types of common bifurcations. Either a simple real eigenvalue approaches zero and we have $\lambda_1 = 0$, or a pair of simple complex eigenvalues reaches the imaginary axis and we have $\lambda_{1,2} = \pm j\omega_0,\ \omega_0 > 0$ for some value of a variable system parameter.

3.13.1 Fold Bifurcation or Saddle-node Bifurcation

Definition 3.3 [104] *In a one-dimensional system, the bifurcation associated with the appearance of* $\lambda_1 = 0$ *is called a fold bifurcation or saddle-node bifurcation.*

The one-dimensional normal form is given by

$$\dot{x} = \alpha + x^2. \tag{3.24}$$

Two equilibrium points are $x_{1,2}(\alpha) = \pm\sqrt{-\alpha}$ when $\alpha < 0$, $-\sqrt{-\alpha}$ is stable and $\sqrt{-\alpha}$ is unstable. At $\alpha = 0$, the two equilibrium points collide, forming an equilibrium point $x = 0$. There are no equilibrium points when $\alpha > 0$.

3.13.2 Hopf Bifurcation

Definition 3.4 [104] *In a two-dimensional system, the bifurcation associated with the presence of $\lambda_{1,2} = \pm j\omega_0, \omega_0 > 0$, is called a Hopf bifurcation.*

The two-dimensional normal form is given by

$$\begin{aligned} \dot{x} &= \alpha x - y - x(x^2 + y^2), \\ \dot{y} &= x + \alpha y - y(x^2 + y^2). \end{aligned} \tag{3.25}$$

The system has the equilibrium point $x = y = 0$ for all α with the Jacobian

$$A = \begin{pmatrix} \alpha & -1 \\ 1 & \alpha \end{pmatrix} \tag{3.26}$$

having eigenvalues $\lambda_{1,2} = \alpha \pm j$. Introduce the complex variable $z = x + jy$, so that $\bar{z} = x - jy$, $|z|^2 = z\bar{z} = x^2 + y^2$ and system (3.25) is rewritten in the following complex form:

$$\dot{z} = (\alpha + j)z - z|z|^2. \tag{3.27}$$

Finally, using the representation $z = \rho e^{j\varphi}$, the polar form of system (3.25) is obtained:

$$\begin{aligned} \dot{\rho} &= \rho(\alpha - \rho^2), \\ \dot{\varphi} &= 1. \end{aligned} \tag{3.28}$$

The system has the equilibrium point $\rho = 0$ for all values of α. The equilibrium point is linearly stable if $\alpha < 0$; it remains stable at $\alpha = 0$; for $\alpha > 0$, the equilibrium point becomes linearly unstable. For $\alpha > 0$, there is a unique and stable closed orbit called limit cycle of radius $\rho_0(\alpha) = \sqrt{\alpha}$. All orbits starting outside or inside except at the origin tend to the cycle as $t \to +\infty$.

3.14 Types of Bifurcation for Discrete-time Dynamical Systems

For discrete-time dynamical systems, there are three types of common bifurcations. Either a simple real positive eigenvalue approaches positive one ($\lambda_1 = 1$),

a simple real negative eigenvalue approaches negative one ($\lambda_1 = -1$), or a pair of simple complex eigenvalues reaches the unit circle ($\lambda_{1,2} = e^{\pm\theta_0},\ 0 \leq \theta_0 < \pi$) for some value of a chosen parameter.

3.14.1 Fold Bifurcation or Saddle-node Bifurcation

Definition 3.5 [104] *For one-dimensional systems, the bifurcation associated with the appearance of $\lambda_1 = 1$ is called a fold bifurcation or saddle-node bifurcation.*

The one-dimensional normal form is given by

$$x_{k+1} = \alpha + x_k + x_k^2. \tag{3.29}$$

Two fixed points are $x_{1,2}(\alpha) = \pm\sqrt{-\alpha}$ when $\alpha < 0$, where $-\sqrt{-\alpha}$ is stable and $\sqrt{-\alpha}$ is unstable. At $\alpha = 0$, the two fixed points collide, forming a fixed point $x = 0$. There are no fixed points when $\alpha > 0$.

3.14.2 Flip Bifurcation or Period-doubling Bifurcation

Definition 3.6 [104] *For one-dimensional systems, the bifurcation associated with the appearance of $\lambda_1 = -1$ is called a flip bifurcation or period-doubling bifurcation.*

The one-dimensional normal form is given by

$$x_{k+1} = -(1+\alpha)x_k + x_k^3. \tag{3.30}$$

One fixed point is $x = 0$ for all $\alpha < 0$, which is stable. For $\alpha > 0$, it becomes unstable and a stable cycle of period two $\{x_1^o, x_2^o\}$ exists.

3.14.3 Neimark-Sacker Bifurcation

Definition 3.7 [104] *For two-dimensional systems, the bifurcation corresponding to the presence of $\lambda_{1,2} = e^{\pm j\theta_0},\ 0 \leq \theta_0 < \pi$, is called a Neimark-Sacker bifurcation.*

The two dimensional normal form is given by

$$\begin{pmatrix} x_{k+1} \\ y_{k+1} \end{pmatrix} = (1+\alpha)\begin{pmatrix} \cos\theta & -\sin\theta \\ \sin\theta & \cos\theta \end{pmatrix}\begin{pmatrix} x_k \\ y_k \end{pmatrix} + (x_k^2+y_k^2)\begin{pmatrix} \cos\theta & -\sin\theta \\ \sin\theta & \cos\theta \end{pmatrix}\begin{pmatrix} a & -b \\ b & a \end{pmatrix}\begin{pmatrix} x_k \\ y_k \end{pmatrix}, \quad (3.31)$$

where α is the bifurcation parameter; $\theta = \theta(\alpha),\ a = a(\alpha),\ b = b(\alpha)$ are smooth functions; and $0 \le \theta(0) < \pi,\ a(0) \neq 0$.

The system has the fixed point $x = y = 0$ for all α, with Jacobian

$$A = (1+\alpha)\begin{pmatrix} \cos\theta & -\sin\theta \\ \sin\theta & \cos\theta \end{pmatrix}. \quad (3.32)$$

The matrix has eigenvalues $\lambda_{1,2} = (1+\alpha)e^{\pm j\theta}$. To analyze the bifurcation, introduce the complex variable $z = x+jy$, so that $\bar{z} = x-jy,\ |z|^2 = z\bar{z} = x^2+y^2$, and set $d = a+jb$. The equation for z becomes

$$z_{k+1} = e^{j\theta}z_k(1+\alpha+d|z_k|^2) = \mu z_k + cz_k|z_k|^2, \quad (3.33)$$

where $\mu = \mu(\alpha) = (1+\alpha)e^{j\theta(\alpha)}$ and $c = c(\alpha) = e^{j\theta(\alpha)}d(\alpha)$ are complex functions of parameter α.

Using the representation $z = \rho e^{j\varphi}$, also from $\rho = |z|$, the following equation is obtained:

$$\rho_{k+1} = \rho_k|1+\alpha+d(\alpha)\rho_k^2|. \quad (3.34)$$

Since

$$|1+\alpha+d(\alpha)\rho^2| = 1+\alpha+a(\alpha)\rho^2+O(\rho^3), \quad (3.35)$$

the following polar form of system (3.31) is obtained:

$$\begin{aligned} \rho_{k+1} &= \rho_k(1+\alpha+a(\alpha)\rho_k^2)+\rho_k^4R_\alpha(\rho_k), \\ \varphi_{k+1} &= \varphi_k+\theta(\alpha)+\rho_k^2Q_\alpha(\rho_k), \end{aligned} \quad (3.36)$$

for some functions R and Q, which are smooth functions of (ρ,α).

The system has a fixed point $\rho = 0$ for all values of α, which is linearly stable for $\alpha < 0$. It remains stable at $\alpha = 0$. For $\alpha > 0$, it becomes linearly unstable; also there is a unique and stable closed invariant curve of radius $\rho_0(\alpha)$.

3.15 Routes to Chaos

3.15.1 Period-doubling Route to Chaos

The period-doubling route to chaos is characterized by a cascade of period-doubling bifurcations. Each period-doubling transforms a limit cycle into one at half the frequency, spreading the energy of the system over a wider range of frequencies. An infinite cascade of such doublings results in a chaotic trajectory of infinite period and a broad-frequency spectrum which contains energy at all frequencies.

The period-doubling routes to chaos is readily identified from a state space plot, time series, power spectrum, or a Poincaré map.

3.15.2 Quasi-periodic Route to Chaos

The quasi-periodic route to chaos results from a sequence of Hopf bifurcations. Starting from a fixed point, the three-torus generated after three Hopf bifurcations is not stable in the sense that there exists an arbitrarily small perturbation of the system (in terms of parameters) for which the three-torus gives way to chaos.

Quasi-periodicity is difficult to detect from a time series; it is more readily identified by means of a Poincaré map.

3.15.3 Intermittency Route to Chaos

The emergence of intermittent behaviour in discrete-time systems is always associated with the loss of stability of a periodic motion. According to where an eigenvalue crosses the unit circle at $+1$ or at -1 or whether a pair of conjugate complex eigenvalues crosses the unit circle, a different type of bifurcation takes place. If λ crosses the circle at $+1$ (saddle-node bifurcation), it is of type I intermittency; if a pair of conjugate complex eigenvalues crosses the unit circle (subcritical Neimark-Sacker bifurcation), it is of type II intermittency and, for $\lambda = -1$ (subcritical flip bifurcation), it is of type III intermittency.

3.16 Common Procedures for Analysis of Power Electronic Circuits

Traditional modelling and analysis methods for linear models usually fail to work in power electronic circuits due to their inherent nonlinearity. In recent years, researchers working in the field of power electronics have developed some tools which are suitable for the analysis of such nonlinear circuits. Much of the literature follows similar procedures in dealing with these systems, and succeeds in achieving novel results with useful conclusions [2], [94].

The common procedures involve three steps. To commence with, a discrete-time iterative map (Poincaré map) of the system being investigated is established. In DC/DC converters, a discrete-time iterative map can be established by sampling the state variables (inductor current and capacitor voltage) at the beginning of each switching period T. Using the map, the dynamics of a DC/DC converter can be described as

$$x_{n+1} = f(x_n, d_n), \tag{3.37}$$

where x is the state vector, d is the duty cycle, and the subscript n denotes the value at the beginning of the nth cycle, i.e., $x_n = x(nT)$. For the closed-loop system, a feedback equation relates d_n to x_n. With this discrete-time equation, the values of the state variables at the beginning of each switching cycle are known.

The next step is the derivation of the Jacobian of the map. Standard bifurcations of discrete-time systems such as saddle-node bifurcation ($\lambda_1 = 1$), period-doubling bifurcation ($\lambda_1 = -1$) and Neimark-Sacker bifurcation ($\lambda_{1,2} = e^{\pm j\theta_0}$, $0 \leq \theta_0 < \pi$) can be located by studying the locus of the eigenvalues of the Jacobian.

The final step is the construction of extensive computer simulations or laboratory experiments to verify the analysis. Time domain waveforms, phase portraits, bifurcation diagrams, Lyapunov exponents and Fourier spectra are commonly used to display the results concerning bifurcation and chaos.

In the following chapters, with the exception of studying autonomous DC/DC converters, the above procedure will be applied to identify various nonlinear phenomena in DC/DC converters. For autonomous converters, a continuous-time approach will be used for studying the nonlinear behaviour.

Chapter 4

Bifurcation in Parallel-connected Buck Converters

4.1 Introduction

Paralleling power converters allows high current to be delivered to loads without the need to employ devices of high power rating. The main design issue in parallel converters is the control of the sharing of current among the constituent converters. If a DC/DC converter is regarded as a voltage regulator that provides very stiff voltage to a load, then it is theoretically impossible to put two such converters in parallel feeding the same load and sharing equal current, unless the two converters are perfectly identical.

In practice, mandatory control is needed to ensure proper current sharing, and many effective control schemes have been proposed in the past [70]–[74], [105]–[107]. One common approach is to employ an active control scheme to force the current in one converter to follow that of the other. The essence of this control approach is to monitor the difference of the output currents in two constituent converters (i.e., *current error*) and incorporate this information in the main voltage control loop. Specifically, for the case of two converters connected in parallel, one converter simply has a voltage feedback control while the other has an additional inner current loop that provides the current error information which is used in turn to "adjust" the voltage feedback loop to ensure equal sharing of current. Such a scheme is commonly known as the *master-slave* current-sharing scheme [105], [107].

In this chapter, we attempt to probe into some nonlinear phenomena of a system of parallel-connected buck converters controlled under a master-slave current-sharing scheme. A usual mode of presentation is to begin with theory and analysis, followed by simulations and/or experiments. However, when studying nonlinear dynamics of physical systems, very often, simulations and experiments precede analysis. In this chapter, we deliberately present our results to reflect this practical mode of investigation. That is, we will begin with a series of computer simulation and experimental studies which identify important bifurcation phenomena. This will be followed by detailed analysis of the system, which establishes formally the possibility of particular bifurcation scenarios.

4.2 Master-Slave Controlled Parallel-connected DC/DC Converters

The system under study consists of two DC/DC converters, which are connected in parallel feeding a common load. The current drawn by the load is shared properly between the two buck converters by the action of a master-slave control scheme, as mentioned briefly in the preceding section. Figure 4.1 shows the block diagram of this master-slave configuration.

Denoting the two converters as Converter 1 and Converter 2, as shown in Fig. 4.1, the operation of the system can be described as follows. Both converters are controlled via a simple pulse-width modulation (PWM) scheme, in which a control voltage, $v_{\rm con}$, is compared with a sawtooth signal to generate a pulse-width modulated signal that drives the switch, as shown in Fig. 4.2. The sawtooth signal of the PWM generator is given by

$$v_{\rm ramp} = V_L + (V_U - V_L)\frac{t \bmod T}{T}, \tag{4.1}$$

where V_L and V_U are the lower and upper voltage limits of the ramp, and T is the switching period. The PWM output is "high" when the control voltage is greater than $v_{\rm ramp}$, and is "low" otherwise.

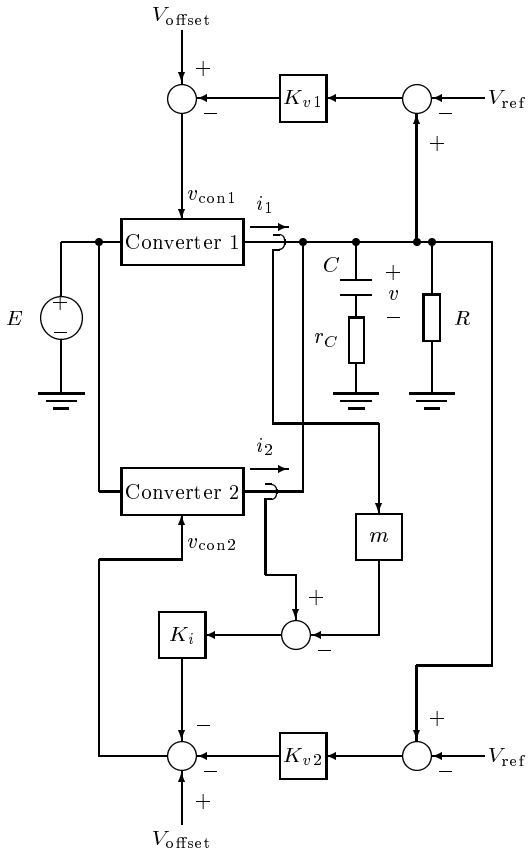

Figure 4.1: Block diagram of parallel-connected DC/DC converters under a master-slave control.

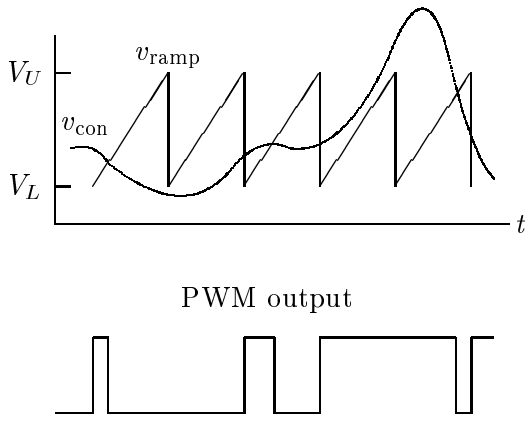

Figure 4.2: Pulse-width modulation (PWM) showing relationship between the control voltage and the PWM output.

For Converter 1, the control voltage is derived from a voltage feedback loop, i.e.,

$$v_{\text{con1}} = V_{\text{offset}} - K_{v1}(v - V_{\text{ref}}), \tag{4.2}$$

where V_{offset} is a dc offset voltage that gives the steady-state duty cycle, V_{ref} is the reference voltage, and K_{v1} is the voltage feedback gain for Converter 1.

For Converter 2, an additional current error signal, which is proportional to the weighted difference of the output currents of the two converters, determines the control voltage. Specifically we write the control voltage for Converter 2 as

$$v_{\text{con2}} = V_{\text{offset}} - K_{v2}(v - V_{\text{ref}}) - K_i(i_2 - mi_1), \tag{4.3}$$

where K_{v2} is the voltage feedback gain of Converter 2, K_i is the current feedback gain, and m is a current weighting factor. Under this scheme, the output current of Converter 2 will follow that of Converter 1 at a ratio of m to 1, where $m > 0$. When $m = 1$, we expect equal current sharing. In much of the literature, Converter 1 is referred to as the "master" which operates independently, and Converter 2 the "slave" which imitates the master's current value.

4.3 State Equations for Two Parallel Buck Converters

The foregoing section defines the essential control scheme that provides current sharing and output voltage regulation. In this section we focus on a specific converter type and derive the state equations that will be needed for subsequent simulation study as well as analysis of the nonlinear phenomena of parallel-connected converters. Specifically, we will focus on the buck converter, which is a second-order circuit comprising an inductor, a diode, a switch and a load resistance connected in parallel with a capacitor. Figure 4.3 shows two buck converters connected in parallel. The presence of four switches (S_1, S_2, D_1 and D_2) allows a total of sixteen possible switch states, and in each switch state the circuit is a linear third-order circuit.

When the converters are operating in the continuous conduction mode, diode D_i is always in complementary state to switch S_i, for $i = 1, 2$. That is, when S_i is on, D_i is off, and vice versa. Hence, only four switch states are possible during a switching cycle, namely, (i) S_1 and S_2 are on; (ii) S_1 is on and S_2 is off; (iii) S_1 is off and S_2 is on; (iv) S_1 and S_2 are off. The state equations corresponding to

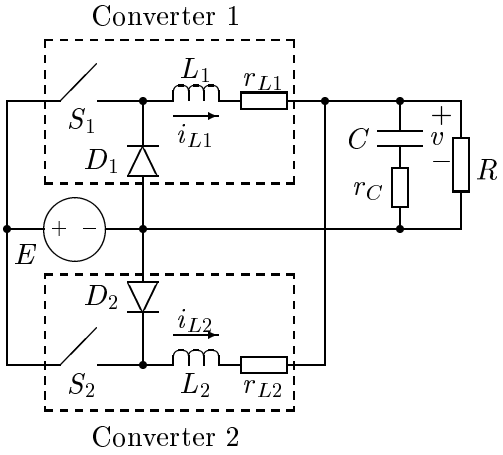

Figure 4.3: Two parallel-connected buck converters.

these switch states are generally given by

$$\begin{aligned} \dot{x} &= A_1 x + B_1 E \qquad \text{for } S_1 \text{ and } S_2 \text{ on} \\ \dot{x} &= A_2 x + B_2 E \qquad \text{for } S_1 \text{ on and } S_2 \text{ off} \\ \dot{x} &= A_3 x + B_3 E \qquad \text{for } S_1 \text{ off and } S_2 \text{ on} \\ \dot{x} &= A_4 x + B_4 E \qquad \text{for } S_1 \text{ and } S_2 \text{ off,} \end{aligned} \tag{4.4}$$

where E is the input voltage, x is the state vector defined as

$$x = [v \;\; i_1 \;\; i_2]^T , \tag{4.5}$$

and the A's and B's for the case of two buck converters are given by

$$\begin{aligned} A_1 &= A_2 = A_3 = A_4 \\ &= \begin{bmatrix} -\dfrac{1}{C(R+r_C)} & \dfrac{R}{C(R+r_C)} & \dfrac{R}{C(R+r_C)} \\ -\dfrac{R}{L_1(R+r_C)} & -\dfrac{1}{L_1}\left(\dfrac{r_C R}{R+r_C} + r_{L1}\right) & -\dfrac{1}{L_1}\left(\dfrac{r_C R}{R+r_C}\right) \\ -\dfrac{R}{L_2(R+r_C)} & -\dfrac{1}{L_2}\left(\dfrac{r_C R}{R+r_C}\right) & -\dfrac{1}{L_2}\left(\dfrac{r_C R}{R+r_C} + r_{L2}\right) \end{bmatrix}, \end{aligned} \tag{4.6}$$

$$B_1 = \begin{bmatrix} 0 \\ \dfrac{1}{L_1} \\ \dfrac{1}{L_2} \end{bmatrix}, \; B_2 = \begin{bmatrix} 0 \\ \dfrac{1}{L_1} \\ 0 \end{bmatrix}, \; B_3 = \begin{bmatrix} 0 \\ 0 \\ \dfrac{1}{L_2} \end{bmatrix}, \; B_4 = \begin{bmatrix} 0 \\ 0 \\ 0 \end{bmatrix}. \tag{4.7}$$

It is worth noting that the sequence of switch states, in general, takes the order as written in (4.4), i.e., starting with "S_1 and S_2 on" and ending with "S_1 and S_2 off" in a switching cycle. However, either "S_1 on S_2 off" or "S_1 off S_2 on" (not both) goes in the middle, depending upon the duty cycles of S_1 and S_2. In the case where S_1 has a larger duty cycle, we should omit the third equation in (4.4), and likewise for the case where S_2 has a larger duty cycle. This should be taken care of in the simulation and analysis.

4.4 Selected Bifurcation Phenomena by Computer Simulations

We now begin our investigation with computer simulations. Since we are primarily concerned with system stability in conjunction with the feedback design, we focus our attention on the effects of varying the various gains on the bifurcation behaviour of the system. In particular, the gains K_{v1}, K_{v2}, K_i and m present themselves as design parameters that can be changed at will. We will henceforth focus on variation of these parameters.

Our simulation is based on the exact state equations derived in Section 4.3. Essentially, for each set of parameter values, time-domain cycle-by-cycle waveforms are generated by solving the appropriate linear equation in any sub-interval of time, according to the states of the switches which are determined from values of the control voltages v_{con1} and v_{con2}. Sampled data are then collected at $t = nT$ in the steady state. With sufficient number of sets of steady-state data, we can construct the bifurcation diagrams as required. Our computer program automatically organizes bifurcation diagrams from time-domain waveforms. The circuit parameters used in our simulations are shown in Table 4.1.

A large number of bifurcation diagrams have been obtained. In the following, only representative bifurcation diagrams are shown, which serve to exemplify the main findings concerning the bifurcation behaviour of a system of parallel buck converters under a master-slave sharing scheme.

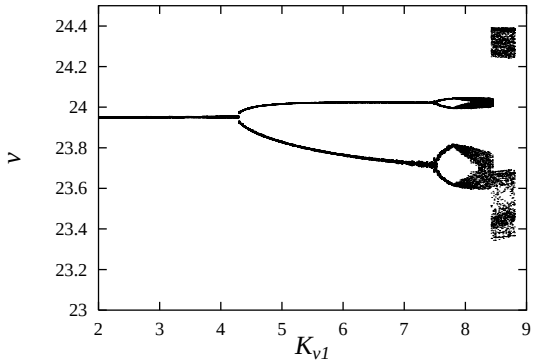

Figure 4.4: Bifurcation diagram with K_{v1} as bifurcation parameter ($K_{v2} = 4$, $K_i = 5$ and $m = 1$), first period-doubling occurs when $K_{v1} = 4.47$.

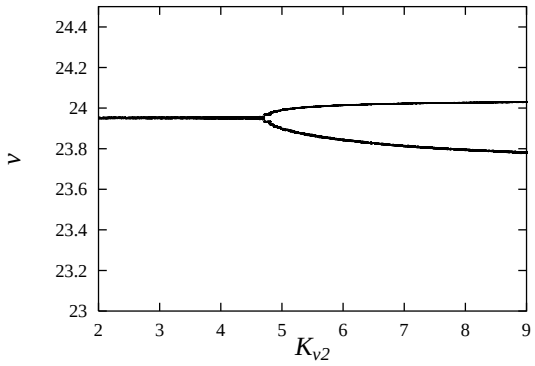

Figure 4.5: Bifurcation diagram with K_{v2} as bifurcation parameter ($K_{v1} = 4$, $K_i = 5$ and $m = 1$), first period-doubling occurs when $K_{v2} = 4.85$.

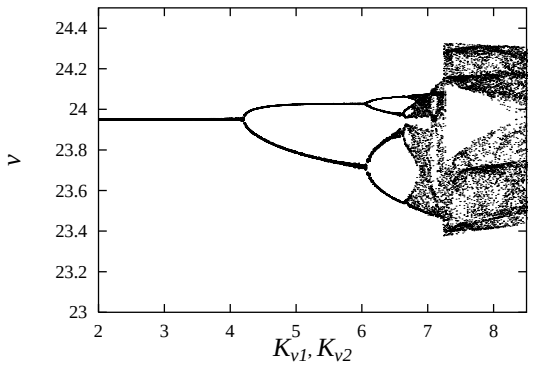

Figure 4.6: Bifurcation diagram with K_{v1} and K_{v2} as bifurcation parameters varying simultaneously ($K_i = 5$, $m = 1$).

Circuit Components	Values
Switching Period T	400μs
Input Voltage E	48V
Output Voltage v	24V
Offset Voltage V_{offset}	5V
Inductance L_1, ESR r_{L1}	0.02H, 0.05Ω
Inductance L_2, ESR r_{L2}	0.04H, 0.2Ω
Capacitance C, ESR r_C	47μF, 0.01Ω
Load Resistance R	10Ω

Table 4.1: Component values and steady-state voltages used in simulation. ESR stands for Equivalent Series Resistance.

4.4.1 Voltage Feedback Gains as Bifurcation Parameters

We first keep K_{v2} constant and vary K_{v1}. The bifurcation diagram, as shown in Fig. 4.4, shows period-doublings to chaos. Next, we keep K_{v1} constant and vary K_{v2}. The bifurcation diagram, as shown in Fig. 4.5, again manifests a period-doubling bifurcation. Finally, we vary K_{v1} and K_{v2} simultaneously, and the corresponding bifurcation diagram is shown in Fig. 4.6. Again, period-doubling bifurcations are observed.

Remarks — The occurrence of period-doubling bifurcations generally agrees with previous findings for the buck converter. Intuitively speaking, if the two converters were identical, the system would reduce to a buck converter feeding a load. Thus, we may expect period-doubling to occur in the parallel system when the voltage feedback gain is varied, as it would occur likewise in a buck converter [14], [15]. We will present detailed analysis in Section 4.6.

4.4.2 Current Gain as Bifurcation Parameter

In studying the bifurcation behaviour in respect of current gain variation, we keep m, K_{v1} and K_{v2} constant, and vary K_i. It is found that the system remains in stable period-1 operation irrespective of the choice of K_i. Basically, K_i only determines how close the slave follows the master. The larger the K_i is, the closer the slave's output current is to the master's.

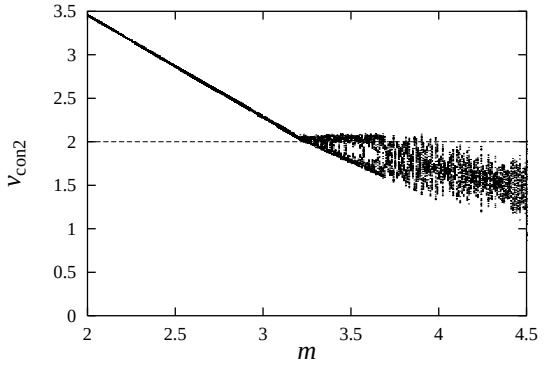

Figure 4.7: Bifurcation diagram with current sharing ratio m as bifurcation parameter ($K_{v1} = 3.5$, $K_{v2} = 3.5$, $K_i = 5$).

4.4.3 Current Sharing Ratio as Bifurcation Parameter

Our next computer investigation is performed for variation of the current sharing ratio m. This time, we fix K_{v1}, K_{v2} and K_i at suitable values such that the system is in stable operation. We then vary m and collect bifurcation diagrams, which look typically as the one shown in Fig. 4.7.

In this type of bifurcation, the stable operation suddenly gives way to chaos. The origin of such a bifurcation is the non-smooth operation of the system near the bifurcation point, which has been studied extensively by Nusse, Ott and Yorke [108] who coined such bifurcation as *border collision* bifurcation, and also by Banerjee *et al.* [24], [25]. To probe further into this bifurcation, we examine the time-domain waveforms of the control voltages v_{con1} and v_{con2} and see how they cross the ramp in the process of generating the PWM signals.

In normal operation, v_{con1} and v_{con2} hit the ramp once per switching cycle, as shown in Fig. 4.9 (a), and the corresponding inductor waveforms are shown in Fig. 4.9 (b). Now, if we increase m and take a close look at the waveform, we observe the following qualitative change near the point of the border collision bifurcation.

- Before border collision — When v_{con2} is slightly larger than V_L, normal operation is maintained, as shown in Fig. 4.10 (a).
- After border collision — When v_{con2} falls below V_L, it fails to hit the ramp. Stable operation is lost and the system bifurcates to chaos. Figure 4.10 (b) shows the waveform just after the bifurcation.

The above bifurcation, which has not been observed previously for parallel converter systems, indicates that stable operation of such systems require keeping m below a certain value. In Section 4.7, we will analyze the condition under which this bifurcation occurs.

4.5 Experimental Verification

Using the parameter values listed in Table 4.1, we build a circuit to verify our simulation results. As we increase K_{v1}, K_{v2} or both, we get results which are in good agreement with our simulations. In our experiments, period-doubling bifurcation takes place at approximately the same location as it does in our simulations. Bifurcation diagrams are captured when we increase K_{v1}, K_{v2} or both. Figure 4.8 (a) shows the bifurcation diagram when K_{v1} is increased. Figure 4.8 (b) shows the bifurcation diagram when K_{v2} is increased. Figure 4.8 (c) shows the bifurcation diagram when both K_{v1} and K_{v2} are increased simultaneously.

4.6 Analysis of Period-doubling Bifurcation

From the foregoing simulation and experimental studies, we have identified period-doubling bifurcation in a system of parallel buck converters when the voltage feedback gains are varied. We have also seen how stability suddenly gives way to chaos when the current sharing ratio is increased. In this and the next sections we analyze these bifurcations in terms of a suitable discrete-time model [27]. We will first derive the model, and examine the Jacobian matrix and the way the system loses stability.

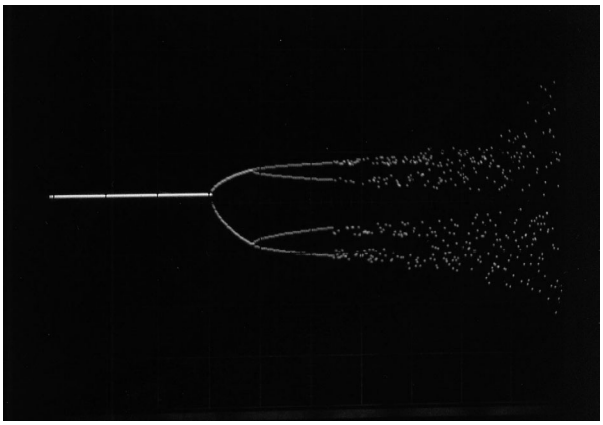

(a)

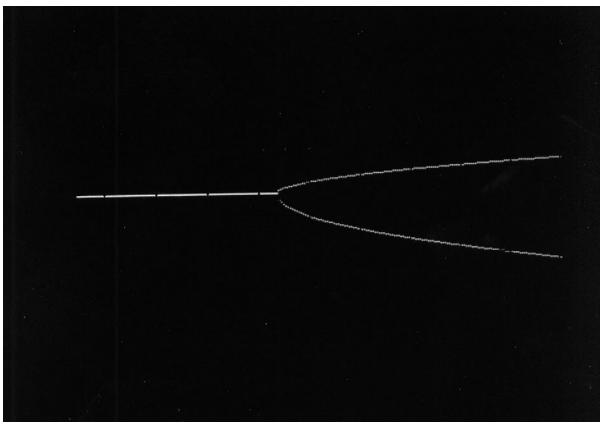

(b)

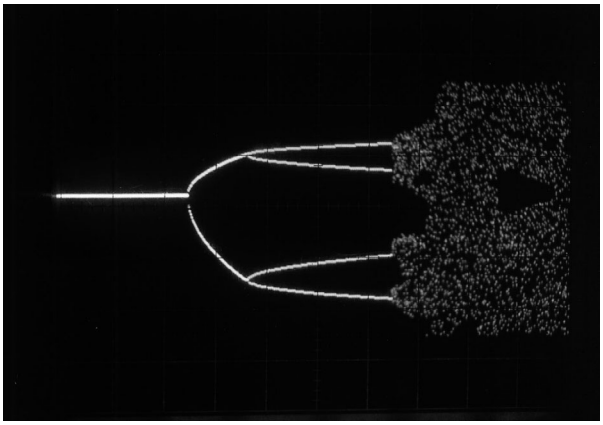

(c)

Figure 4.8: (a) Bifurcation diagram when K_{v1} is increased; (b) bifurcation diagram when K_{v2} is increased; (c) bifurcation diagram when both K_{v1} and K_{v2} are increased simultaneously. (Vertical scale: 0.2V/div.)

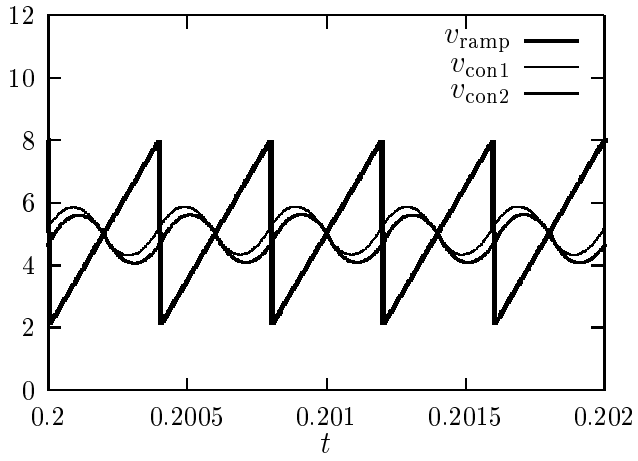

(a)

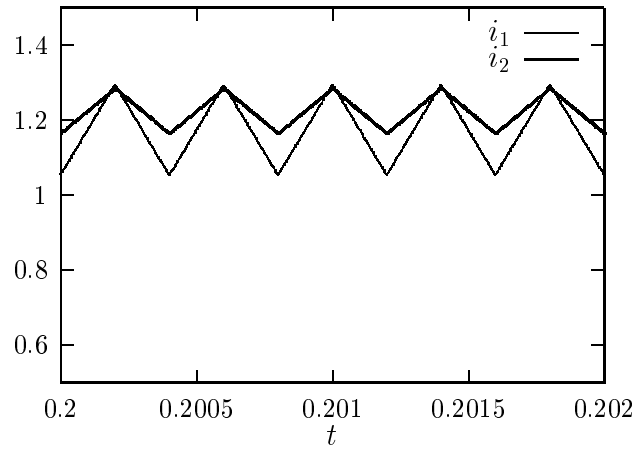

(b)

Figure 4.9: Stable period-1 operation. (a) Control voltages and ramp; (b) inductor currents.

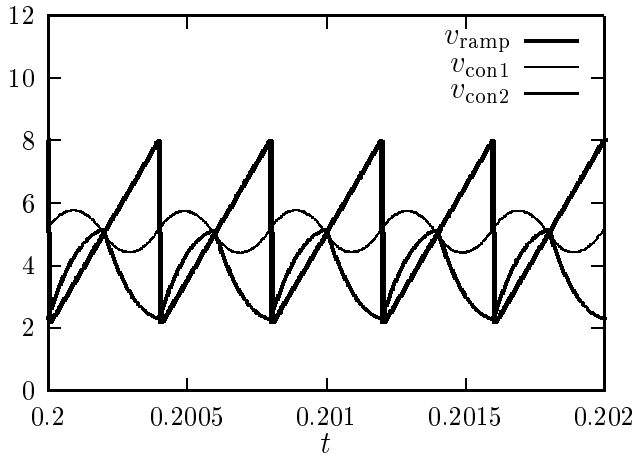

(a)

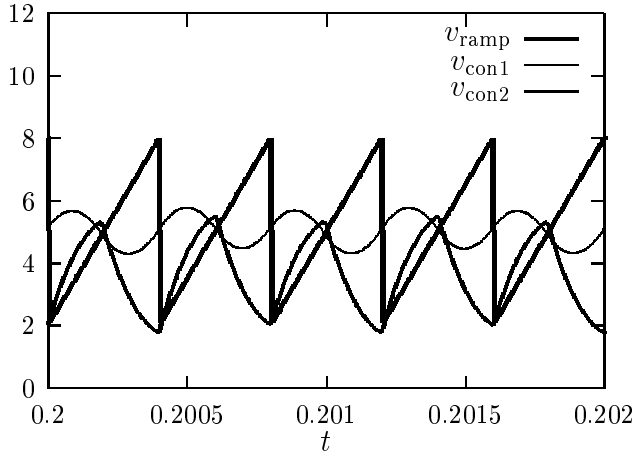

(b)

Figure 4.10: Control voltage waveforms (a) just before border collision bifurcation ($m = 3$); and (b) just after border collision bifurcation ($m = 3.5$).

4.6.1 Derivation of the Discrete-time Map

Our purpose in this subsection is to derive a discrete-time map that describes the dynamics of a system of two buck converters connected in parallel, as defined earlier in Section 4.3 (see Fig. 4.3), in the neighborhood of the T-periodic steady state. We let x be the state variables as defined previously, and further let d_1 and d_2 be the duty cycle of Converter 1 (master) and Converter 2 (slave), respectively. The discrete-time map that we aim to find takes the following form:

$$x_{n+1} = f(x_n, d_{1,n}, d_{2,n}), \tag{4.8}$$

where subscript n denotes the value at the beginning of the nth cycle, i.e., $x_n = x(nT)$. For the closed-loop system, we need also to find the feedback equations that relate $d_{1,n}$ and $d_{2,n}$ to x_n.

The state equations are given in (4.4) for different switch states. The order in which the system toggles between the switch states depends on d_1 and d_2. Thus, we need to assume that $d_2 > d_1$ in the neighbourhood of the T-periodic state, or otherwise, in order to derive the discrete-time model. In particular, the assumption $d_2 > d_1$ is consistent with our simulation study since r_{L1} has a lower value than r_{L2}. Note that such an assumption loses no generality.

Recall that if $d_2 > d_1$, the state "S_1 on and S_2 off" should be omitted. Hence, we have three switch states:

1. For $nT < t \leq nT + d_{1,n}T$, both S_1 and S_2 are turned on.
2. For $nT + d_{1,n}T < t \leq nT + d_{2,n}T$, S_1 is turned off and S_2 remains on.
3. For $nT + d_{2,n}T < t \leq (n+1)T$, both S_1 and S_2 are off.

In each switch state, the describing state equation is $\dot{x} = A_j x + B_j E$, where $j = 1, 3, 4$. (Note that $j = 2$ does not appear here.) For each state equation we can derive the solution, and by stacking up the solutions, x_{n+1} can be expressed in terms of x_n, $d_{1,n}$ and $d_{2,n}$, i.e.,

$$\begin{aligned} x_{n+1} \;=\; & \Phi_4((1-d_{2,n})T)\Phi_3((d_{2,n}-d_{1,n})T)\Phi_1(d_{1,n}T)x_n \\ & +\Phi_4((1-d_{2,n})T)\Phi_3((d_{2,n}-d_{1,n})T)(\Phi_1(d_{1,n}T)-\mathbf{1})A_1^{-1}B_1E \\ & +\Phi_4((1-d_{2,n})T)(\Phi_3((d_{2,n}-d_{1,n})T)-\mathbf{1})A_3^{-1}B_3E \\ & +(\Phi_4((1-d_{2,n})T)-\mathbf{1})A_4^{-1}B_4E, \end{aligned} \tag{4.9}$$

where $\mathbf{1}$ is the identity matrix, and $\Phi_j(\xi)$ is the transition matrix corresponding

to A_j and is given by

$$\Phi_j(\xi) = e^{A_j\xi} = \mathbf{1} + \sum_{k=1}^{\infty} \frac{1}{k!} A_j^k \xi^k, \quad \text{for} \quad j = 1, 2, 3, 4. \tag{4.10}$$

For parallel-connected buck converters, we let $A = A_1 = A_2 = A_3 = A_4$ and $\Phi(\xi) = \Phi_1(\xi) = \Phi_2(\xi) = \Phi_3(\xi) = \Phi_4(\xi)$. Hence, (4.9) can be written as

$$\begin{aligned} x_{n+1} &= \Phi(T)x_n + \Phi(T)A^{-1}B_1E + \Phi((1-d_{1,n})T)A^{-1}(B_3 - B_1)E \\ &\quad + \Phi((1-d_{2,n})T)A^{-1}(B_4 - B_3)E - A^{-1}B_4E. \end{aligned} \tag{4.11}$$

Our next step is to find the feedback relations that connect the duty cycles and the state variables. The control voltages v_{con1} and v_{con2}, as given before by (4.2) and (4.3), can be rewritten as

$$v_{\text{con1}} = U_1 + \kappa_1^T x \tag{4.12}$$

$$v_{\text{con2}} = U_2 + \kappa_2^T x, \tag{4.13}$$

where U_1 and U_2 are constants, and the gain vectors κ_1 and κ_2 are

$$\kappa_1^T = [-K_{v1}\ 0\ 0] \quad \text{and} \quad \kappa_2^T = [-K_{v2}\ K_i m\ -K_i]. \tag{4.14}$$

The ramp function can also be rewritten simply as

$$v_{\text{ramp}} = \alpha + \beta(t \bmod T), \tag{4.15}$$

where α and β are constants. To find the defining equations for the duty cycles, we first note that the switches are turned off when $v_{\text{con1}} = v_{\text{ramp}}$ and $v_{\text{con2}} = v_{\text{ramp}}$. Now, define $s_1(x_n, d_{1,n})$ and $s_2(x_n, d_{1,n}, d_{2,n})$ as

$$\begin{aligned} s_1(x_n, d_{1,n}) &\stackrel{\text{def}}{=} v_{\text{con1}} - v_{\text{ramp}} \\ &= U_1 + \kappa_1^T x(d_{1,n}T) - (\alpha + \beta d_{1,n}T) \\ &= U_1 + \kappa_1^T[\Phi(d_{1,n}T)x_n + (\Phi(d_{1,n}T) - \mathbf{1})A^{-1}B_1E] \\ &\quad -(\alpha + \beta d_{1,n}T), \end{aligned} \tag{4.16}$$

$$\begin{aligned} s_2(x_n, d_{1,n}, d_{2,n}) &\stackrel{\text{def}}{=} v_{\text{con2}} - v_{\text{ramp}} \\ &= U_2 + \kappa_2^T x(d_{2,n}T) - (\alpha + \beta d_{2,n}T) \\ &= U_2 + \kappa_2^T[\Phi(d_{2,n}T)x_n + \Phi(d_{2,n}T)A^{-1}B_1E \\ &\quad +\Phi((d_{2,n} - d_{1,n})T)A^{-1}(B_3 - B_1)E - A^{-1}B_3E] \\ &\quad -(\alpha + \beta d_{2,n}T). \end{aligned} \tag{4.17}$$

Thus, S_1 and S_2 are turned off, respectively, when

$$s_1(x_n, d_{1,n}) = 0 \tag{4.18}$$

and

$$s_2(x_n, d_{1,n}, d_{2,n}) = 0. \tag{4.19}$$

Solving (4.18) and (4.19), $d_{1,n}$ and $d_{2,n}$ can be obtained. Combining with (4.11), we have the discrete-time iterative map for the closed-loop system.

4.6.2 Derivation of the Jacobian

The Jacobian plays an important role in the study of dynamical systems [109]. The essence of using a Jacobian matrix in the analysis of dynamical systems lies in the capture of the dynamics in the small neighbourhood of an equilibrium point or orbit (stable or unstable). We will make use of this conventional method to examine the bifurcation phenomena in Section 4.6.3. But before we move on, we need to find the necessary expressions that enable the Jacobian to be computed.

Suppose the equilibrium point is given by $x(nT) = X_Q$. The Jacobian of the discrete-time map evaluated at the equilibrium point can be written as follows:

$$\begin{aligned} J(X_Q) &= \frac{\partial f}{\partial x_n} - \frac{\partial f}{\partial d_{1,n}}\left(\frac{\partial s_1}{\partial d_{1,n}}\right)^{-1}\left(\frac{\partial s_1}{\partial x_n}\right) \\ &\quad -\frac{\partial f}{\partial d_{2,n}}\left(\frac{\partial s_2}{\partial d_{2,n}}\right)^{-1}\left[\left(\frac{\partial s_2}{\partial x_n}\right) + \frac{\partial s_2}{\partial d_{1,n}}\left(\frac{\partial s_1}{\partial d_{1,n}}\right)^{-1}\left(\frac{\partial s_1}{\partial x_n}\right)\right]\Bigg|_{x_n = X_Q}, \end{aligned} \tag{4.20}$$

where

$$\frac{\partial f}{\partial x_n} = \begin{bmatrix} \frac{\partial f_1}{\partial v_n} & \frac{\partial f_1}{\partial i_{1,n}} & \frac{\partial f_1}{\partial i_{2,n}} \\ \frac{\partial f_2}{\partial v_n} & \frac{\partial f_2}{\partial i_{1,n}} & \frac{\partial f_2}{\partial i_{2,n}} \\ \frac{\partial f_3}{\partial v_n} & \frac{\partial f_3}{\partial i_{1,n}} & \frac{\partial f_3}{\partial i_{2,n}} \end{bmatrix}, \tag{4.21}$$

$$\frac{\partial f}{\partial d_{1,n}} = \begin{bmatrix} \frac{\partial f_1}{\partial d_{1,n}} & \frac{\partial f_2}{\partial d_{1,n}} & \frac{\partial f_3}{\partial d_{1,n}} \end{bmatrix}^T, \tag{4.22}$$

$$\frac{\partial s_1}{\partial x_n} = \begin{bmatrix} \frac{\partial s_1}{\partial v_n} & \frac{\partial s_1}{\partial i_{1,n}} & \frac{\partial s_1}{\partial i_{2,n}} \end{bmatrix}, \tag{4.23}$$

$$\frac{\partial f}{\partial d_{2,n}} = \begin{bmatrix} \frac{\partial f_1}{\partial d_{2,n}} & \frac{\partial f_2}{\partial d_{2,n}} & \frac{\partial f_3}{\partial d_{2,n}} \end{bmatrix}^T, \tag{4.24}$$

$$\frac{\partial s_2}{\partial x_n} = \begin{bmatrix} \frac{\partial s_2}{\partial v_n} & \frac{\partial s_2}{\partial i_{1,n}} & \frac{\partial s_2}{\partial i_{2,n}} \end{bmatrix}. \tag{4.25}$$

Using (4.16), (4.17) and (4.11), we can find all the derivatives in (4.20). First, $\partial f/\partial x_n$ can be found from (4.11), i.e.,

$$\frac{\partial f}{\partial x_n} = \Phi(T). \tag{4.26}$$

Also, a direct differentiation gives $\partial f/\partial d_{1,n}$ as

$$\frac{\partial f}{\partial d_{1,n}} = -T\Phi((1-d_{1,n})T)(B_3 - B_1)E. \tag{4.27}$$

Likewise, we get $\partial f/\partial d_{2,n}$ as

$$\frac{\partial f}{\partial d_{2,n}} = -T\Phi((1-d_{2,n})T)(B_4 - B_3)E. \tag{4.28}$$

From (4.16), we obtain $\partial s_1/\partial x_n$ readily as

$$\frac{\partial s_1}{\partial x_n} = \kappa_1^T \Phi(d_{1,n}T). \tag{4.29}$$

Again by a direct differentiation, we get

$$\begin{aligned}
\frac{\partial s_1}{\partial d_{1,n}} &= \kappa_1^T \frac{\partial \Phi(d_{1,n}T)}{\partial d_{1,n}} x_n + \kappa_1^T \frac{\partial (\Phi(d_{1,n}T) - \mathbf{1})A^{-1}B_1}{\partial d_{1,n}} E - \beta T \\
&= \kappa_1^T (AT\Phi(d_{1,n}T))x_n + \kappa_1^T (\Phi(d_{1,n}T)B_1 T)E - \beta T \\
&= T\kappa_1^T \Phi(d_{1,n}T)(Ax_n + B_1 E) - \beta T.
\end{aligned} \tag{4.30}$$

And from (4.17), we get

$$\frac{\partial s_2}{\partial x_n} = \kappa_2^T \Phi(d_{2,n}T). \tag{4.31}$$

Finally, we need to get $\partial s_2/\partial d_{2,n}$ and $\partial s_2/\partial d_{1,n}$. From (4.17) we have

$$\begin{aligned}
\frac{\partial s_2}{\partial d_{2,n}} &= \kappa_2^T \frac{\partial \Phi(d_{2,n}T)}{\partial d_{2,n}} x_n + \kappa_2^T \frac{\partial \Phi(d_{2,n}T)A^{-1}B_1}{\partial d_{2,n}} E \\
&\quad + \kappa_2^T \frac{\partial \Phi((d_{2,n} - d_{1,n})T)A^{-1}(B_3 - B_1)}{\partial d_{2,n}} E - \beta T \\
&= \kappa_2^T (AT\Phi(d_{2,n}T)x_n + \kappa_2^T (\Phi(d_{2,n}T)B_1 T)E \\
&\quad + \kappa_2^T \Phi((d_{2,n} - d_{1,n})T)(B_3 - B_1)TE - \beta T \\
&= T\kappa_2^T \Phi(d_{2,n}T)(Ax_n + B_1 E) + T\kappa_2^T \Phi((d_{2,n} - d_{1,n})T)(B_3 - B_1)E - \beta T.
\end{aligned} \tag{4.32}$$

and

$$\begin{aligned}
\frac{\partial s_2}{\partial d_{1,n}} &= \kappa_2^T \frac{\partial \Phi((d_{2,n} - d_{1,n})T)A^{-1}(B_3 - B_1)E}{\partial d_{1,n}} \\
&= -T\kappa_2^T \Phi((d_{2,n} - d_{1,n})T)(B_3 - B_1)E.
\end{aligned} \tag{4.33}$$

Now, putting all the derivatives into (4.20) gives

$$\begin{aligned}
J(X_Q) &= \Phi(T) - \frac{-\Phi((1-d_{1,n})T)(B_3 - B_1)E\kappa_1^T \Phi(d_{1,n}T)}{\kappa_1^T \Phi(d_{1,n}T)(Ax_n + B_1 E) - \beta} \\
&\quad - \frac{-\Phi((1-d_{2,n})T)(B_4 - B_3)E\left[\kappa_2^T \Phi(d_{2,n}T) + \frac{-\kappa_2^T \Phi((d_{2,n}-d_{1,n})T)(B_3 - B_1)E\kappa_1^T \Phi(d_{1,n}T)}{\kappa_1^T \Phi(d_{1,n}T)(Ax_n + B_1 E) - \beta}\right]}{\kappa_2^T \Phi(d_{2,n}T)(Ax_n + B_1 E) + \kappa_2^T \Phi((d_{2,n} - d_{1,n})T)(B_3 - B_1)E - \beta}.
\end{aligned} \tag{4.34}$$

Numerical algorithms can now be developed for computing $J(X_Q)$ and, hence, the characteristic multipliers. This is further discussed in the next subsection.

4.6.3 Characteristic Multipliers and Period-doubling Bifurcation

The Jacobian derived in the foregoing subsection provides a means to evaluate the dynamics of the system. We will, in particular, study the loci of the characteristic multipliers (also called eigenvalues), the aim being to find out possible bifurcation scenarios as the voltage feedback gains are varied. To find the characteristic multipliers, we solve the following polynomial equation in λ, whose roots actually give the characteristic multipliers:

$$\det[\lambda \mathbf{1} - J(X_Q)] = 0, \tag{4.35}$$

where $J(X_Q)$ is the Jacobian found previously. We will pay attention to the movement of the characteristic multipliers as K_{v1} and K_{v2} are varied. Any crossing from the interior of the unit circle to the exterior indicates a possible bifurcation. In particular, if a real characteristic multiplier goes through -1, as it moves out of the unit circle, a period-doubling occurs.

Using (4.34), we can generate loci of characteristic multipliers numerically. Since we are interested here in varying K_{v1} and K_{v2}, we keep $m = 1$, thereby ensuring that the system is remote from any border collision due possibly to large m, as we have seen previously in the simulation. The parameter values of the system are the same as in Tables 4.2 and 4.3 and in Figs. 4.4 and 4.5. To maintain conciseness, we exemplify here the typical loci shown in Tables 4.2 and 4.3, which are graphically illustrated in Figs. 4.11 and 4.12. Both loci indicate a period-doubling bifurcation as K_{v1} and K_{v2} vary. This agrees with our simulation results in Section 4.4.

K_{v1}	Char. Mult.	Remarks
3.00	-0.542$\pm$ j0.363, 0.998	Stable 1T
3.50	-0.608$\pm$ j0.236, 0.998	Stable 1T
3.80	-0.643$\pm$ j0.106, 0.998	Stable 1T
3.85	-0.649, -0.649, 0.998	Stable 1T
4.00	-0.801, -0.531, 0.998	Stable 1T
4.20	-0.903, -0.471, 0.998	Stable 1T
4.40	-0.981, -0.433, 0.998	Stable 1T
4.47	-1.000, -0.425, 0.998	Period-doubling

Table 4.2: Characteristic multipliers for different values of K_{v1}.

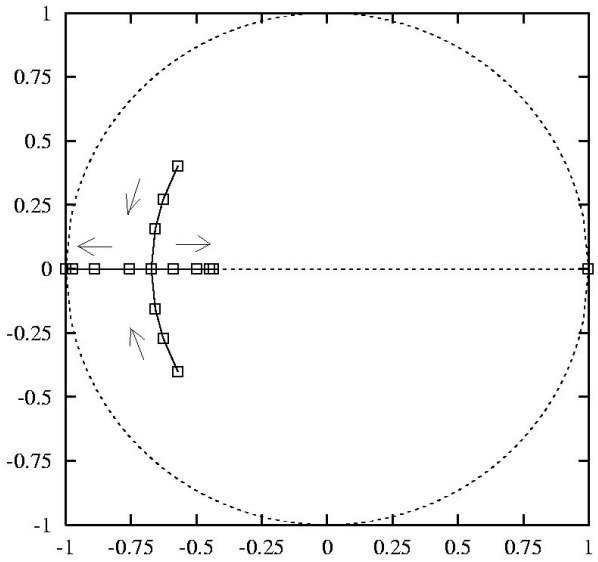

Figure 4.11: Loci of characteristic multipliers as K_{v1} varies. Arrows indicate increasing K_{v1}.

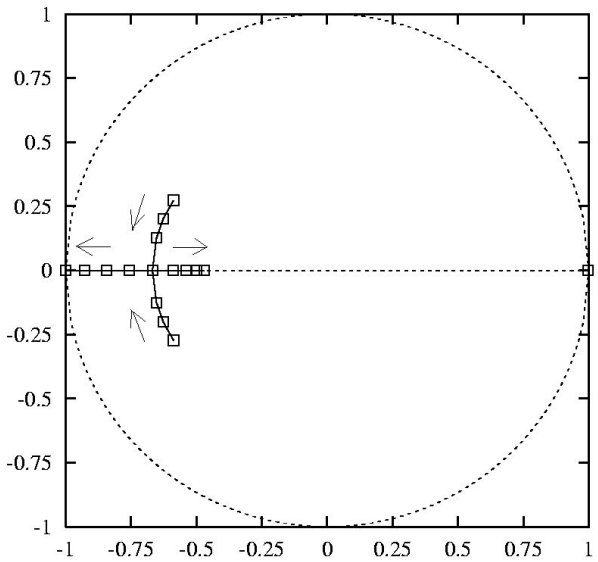

Figure 4.12: Loci of characteristic multipliers as K_{v2} varies. Arrows indicate increasing K_{v2}.

K_{v2}	Char. Mult.	Remarks
3.00	-0.604$\pm$ j0.246, 0.998	Stable 1T
3.40	-0.631$\pm$ j0.166, 0.998	Stable 1T
3.60	-0.643$\pm$ j0.109, 0.998	Stable 1T
3.70	-0.649, -0.649, 0.998	Stable 1T
4.00	-0.801, -0.531, 0.998	Stable 1T
4.20	-0.856, -0.497, 0.998	Stable 1T
4.50	-0.921, -0.461, 0.998	Stable 1T
4.85	-1.000, -0.426, 0.998	Period-doubling

Table 4.3: Characteristic multipliers for different values of K_{v2}.

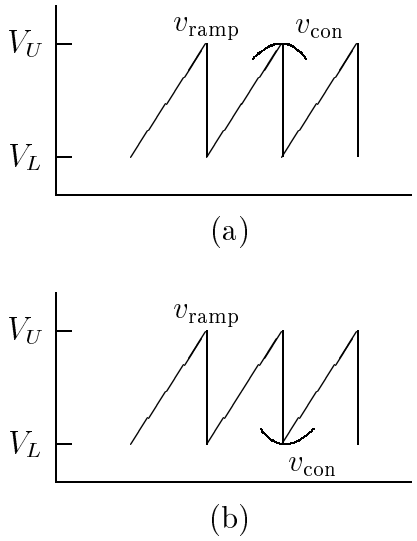

Figure 4.13: The two possible border collision scenarios.

4.7 Analysis of Border Collision Bifurcation with Respect to Variation of Current Sharing Ratio

As observed in the simulation, a border collision bifurcation occurs when m increases beyond a certain limit. In this section, we attempt to analyze this border collision and specifically to find the limit of m below which the system maintains stable operation. In the following study, we assume that K_{v1} and K_{v2} are kept within the stable range, so that the system is remote from any period-doubling bifurcation due possibly to large values of K_{v1} and K_{v2}.

Inspection of the loci of the characteristic multipliers reveals that a sudden "jump" occurs as m increases, which is typical of border collision bifurcation [24],

[108]. Such a bifurcation arises when v_{con1} or v_{con2} begins to pass over or under the ramp without hitting it during the whole switching period. This situation is illustrated in Fig. 4.13. As m increases, the system traverses from one situation where v_{con1} and v_{con2} both hit the ramp, to another where v_{con1} or v_{con2} misses the ramp. Such a transition is *non-smooth* at the point where v_{con1} or v_{con2} just misses the ramp, and at this point, border collision bifurcation occurs.

By studying the expressions of v_{con1}, v_{con2} and v_{ramp}, we can estimate the critical value of m, at which border collision takes place. Ignoring the ripple, we have $v \approx V_{\text{ref}}$ in the steady state. Thus, (4.2) and (4.3) can be approximated by

$$v_{\text{con1}}(t) \approx V_{\text{offset}}, \tag{4.36}$$

$$v_{\text{con2}}(t) \approx V_{\text{offset}} - K_i[i_2(t) - mi_1(t)]. \tag{4.37}$$

Since V_{offset} is always set between V_L and V_U, v_{con1} will always hit the ramp during a switching cycle. We therefore need only to focus on $v_{\text{con2}}(nT)$. As mentioned before, we assume that $d_2 > d_1$ in the neighbourhood of T periodic state. Also, neglecting the middle period $(d_{2,n} - d_{1,n})T$ in the T periodic state, assuming $i_2(d_{1,n}T) \approx mi_1(d_{1,n}T)$, and neglecting ESR of inductors, we may express $i_1(nT)$ and $i_2(nT)$ as

$$i_1(nT) = i_1(d_{1,n}T) - \frac{v}{L_1}(1 - d_{1,n})T, \tag{4.38}$$

$$i_2(nT) = i_2(d_{1,n}T) - \frac{v}{L_2}(1 - d_{1,n})T. \tag{4.39}$$

Putting (4.38) and (4.39) in (4.37), we get

$$v_{\text{con2}}(nT) = V_{\text{offset}} - K_i v(1 - d_{1,n})T\left(\frac{m}{L_1} - \frac{1}{L_2}\right). \tag{4.40}$$

Now, we may substitute either $v_{\text{con2}}(nT) = V_L$ or $v_{\text{con2}}(nT) = V_U$ in (4.40) to obtain the critical value of m. In particular, putting $v_{\text{con2}}(nT) = V_L$ in (4.40) gives

$$m_{\text{crit}} = \left(\frac{V_{\text{offset}} - V_L}{K_i v(1 - d_{1,n})T} + \frac{1}{L_2}\right) L_1, \tag{4.41}$$

where m_{crit} is the critical value of m at which v_{con2} just hits V_L at $t = nT$. Furthermore, $v_{\text{con2}}(nT) = V_U$ gives a negative value for m, which is not possible, thus ruling out the possibility of a border collision with v_{con2} hitting V_U.

Using the same set of parameter values and voltages as in Section 4.4.3, we find that $m_{\text{crit}} = 3.0$, which agrees very well with the bifurcation diagram shown in Fig. 4.7.

The above result clearly illustrates that the current sharing ratio m in a master-slave controlled parallel converter system must be kept below a certain value in order to ensure stable operation.

4.8 Conclusion

Despite the popularity of parallel converter systems in power electronics applications, their bifurcation phenomena are rarely studied. This chapter reports some selected bifurcation phenomena in a parallel system of two buck converters, which share current under a master-slave control scheme. The study of stability is a complex issue in this type of system [70], [107]. This chapter focuses on the effects of variation of some voltage feedback gains and current sharing ratio. It has been found that period-doubling bifurcations are possible when voltage feedback gains are varied, and that a border collision bifurcation is also possible when the current sharing ratio is varied. These results are useful for practical design of parallel converter systems to ensure stable period-1 operation in the expected stable region.

Chapter 5

Bifurcation in Parallel-connected Boost Converters

5.1 Introduction

In the previous chapter, some bifurcation behaviours of parallel-connected buck converters under the master-slave current sharing scheme were reported. In this chapter, we employ similar approaches to study a system of parallel-connected boost converters under the same master-slave current sharing scheme. We study the bifurcation behaviour, beginning with a series of computer simulations and experimental measurements. Finally, we analyze the system using the same discrete-time approach as in the previous chapter.

5.2 State Equations for Two Parallel Boost Converters

We begin our study by deriving the state equations for the system of parallel-connected boost converters shown in Fig. 5.1. These state equations will be needed for subsequent simulation study as well as analysis of the nonlinear phenomena of parallel-connected converters. Specifically, we will focus on the boost converter which is a second-order circuit comprising an inductor, a switch, a diode and a load resistance connected in parallel with a capacitor. The presence of four switches (S_1, S_2, D_1 and D_2) allows a total of sixteen possible switch states, and in each switch state the circuit is a linear third-order circuit.

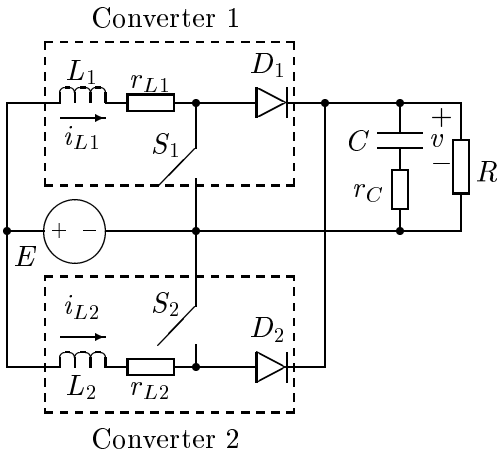

Figure 5.1: Two parallel-connected boost converters.

When the converters are operating in continuous conduction mode, diode D_i is always in complementary state to switch S_i, for $i = 1, 2$. That is, when S_i is on, D_i is off, and vice versa. Hence, only four switch states are possible during a switching cycle, namely, (i) S_1 and S_2 are on; (ii) S_1 is on and S_2 is off; (iii) S_1 is off and S_2 is on; (iv) S_1 and S_2 are off. The state equations corresponding to these switch states are given by

$$\begin{array}{ll} \dot{x} = A_1 x + B_1 E & \text{for } S_1 \text{ and } S_2 \text{ on} \\ \dot{x} = A_2 x + B_2 E & \text{for } S_1 \text{ on and } S_2 \text{ off} \\ \dot{x} = A_3 x + B_3 E & \text{for } S_1 \text{ off and } S_2 \text{ on} \\ \dot{x} = A_4 x + B_4 E & \text{for } S_1 \text{ and } S_2 \text{ off,} \end{array} \tag{5.1}$$

where E is the input voltage, x is the state vector defined as

$$x = [v \;\; i_1 \;\; i_2]^T , \tag{5.2}$$

and the A's and B's are given by

$$A_1 = \begin{bmatrix} -\dfrac{1}{C(R+r_C)} & 0 & 0 \\ 0 & -\dfrac{r_{L1}}{L_1} & 0 \\ 0 & 0 & -\dfrac{r_{L2}}{L_2} \end{bmatrix}, \tag{5.3}$$

$$A_2 = \begin{bmatrix} -\dfrac{1}{C(R+r_C)} & 0 & \dfrac{R}{C(R+r_C)} \\ 0 & -\dfrac{r_{L1}}{L_1} & 0 \\ -\dfrac{R}{L_2(R+r_C)} & 0 & -\dfrac{1}{L_2}\left(\dfrac{r_C R}{R+r_C} + r_{L2}\right) \end{bmatrix}, \tag{5.4}$$

$$A_3 = \begin{bmatrix} -\frac{1}{C(R+r_C)} & \frac{R}{C(R+r_C)} & 0 \\ -\frac{R}{L_1(R+r_C)} & -\frac{1}{L_1}(\frac{r_C R}{R+r_C}+r_{L1}) & 0 \\ 0 & 0 & -\frac{r_{L2}}{L_2} \end{bmatrix}, \tag{5.5}$$

$$A_4 = \begin{bmatrix} -\frac{1}{C(R+r_C)} & \frac{R}{C(R+r_C)} & \frac{R}{C(R+r_C)} \\ -\frac{R}{L_1(R+r_C)} & -\frac{1}{L_1}(\frac{r_C R}{R+r_C}+r_{L1}) & 0 \\ -\frac{R}{L_2(R+r_C)} & 0 & -\frac{1}{L_2}(\frac{r_C R}{R+r_C}+r_{L2}) \end{bmatrix}, \tag{5.6}$$

$$B_1 = B_2 = B_3 = B_4 = \begin{bmatrix} 0 \\ \frac{1}{L_1} \\ \frac{1}{L_2} \end{bmatrix}. \tag{5.7}$$

It is worth noting that the sequence of switch states, in general, takes the order as written in (5.1), i.e., starting with "S_1 and S_2 on" and ending with "S_1 and S_2 off" in a switching cycle. However, either "S_1 on S_2 off" or "S_1 off S_2 on" (not both) goes in the middle, depending upon the duty cycles of S_1 and S_2. In the case where S_1 has a larger duty cycle, we should omit the third equation in (5.1), and likewise for the case where S_2 has a larger duty cycle. This should be taken care of in the simulation and analysis.

5.3 Selected Bifurcation Phenomena by Computer Simulations

We now begin our investigation with computer simulations. Since we are primarily concerned with system stability in conjunction with the feedback design, we focus our attention on the effects of varying the various gains on the bifurcation behaviour of the system. In particular, the gains K_{v1}, K_{v2}, K_i and m present themselves as design parameters that can be changed at will. We will henceforth focus on variation of these parameters.

Our simulation is based on the exact state equations derived in Section 5.2. Essentially, for each set of parameter values, time-domain cycle-by-cycle waveforms are generated by solving the appropriate linear equation in any sub-interval of time, according to the states of the switches which are determined from values of the control voltages v_{con1} and v_{con2}. Sampled data are then collected at $t = nT$ in the steady state. With sufficient number of sets of steady-state data,

we can construct the bifurcation diagrams as required. Our computer program automatically organizes bifurcation diagrams from time-domain waveforms. The circuit parameters used in our simulations are shown in Table 5.1.

Circuit Components	Values
Switching Period T	40μs
Input Voltage E	12V
Output Voltage v	24V
Inductance L_1, ESR r_{L1}	4mH, 0.05Ω
Inductance L_2, ESR r_{L2}	4mH, 0.2Ω
Capacitance C, ESR r_C	10μF, 0.01Ω
Load Resistance R	10Ω

Table 5.1: Component values and steady-state voltages used in simulation. ESR stands for Equivalent Series Resistance.

A large number of trajectories and bifurcation diagrams have been obtained. In the following, only representative bifurcation figures and diagrams are shown, which serve to exemplify the main findings concerning the bifurcation behaviour of a system of parallel boost converters under a master-slave sharing scheme.

5.3.1 Voltage Feedback Gains as Bifurcation Parameters

We first keep K_{v1} constant and vary K_{v2}. A bifurcation diagram is shown in Fig. 5.2 (a). The sequence of simulated trajectories, as shown in Figs. 5.2 (b), (c) and (e), reveals a typical Neimark-Sacker bifurcation in which a stable equilibrium state breaks down to quasi-periodic orbits and limit cycles. The corresponding stroboscopic maps showing a quasi-periodic orbit and a limit cycle are shown in Figs. 5.2 (d) and (f). Next, we keep K_{v2} constant and vary K_{v1}. Similar bifurcation diagram and trajectories are obtained. For brevity, they are not repeated here. We will present detailed analysis in Section 5.5.

5.3.2 Current Gain as Bifurcation Parameter

In studying the bifurcation behaviour in respect of current gain variation, we keep m, K_{v1} and K_{v2} constant, and vary K_i. It is found that the system remains in stable period-1 operation irrespective of the choice of K_i. Basically, K_i only determines how close the slave follows the master. The larger the K_i is, the closer the slave's output current is to the master's.

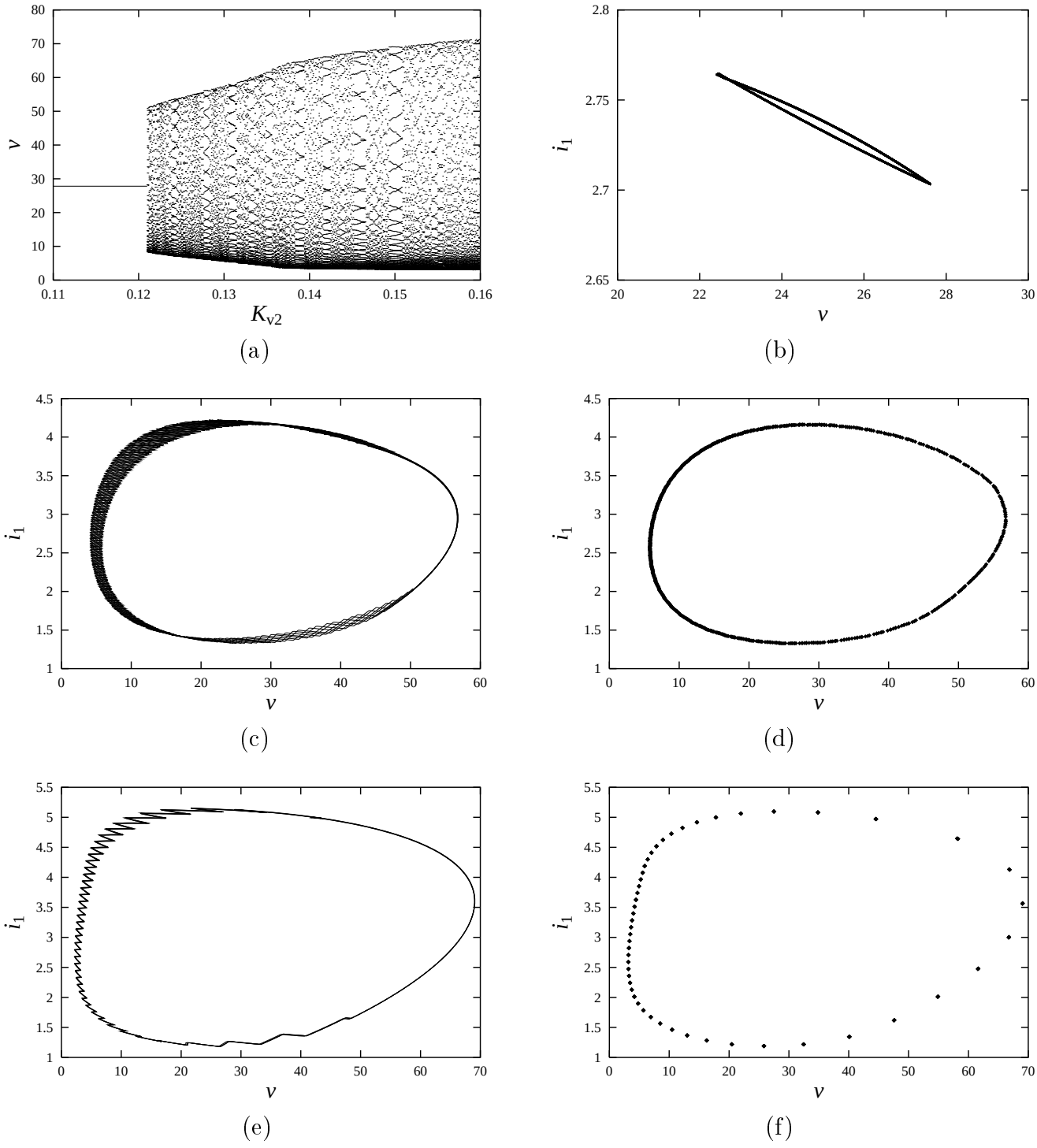

Figure 5.2: (a) Bifurcation diagram with K_{v2} as bifurcation parameter (K_{v1} = 0.11, K_i = 1 and m = 1); (b) stable period-1 orbit (K_{v1} = 0.11, K_{v2} = 0.11, K_i = 1 and m = 1); (c) quasi-periodic orbit (K_{v1} = 0.11, K_{v2} = 0.13, K_i = 1 and m = 1); (d) stroboscopic map of (c); (e) limit cycle (K_{v1} = 0.11, K_{v2} = 0.15, K_i = 1 and m = 1); (f) stroboscopic map of (e).

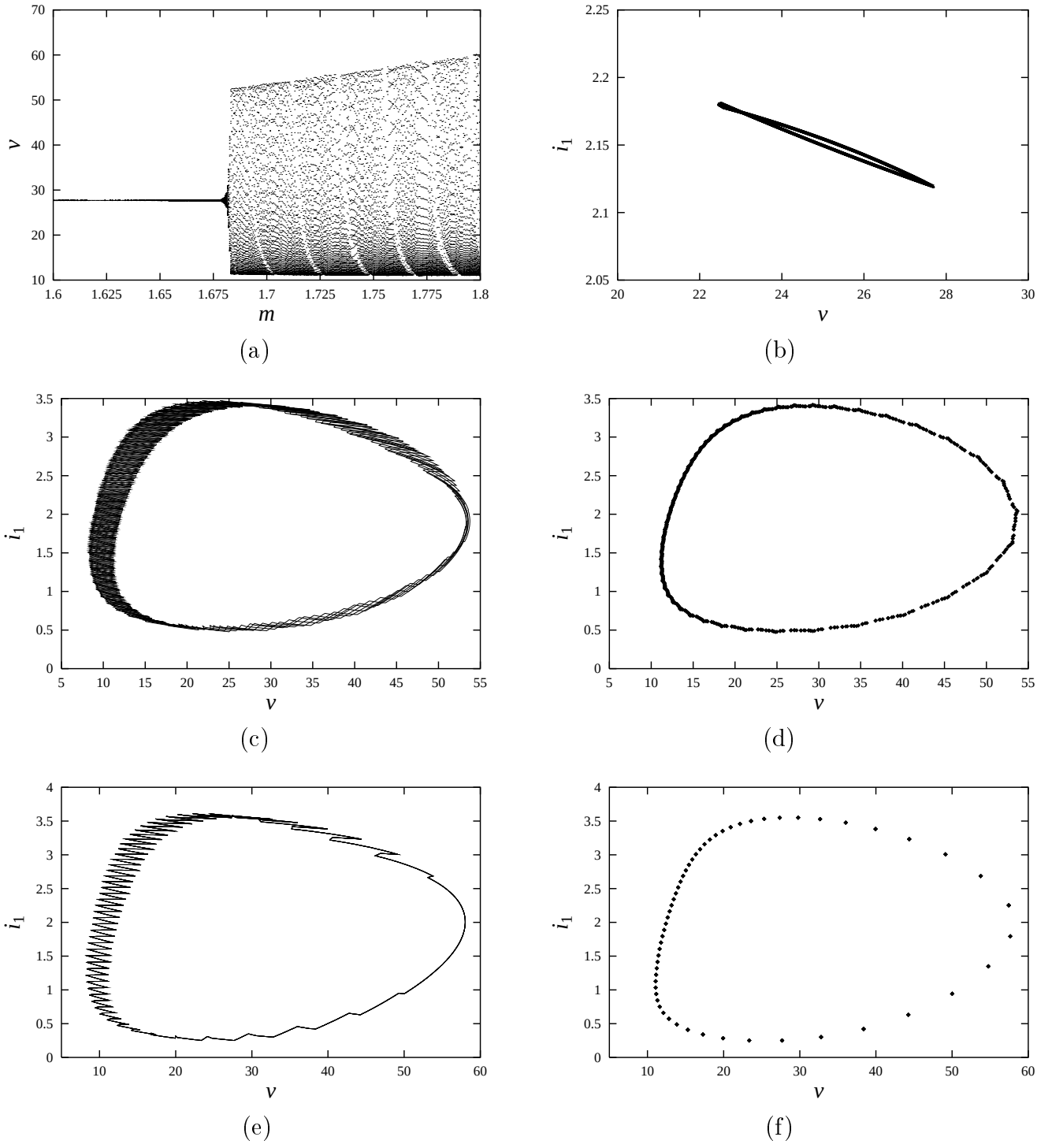

Figure 5.3: (a) Bifurcation diagram with m as bifurcation parameter ($K_{v1} = 0.1$, $K_{v2} = 0.1$ and $K_i = 1$); (b) stable period-1 orbit ($K_{v1} = 0.1$, $K_{v2} = 0.1$, $K_i = 1$ and $m = 1.60$); (c) quasi-periodic orbit ($K_{v1} = 0.1$, $K_{v2} = 0.1$, $K_i = 1$ and $m = 1.70$); (d) stroboscopic map of (c); (e) limit cycle ($K_{v1} = 0.1$, $K_{v2} = 0.1$, $K_i = 1$ and $m = 1.775$); (f) stroboscopic map of (e).

5.3.3 Current Sharing Ratio as Bifurcation Parameter

Our next computer investigation is performed for variation of the current sharing ratio m. This time, we fix K_{v1}, K_{v2} and K_i at suitable values such that the system is in stable operation. We vary m and find that the bifurcation is similar to that of varying K_{v1} or K_{v2}. A bifurcation diagram is shown in Fig. 5.3 (a). Trajectories are shown in Figs. 5.3 (b), (c) and (e) and the corresponding stroboscopic maps in Figs. 5.3 (d) and (f).

5.4 Experimental Verification

Using the parameter values listed in Table 5.1, we build a circuit to verify our simulation results. As we increase K_{v2} or m, we get results which are in good agreement with our simulations. In our experiments, Neimark-Sacker bifurcation takes place at approximately the same location as it does in our simulations. Trajectories of stable period-1 orbit, quasi-periodic orbit and limit cycle are captured, along with stroboscopic maps showing quasi-periodic orbits and limit cycles. In all the oscilloscope pictures, y-axis corresponds to i_1 and x-axis corresponds to v. Figures 5.4 (a)–(e) show the sequence of changes when we increase K_{v2}. Figure 5.4 (a) shows a stable period-1 orbit. Figure 5.4 (b) shows a quasi-periodic orbit and Fig. 5.4 (c) gives its the stroboscopic map. Figure 5.4 (d) shows a limit cycle and Fig. 5.4 (e) gives its the stroboscopic map. Similarly, Figs. 5.5 (a)–(e) show the sequence of changes when we increase m. Figure 5.5 (a) shows the stable period-1 orbit. Figure 5.5 (b) shows the quasi-periodic orbit and Fig. 5.5 (c) gives its the stroboscopic map. Figure 5.5 (d) shows the limit cycle and Fig. 5.5 (e) gives its the stroboscopic map.

5.5 Analysis of Neimark-Sacker Bifurcation

From the foregoing simulation and experimental studies, we have identified Neimark-Sacker bifurcation in a system of parallel boost converters when the voltage feedback gains are varied. We have also observed similar behaviour when the current sharing ratio is increased. In this and the next sections, we analyze this kind of bifurcation in terms of a suitable discrete-time model [27]. We first derive the model, then examine the Jacobian and the way the system loses stability.

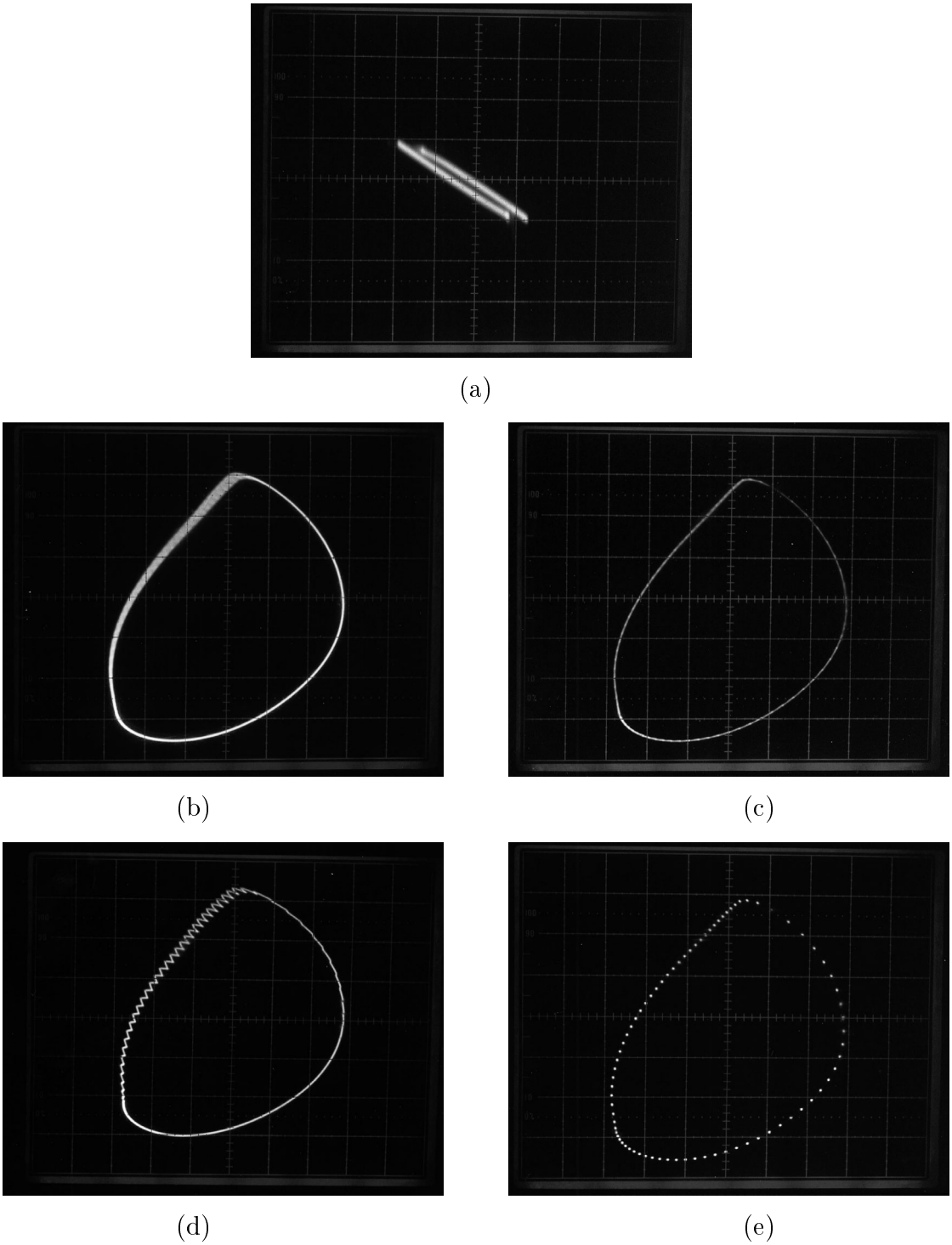

(a)

(b)

(c)

(d)

(e)

Figure 5.4: Sequence of changes observed experimentally when K_{v2} is increased. (a) Stable period-1 orbit; (b) quasi-periodic orbit; (c) stroboscopic map of (b); (d) limit cycle; (e) stroboscopic map of (d). (Horizontal scale: 5V/div, vertical scale: 0.04A/div for (a); horizontal scale: 10V/div, vertical scale: 0.4A/div for (b)—(e).)

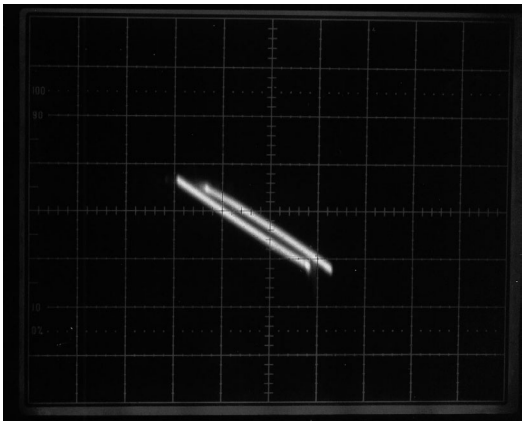

(a)

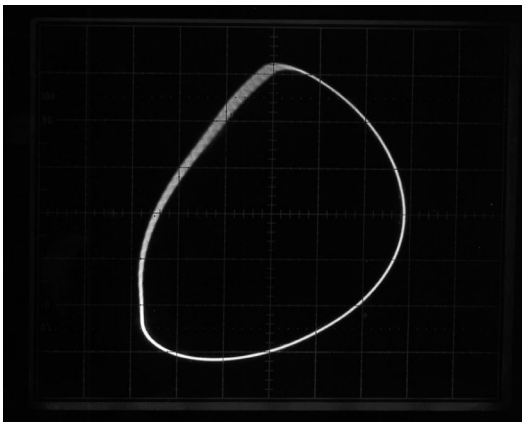

(b)

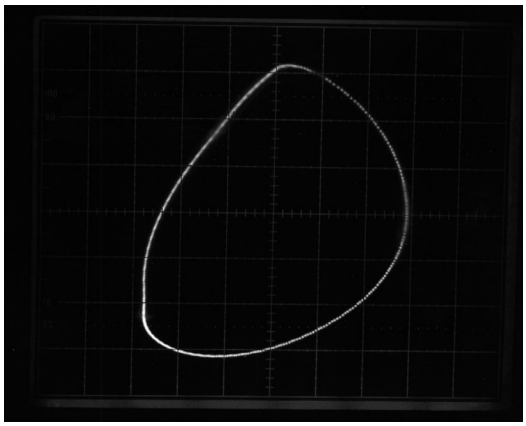

(c)

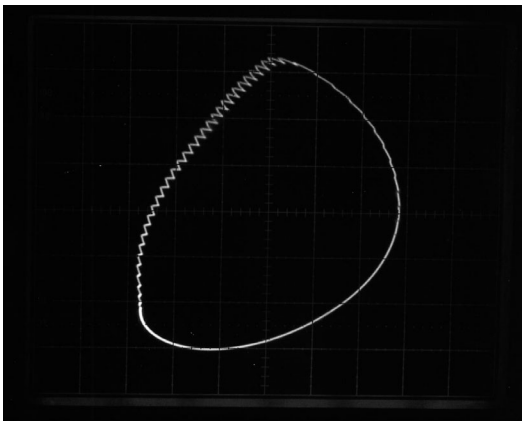

(d)

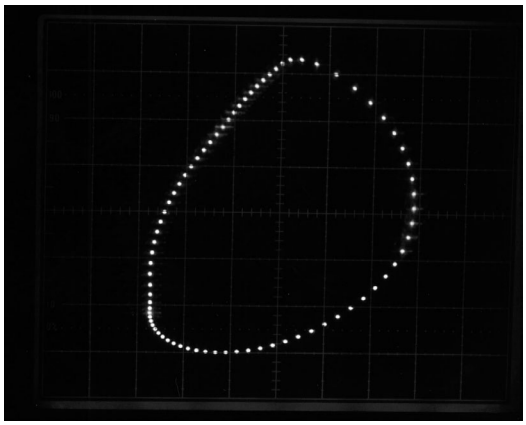

(e)

Figure 5.5: Sequence of changes observed experimentally when m is increased. (a) Stable period-1 orbit; (b) quasi-periodic orbit; (c) stroboscopic map of (b); (d) limit cycle; (e) stroboscopic map of (d). (Horizontal scale: 5V/div, vertical scale: 0.04A/div for (a); horizontal scale: 10V/div, vertical scale: 0.4A/div for (b)—(e).)

5.5.1 Derivation of the Discrete-time Map

Our purpose in this subsection is to derive a discrete-time map that describes the dynamics of a system of two boost converters connected in parallel, as defined earlier in Section 5.2 (see Fig. 5.1). We let x be the state variables as defined previously, and further let d_1 and d_2 be the duty cycle of Converter 1 (master) and Converter 2 (slave), respectively. The discrete-time map that we aim to find takes the following form:

$$x_{n+1} = f(x_n, d_{1,n}, d_{2,n}), \tag{5.8}$$

where subscript n denotes the value at the beginning of the nth cycle, i.e., $x_n = x(nT)$. For the closed-loop system, we need also to find the feedback equations that relate $d_{1,n}$ and $d_{2,n}$ to x_n.

The state equations are given in (5.1) for different switch states. The order in which the system toggles between the switch states depends on d_1 and d_2. Thus, we need to assume that $d_2 > d_1$ in the neighbourhood of the T-periodic state, or otherwise, in order to derive the discrete-time model. In particular, the assumption $d_2 > d_1$ is consistent with our simulation study since r_{L1} has a lower value than r_{L2}. Note that such an assumption loses no generality.

Recall that if $d_2 > d_1$, the state "S_1 on and S_2 off" should be omitted. Hence, we have three switch states:

1. For $nT < t \leq nT + d_{1,n}T$, both S_1 and S_2 are turned on.
2. For $nT + d_{1,n}T < t \leq nT + d_{2,n}T$, S_1 is turned off and S_2 remains on.
3. For $nT + d_{2,n}T < t \leq (n+1)T$, both S_1 and S_2 are off.

In each switch state, the describing state equation is $\dot{x} = A_j x + B_j E$, where $j = 1, 3, 4$. (Note that $j = 2$ does not appear here.) For each state equation we can derive the solution, and by stacking up the solutions, x_{n+1} can be expressed in terms of x_n, $d_{1,n}$ and $d_{2,n}$, i.e.,

$$\begin{aligned} x_{n+1} \;=\; & \Phi_4((1-d_{2,n})T)\Phi_3((d_{2,n}-d_{1,n})T)\Phi_1(d_{1,n}T)x_n \\ & +\Phi_4((1-d_{2,n})T)\Phi_3((d_{2,n}-d_{1,n})T)(\Phi_1(d_{1,n}T)-\mathbf{1})A_1^{-1}B_1E \\ & +\Phi_4((1-d_{2,n})T)(\Phi_3((d_{2,n}-d_{1,n})T)-\mathbf{1})A_3^{-1}B_3E \\ & +(\Phi_4((1-d_{2,n})T)-\mathbf{1})A_4^{-1}B_4E, \end{aligned} \tag{5.9}$$

where $\mathbf{1}$ is the unit matrix, and $\Phi_j(\xi)$ is the transition matrix corresponding to

A_j and is given by

$$\Phi_j(\xi) = e^{A_j\xi} = \mathbf{1} + \sum_{k=1}^{\infty} \frac{1}{k!} A_j^k \xi^k, \quad \text{for} \quad j = 1, 2, 3, 4. \tag{5.10}$$

For parallel-connected boost converters, we let $B = B_1 = B_2 = B_3 = B_4$. Hence, (5.9) can be rewritten as

$$\begin{aligned} x_{n+1} &= \Phi_4((1-d_{2,n})T)\Phi_3((d_{2,n}-d_{1,n})T)\Phi_1(d_{1,n}T)x_n \\ &\quad +\Phi_4((1-d_{2,n})T)\Phi_3((d_{2,n}-d_{1,n})T)(\Phi_1(d_{1,n}T)-\mathbf{1})A_1^{-1}BE \\ &\quad +\Phi_4((1-d_{2,n})T)(\Phi_3((d_{2,n}-d_{1,n})T)-\mathbf{1})A_3^{-1}BE \\ &\quad +(\Phi_4((1-d_{2,n})T)-\mathbf{1})A_4^{-1}BE. \end{aligned} \tag{5.11}$$

Our next step is to find the feedback relations that connect the duty cycles and the state variables. The control voltages v_{con1} and v_{con2}, as given before by (4.2) and (4.3), can be rewritten as

$$v_{\text{con1}} = U_1 + \kappa_1^T x \tag{5.12}$$

$$v_{\text{con2}} = U_2 + \kappa_2^T x, \tag{5.13}$$

where U_1 and U_2 are constants, and the gain vectors κ_1 and κ_2 are

$$\kappa_1^T = [-K_{v1}\ 0\ 0] \quad \text{and} \quad \kappa_2^T = [-K_{v2}\ K_i m\ -K_i]. \tag{5.14}$$

The ramp function can also be rewritten simply as

$$v_{\text{ramp}} = \alpha + \beta(t \bmod T), \tag{5.15}$$

where α and β are constants. To find the defining equations for the duty cycles, we first note that the switches are turned off when $v_{\text{con1}} = v_{\text{ramp}}$ and $v_{\text{con2}} = v_{\text{ramp}}$. Now, define $s_1(x_n, d_{1,n})$ and $s_2(x_n, d_{1,n}, d_{2,n})$ as

$$\begin{aligned} s_1(x_n, d_{1,n}) &\stackrel{\text{def}}{=} v_{\text{con1}} - v_{\text{ramp}} \\ &= U_1 + \kappa_1^T x(d_{1,n}T) - (\alpha + \beta d_{1,n}T) \\ &= U_1 + \kappa_1^T[\Phi_1(d_{1,n}T)x_n + (\Phi_1(d_{1,n}T)-\mathbf{1})A_1^{-1}BE] \\ &\quad -(\alpha + \beta d_{1,n}T), \end{aligned} \tag{5.16}$$

$$\begin{aligned} s_2(x_n, d_{1,n}, d_{2,n}) &\stackrel{\text{def}}{=} v_{\text{con2}} - v_{\text{ramp}} \\ &= U_2 + \kappa_2^T x(d_{2,n}T) - (\alpha + \beta d_{2,n}T) \\ &= U_2 + \kappa_2^T[\Phi_3((d_{2,n}-d_{1,n})T)\Phi_1(d_{1,n}T)x_n \\ &\quad +\Phi_3((d_{2,n}-d_{1,n})T)(\Phi_1(d_{1,n}T)-\mathbf{1})A_1^{-1}BE \\ &\quad +(\Phi_3((d_{2,n}-d_{1,n})T)-\mathbf{1})A_3^{-1}BE] - (\alpha + \beta d_{2,n}T). \end{aligned} \tag{5.17}$$

Thus, S_1 and S_2 are turned off, respectively, when

$$s_1(x_n, d_{1,n}) = 0 \tag{5.18}$$

and

$$s_2(x_n, d_{1,n}, d_{2,n}) = 0. \tag{5.19}$$

Solving (5.18) and (5.19), $d_{1,n}$ and $d_{2,n}$ can be obtained. Combining with (5.11), we have the discrete-time iterative map for the closed-loop system.

5.5.2 Derivation of the Jacobian

We will make use of the system Jacobian to examine the bifurcation phenomena in Section 5.5.3. But before we move on, we need to find the necessary expressions that enable the Jacobian to be computed.

Suppose the equilibrium point is given by $x(nT) = X_Q$. The Jacobian of the discrete-time map evaluated at the equilibrium point can be written as follows:

$$\begin{aligned} J(X_Q) \;=\; & \frac{\partial f}{\partial x_n} - \frac{\partial f}{\partial d_{1,n}} \left(\frac{\partial s_1}{\partial d_{1,n}}\right)^{-1} \left(\frac{\partial s_1}{\partial x_n}\right) \\ & - \frac{\partial f}{\partial d_{2,n}} \left(\frac{\partial s_2}{\partial d_{2,n}}\right)^{-1} \left[\left(\frac{\partial s_2}{\partial x_n}\right) + \frac{\partial s_2}{\partial d_{1,n}} \left(\frac{\partial s_1}{\partial d_{1,n}}\right)^{-1} \left(\frac{\partial s_1}{\partial x_n}\right)\right] \Bigg|_{x_n = X_Q}, \end{aligned} \tag{5.20}$$

where

$$\frac{\partial f}{\partial x_n} = \begin{bmatrix} \frac{\partial f_1}{\partial v_n} & \frac{\partial f_1}{\partial i_{1,n}} & \frac{\partial f_1}{\partial i_{2,n}} \\ \frac{\partial f_2}{\partial v_n} & \frac{\partial f_2}{\partial i_{1,n}} & \frac{\partial f_2}{\partial i_{2,n}} \\ \frac{\partial f_3}{\partial v_n} & \frac{\partial f_3}{\partial i_{1,n}} & \frac{\partial f_3}{\partial i_{2,n}} \end{bmatrix}, \tag{5.21}$$

$$\frac{\partial f}{\partial d_{1,n}} = \begin{bmatrix} \frac{\partial f_1}{\partial d_{1,n}} & \frac{\partial f_2}{\partial d_{1,n}} & \frac{\partial f_3}{\partial d_{1,n}} \end{bmatrix}^T, \tag{5.22}$$

$$\frac{\partial s_1}{\partial x_n} = \begin{bmatrix} \frac{\partial s_1}{\partial v_n} & \frac{\partial s_1}{\partial i_{1,n}} & \frac{\partial s_1}{\partial i_{2,n}} \end{bmatrix}, \tag{5.23}$$

$$\frac{\partial f}{\partial d_{2,n}} = \begin{bmatrix} \frac{\partial f_1}{\partial d_{2,n}} & \frac{\partial f_2}{\partial d_{2,n}} & \frac{\partial f_3}{\partial d_{2,n}} \end{bmatrix}^T, \tag{5.24}$$

$$\frac{\partial s_2}{\partial x_n} = \begin{bmatrix} \frac{\partial s_2}{\partial v_n} & \frac{\partial s_2}{\partial i_{1,n}} & \frac{\partial s_2}{\partial i_{2,n}} \end{bmatrix}. \tag{5.25}$$

Using (5.16), (5.17) and (5.11), we can find all the derivatives in (5.20). First, $\partial f/\partial x_n$ can be found from (5.11), i.e.,

$$\frac{\partial f}{\partial x_n} = \Phi_4((1-d_{2,n})T)\Phi_3((d_{2,n}-d_{1,n})T)\Phi_1(d_{1,n}T). \tag{5.26}$$

Also, a direct differentiation gives $\partial f/\partial d_{1,n}$ as

$$\begin{aligned}
\frac{\partial f}{\partial d_{1,n}} &= \left(\Phi_4((1-d_{2,n})T)\Phi_3((d_{2,n}-d_{1,n})T)\frac{\partial \Phi_1(d_{1,n}T)}{\partial d_{1,n}}\right)x_n \\
&\quad + \left(\Phi_4((1-d_{2,n})T)\frac{\partial \Phi_3((d_{2,n}-d_{1,n})T)}{\partial d_{1,n}}\Phi_1(d_{1,n}T)\right)x_n \\
&\quad + \Phi_4((1-d_{2,n})T)\Phi_3((d_{2,n}-d_{1,n})T)\frac{\partial(\Phi_1(d_{1,n}T)-\mathbf{1})A_1^{-1}B}{\partial d_{1,n}}E \\
&\quad + \Phi_4((1-d_{2,n})T)\frac{\partial \Phi_3((d_{2,n}-d_{1,n})T)}{\partial d_{1,n}}(\Phi_1(d_{1,n}T)-\mathbf{1})A_1^{-1}BE \\
&\quad + \Phi_4((1-d_{2,n})T)\frac{\partial(\Phi_3((d_{2,n}-d_{1,n})T)-\mathbf{1})A_3^{-1}B}{\partial d_{1,n}}E \\
&= T\Phi_4((1-d_{2,n})T)\Phi_3((d_{2,n}-d_{1,n})T)(A_1-A_3)\Phi_1(d_{1,n}T)x_n \\
&\quad + T\Phi_4((1-d_{2,n})T)\Phi_3((d_{2,n}-d_{1,n})T)[\Phi_1(d_{1,n}T) \\
&\quad - A_3(\Phi_1(d_{1,n}T)-\mathbf{1})A_1^{-1}-\mathbf{1}]BE.
\end{aligned} \tag{5.27}$$

Likewise, we get $\partial f/\partial d_{2,n}$ as

$$\begin{aligned}
\frac{\partial f}{\partial d_{2,n}} &= \left(\frac{\partial \Phi_4((1-d_{2,n})T)}{\partial d_{2,n}}\Phi_3((d_{2,n}-d_{1,n})T)\Phi_1(d_{1,n}T)\right)x_n \\
&\quad + \left(\Phi_4((1-d_{2,n})T)\frac{\partial \Phi_3((d_{2,n}-d_{1,n})T)}{\partial d_{2,n}}\Phi_1(d_{1,n}T)\right)x_n \\
&\quad + \frac{\partial \Phi_4((1-d_{2,n})T)}{\partial d_{2,n}}\Phi_3((d_{2,n}-d_{1,n})T)(\Phi_1(d_{1,n}T)-\mathbf{1})A_1^{-1}BE \\
&\quad + \Phi_4((1-d_{2,n})T)\frac{\partial \Phi_3((d_{2,n}-d_{1,n})T)}{\partial d_{2,n}}(\Phi_1(d_{1,n}T)-\mathbf{1})A_1^{-1}BE \\
&\quad + \frac{\partial \Phi_4((1-d_{2,n})T)}{\partial d_{2,n}}(\Phi_3((d_{2,n}-d_{1,n})T)-\mathbf{1})A_3^{-1}BE \\
&\quad + \Phi_4((1-d_{2,n})T)\frac{\partial(\Phi_3((d_{2,n}-d_{1,n})T)-\mathbf{1})A_3^{-1}B}{\partial d_{2,n}}E \\
&\quad + \frac{\partial(\Phi_4((1-d_{2,n})T)-\mathbf{1})A_4^{-1}B}{\partial d_{2,n}}E \\
&= T\Phi_4((1-d_{2,n})T)(A_3-A_4)\Phi_3((d_{2,n}-d_{1,n})T)\Phi_1(d_{1,n}T)x_n \\
&\quad + T\Phi_4((1-d_{2,n})T)(A_3-A_4)\Phi_3((d_{2,n}-d_{1,n})T)(\Phi_1(d_{1,n}T)-\mathbf{1})A_1^{-1}BE \\
&\quad + T\Phi_4((1-d_{2,n})T)[\Phi_3((d_{2,n}-d_{1,n})T) \\
&\quad - A_4(\Phi_3((d_{2,n}-d_{1,n})T)-\mathbf{1})A_3^{-1}-\mathbf{1})]BE.
\end{aligned} \tag{5.28}$$

From (5.16), we obtain $\partial s_1/\partial x_n$ readily as

$$\frac{\partial s_1}{\partial x_n} = \kappa_1^T \Phi_1(d_{1,n}T). \tag{5.29}$$

Again by a direct differentiation, we get

$$\begin{aligned}
\frac{\partial s_1}{\partial d_{1,n}} &= \kappa_1^T \frac{\partial \Phi_1(d_{1,n}T)}{\partial d_{1,n}} x_n + \kappa_1^T \frac{\partial (\Phi_1(d_{1,n}T) - \mathbf{1}) A_1^{-1} B}{\partial d_{1,n}} E - \beta T \\
&= \kappa_1^T (A_1 T \Phi_1(d_{1,n}T)) x_n + \kappa_1^T (\Phi_1(d_{1,n}T) B T) E - \beta T \\
&= T \kappa_1^T \Phi_1(d_{1,n}T)(A_1 x_n + BE) - \beta T.
\end{aligned} \tag{5.30}$$

And from (5.17), we get

$$\frac{\partial s_2}{\partial x_n} = \kappa_2^T \Phi_3((d_{2,n} - d_{1,n})T) \Phi_1(d_{1,n}T). \tag{5.31}$$

Finally, we need to find $\partial s_2/\partial d_{2,n}$ and $\partial s_2/\partial d_{1,n}$. From (5.17) we have

$$\begin{aligned}
\frac{\partial s_2}{\partial d_{2,n}} &= \kappa_2^T \frac{\partial \Phi_3((d_{2,n} - d_{1,n})T)}{\partial d_{2,n}} \Phi_1(d_{1,n}T) x_n \\
&\quad + \kappa_2^T \frac{\partial \Phi_3((d_{2,n} - d_{1,n})T)}{\partial d_{2,n}} (\Phi_1(d_{1,n}T) - \mathbf{1}) A_1^{-1} BE \\
&\quad + \kappa_2^T \frac{\partial (\Phi_3((d_{2,n} - d_{1,n})T) - \mathbf{1}) A_3^{-1} B}{\partial d_{2,n}} E - \beta T \\
&= T \kappa_2^T \Phi_3((d_{2,n} - d_{1,n})T)[A_3 \Phi_1(d_{1,n}T) x_n \\
&\quad + A_3(\Phi_1(d_{1,n}T) - \mathbf{1}) A_1^{-1} BE + BE] - \beta T,
\end{aligned} \tag{5.32}$$

and

$$\begin{aligned}
\frac{\partial s_2}{\partial d_{1,n}} &= \kappa_2^T \frac{\partial \Phi_3((d_{2,n} - d_{1,n})T)}{\partial d_{1,n}} \Phi_1(d_{1,n}T) x_n \\
&\quad + \kappa_2^T \Phi_3((d_{2,n} - d_{1,n})T) \frac{\partial \Phi_1(d_{1,n}T)}{\partial d_{1,n}} x_n \\
&\quad + \kappa_2^T \frac{\partial \Phi_3((d_{2,n} - d_{1,n})T)}{\partial d_{1,n}} (\Phi_1(d_{1,n}T) - \mathbf{1}) A_1^{-1} BE \\
&\quad + \kappa_2^T \Phi_3((d_{2,n} - d_{1,n})T) \frac{\partial (\Phi_1(d_{1,n}T) - \mathbf{1}) A_1^{-1} B}{\partial d_{1,n}} E \\
&\quad + \kappa_2^T \frac{\partial (\Phi_3((d_{2,n} - d_{1,n})T) - \mathbf{1}) A_3^{-1} B}{\partial d_{1,n}} E. \\
&= T \kappa_2^T \Phi_3((d_{2,n} - d_{1,n})T)[(A_1 - A_3) \Phi_1(d_{1,n}T) x_n \\
&\quad + \Phi_1(d_{1,n}T) BE - A_3(\Phi_1(d_{1,n}T) - \mathbf{1}) A_1^{-1} BE - BE].
\end{aligned} \tag{5.33}$$

Now, putting all the derivatives into (5.20) gives an expression of $J(X_Q)$ that can be computed numerically. Numerical algorithms can now be developed for computing $J(X_Q)$ and hence the characteristic multipliers, as will be shown in the next subsection.

5.5.3 Characteristic Multipliers and Neimark-Sacker Bifurcation

The Jacobian derived in the foregoing subsection provides a means to evaluate the dynamics of the system. We will, in particular, study the loci of the characteristic multipliers, the aim being to find out possible bifurcation scenarios as the voltage feedback gains are varied. To find the characteristic multipliers, we solve the following polynomial equation in λ, whose roots actually give the characteristic multipliers:

$$\det[\lambda \mathbf{1} - J(X_Q)] = 0, \tag{5.34}$$

where $J(X_Q)$ is the Jacobian found previously. We will pay attention to the movement of the characteristic multipliers as K_{v2} and m are varied. Any crossing from the interior of the unit circle to the exterior indicates a possible bifurcation. In particular, if a pair of complex characteristic multipliers move out of the unit circle, a Neimark-Sacker bifurcation occurs [104], [110].

Using (5.20) and (5.34), we can generate loci of characteristic multipliers numerically. Since we are interested here in varying K_{v2}, we keep $m = 1$, thereby ensuring that the system will not undergo any bifurcation due possibly to large m, as we have seen previously in the simulation. Then, we keep K_{v1} and K_{v2} relatively small and vary m. To maintain conciseness, we exemplify here the typical loci shown in Tables 5.2 and 5.3, which are graphically illustrated in Figs. 5.6 and 5.7. Both loci indicate a Neimark-Sacker bifurcation as K_{v2} and m vary. This agrees with our simulation results in Section 5.3.

K_{v2}	Char. Mult.	Remarks
0.02	$0.901 \pm j0.131$, 0.999	Stable 1T
0.04	$0.916 \pm j0.146$, 0.999	Stable 1T
0.06	$0.932 \pm j0.159$, 0.999	Stable 1T
0.08	$0.949 \pm j0.170$, 0.999	Stable 1T
0.10	$0.967 \pm j0.179$, 0.999	Stable 1T
0.125	$0.992 \pm j0.188$, 0.999	Neimark-Sacker bifurcation

Table 5.2: Characteristic multipliers for different values of K_{v2}.

5.6 Conclusion

This chapter reports, for the first time, some selected bifurcation phenomena in a parallel system of two boost converters which share current under a master-

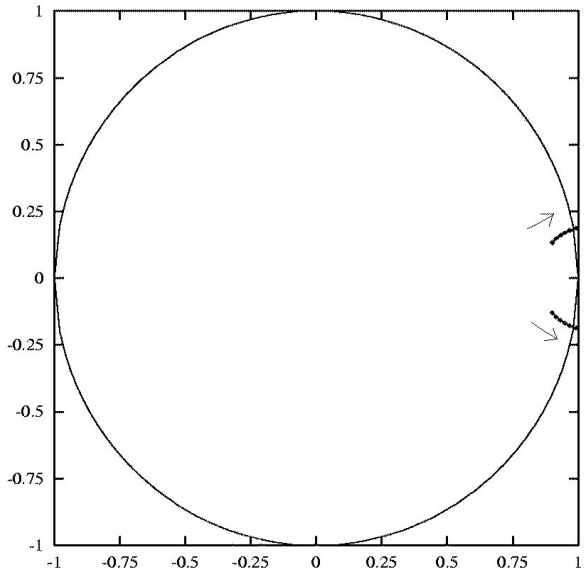

Figure 5.6: Loci of characteristic multipliers as K_{v2} varies. Arrows indicate increasing K_{v2}.

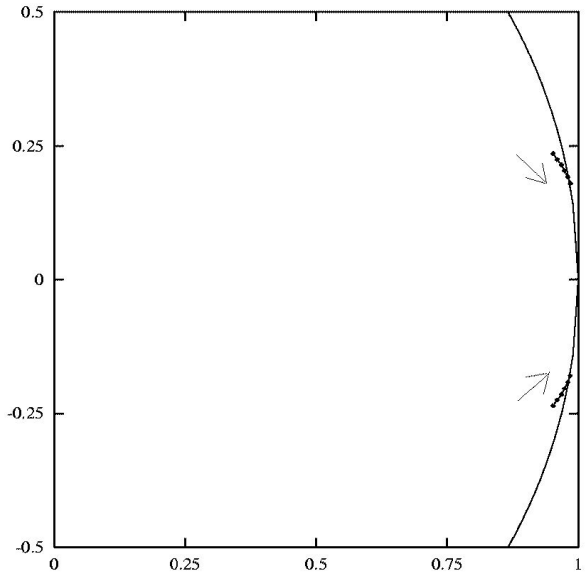

Figure 5.7: Loci of characteristic multipliers as m varies. Arrows indicate increasing m.

m	Char. Mult.	Remarks
0.7	$0.952 \pm j0.238, 0.999$	Stable 1T
0.9	$0.960 \pm j0.226, 0.999$	Stable 1T
1.1	$0.968 \pm j0.215, 0.999$	Stable 1T
1.3	$0.974 \pm j0.204, 0.999$	Stable 1T
1.5	$0.980 \pm j0.192, 0.998$	Stable 1T
1.7	$0.985 \pm j0.180, 0.998$	Neimark-Sacker bifurcation

Table 5.3: Characteristic multipliers for different values of m.

slave control scheme. The study of stability is a complex issue in this type of system [70], [107]. This chapter focuses on the effects of variation of some voltage feedback gains and current sharing ratio. It has been found that Neimark-sacker bifurcations are possible when voltage feedback gains or current-sharing ratio are varied. These results are useful for practical design of parallel converter systems to ensure stable period-1 operation in the expected stable region.

Remarks — The analysis approach we use for studying parallel DC/DC converters in Chapter 4 and this chapter is mainly based on a discrete-time map. It is effective in analyzing a small number of converters connected in parallel. However, the number of converters may be quite large in practical situations. When the number of parallel converters increases, the complexity of the system escalates drastically. The order of the system matrices involved becomes very high and it will be difficult to establish the discrete-time map. In this case, we need to make some simplifying assumptions in order to reduce the order of the system matrices. For example, we can assume some of the converters and their control methods are identical. When the order of the system is reduced, we can adopt the same approach of analysis.

Chapter 6

Hopf Bifurcation and Chaos from Autonomous DC/DC Converters

6.1 Introduction

Self-oscillating or free-running current-controlled switching converters are often used in low-cost switching power supplies, since they require no external clocks and their constructions are relatively simple. In contrast to their non-autonomous counterparts for which chaos is observed even for the simplest first-order discontinuous-mode converters [11]–[12], free-running converters of order below three cannot exhibit chaos. The essential feature of an autonomous switching converter is the absence of any external driving signal, which is mandatory in the non-autonomous case for periodic switching of the power switch. Up to now, much has been reported on the bifurcation and chaotic behaviour of non-autonomous switching converters [10]–[29], while very little work has been performed in identifying bifurcation and chaos in autonomous switching converters.

In this chapter, we study the dynamics of the Ćuk converter, which is widely used in power electronics. Being of fourth-order, the Ćuk converter can operate chaotically in free-running (autonomous) mode. We report, in this chapter, the bifurcation behaviour of a free-running current-controlled Ćuk converter. In particular, our study covers the following aspects: 1) derivation of describing state equation; 2) study of stability of the equilibrium state and identification of Hopf bifurcation based on the describing state equation; 3) computer simulations of the circuits revealing the bifurcation from stable equilibrium state (fixed point), through limit cycles and quasi-periodic orbits, and eventually to chaos; and 4) experimental verification of the bifurcation scenario.

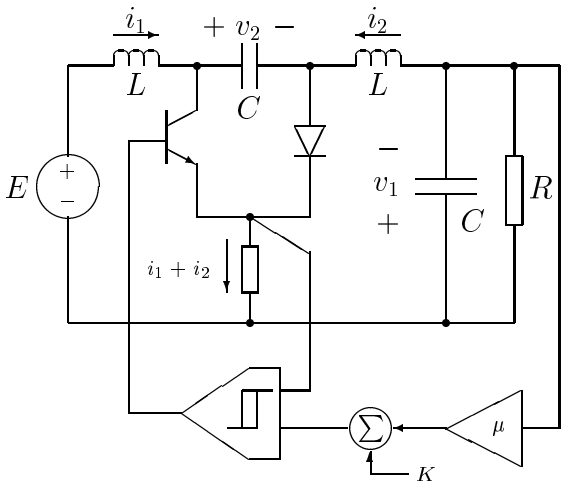

Figure 6.1: Ćuk converter under hysteretic current-mode control.

6.2 System Description

Specifically, the system under study consists of a Ćuk converter whose operation is based on a free-running hysteretic current-mode control. In actual implementation, the switch is turned on and off, in a hysteretic fashion, when the sum of the inductor currents falls below or rises above a certain pre-set hysteretic band [111, 112]. The average value and width of this pre-set band are adjusted by a feedback Schmitt trigger circuit. Also, the output voltage is fed back to set the average value of the hysteretic band, forcing the control variable to be related by the following control equation:

$$i_1 + i_2 = g(v_1), \tag{6.1}$$

where i_1 and i_2 are the inductor currents, v_1 is the output voltage, and $g(.)$ is the control function. For example, a simple proportional control takes the form of

$$\Delta(i_1 + i_2) = -\mu \Delta v_1, \tag{6.2}$$

where μ is the gain factor. This equation has the following equivalent form, assuming regulated output:

$$i_1 + i_2 = K - \mu v_1, \tag{6.3}$$

where K and μ are the control parameters. Figure 6.1 shows a simplified schematic of the system.

6.2.1 Derivation of Autonomous State Equations

The system can be represented by the following state-space equations, where $s = 1$ when the switch is turned on, and $s = 0$ when the switch is off:

$$\begin{cases} \dfrac{di_1}{dt} &= -\dfrac{(1-s)v_2}{L} + \dfrac{E}{L} \\ \dfrac{di_2}{dt} &= \dfrac{v_2 s}{L} - \dfrac{v_1}{L} \\ \dfrac{dv_1}{dt} &= \dfrac{i_2}{C} - \dfrac{v_1}{CR} \\ \dfrac{dv_2}{dt} &= \dfrac{(1-s)i_1}{C} - \dfrac{i_2 s}{C}. \end{cases} \tag{6.4}$$

The state-space averaged model has the same form as above, with s replaced by the duty cycle δ, which is the fraction of the switching period, for which the switch is turned on.

Since $i_1 + i_2$ is related to v_1 by a linear algebraic equation, the system reduces its order by one. Specifically, when the control equation (6.3) is taken into account, the system can be reduced to the following third-order system:

$$\begin{cases} \dfrac{di_2}{dt} &= \dfrac{v_2 \delta}{L} - \dfrac{v_1}{L} \\ \dfrac{dv_1}{dt} &= \dfrac{i_2}{C} - \dfrac{v_1}{CR} \\ \dfrac{dv_2}{dt} &= \dfrac{(1-\delta)(K - \mu v_1)}{C} - \dfrac{i_2}{C}, \end{cases} \tag{6.5}$$

where δ is the duty cycle. Also, from (6.3), $d(i_1+i_2)/dt = -\mu dv_1/dt$. Substitution of the involving derivatives gives

$$\delta = \frac{1}{2} - \frac{\dfrac{\mu L}{C} i_2 - \left(1 + \dfrac{\mu L}{CR}\right) v_1 + E}{2v_2}, \tag{6.6}$$

which must satisfy $0 < \delta < 1$. Finally, putting (6.6) into (6.5) results in the following state equations that describe the dynamics of the autonomous system:

$$\begin{cases} \dfrac{di_2}{dt} &= -\dfrac{\mu i_2}{2C} - \left(1 - \dfrac{\mu L}{CR}\right)\dfrac{v_1}{2L} + \dfrac{v_2}{2L} - \dfrac{E}{2L} \\ \dfrac{dv_1}{dt} &= \dfrac{i_2}{C} - \dfrac{v_1}{CR} \\ \dfrac{dv_2}{dt} &= -\dfrac{i_2}{C} + \left(\dfrac{K - \mu v_1}{2C}\right)\left(1 + \dfrac{\frac{\mu L}{C} i_2 - \left(1 + \frac{\mu L}{CR}\right) v_1 + E}{v_2}\right). \end{cases} \tag{6.7}$$

Note that this representation is valid only if $0 < \delta < 1$. Such a condition is satisfied when the system is operating in a stable equilibrium state, corresponding to a fixed point in the above averaged model.

Remarks — It should be noted that averaged models have limited validity for nonlinear analysis. Specifically, the averaged model, as derived above, is valid when the system remains in continuous mode and the switching frequency is relatively high. Thus, we may use such a model only to study the behaviour of the system up to the point of losing stability. Nonetheless, as we will see, the averaged model gives useful clues to the way the system loses stability, although it falls short of predicting the behaviour beyond the bifurcation point.

6.2.2 Equilibrium Point Calculation

To find the equilibrium point, we set all the time-derivatives to zero and solve for i_2, v_1 and v_2. This gives

$$\begin{cases} I_2 &= -\dfrac{E(1+\mu R)}{2R} \pm \dfrac{E}{2R}\sqrt{(1+\mu R)^2 + \dfrac{4KR}{E}} \\ V_1 &= -\dfrac{E(1+\mu R)}{2} \pm \dfrac{E}{2}\sqrt{(1+\mu R)^2 + \dfrac{4KR}{E}} \\ V_2 &= \dfrac{E(1-\mu R)}{2} \pm \dfrac{E}{2}\sqrt{(1+\mu R)^2 + \dfrac{4KR}{E}}. \end{cases} \tag{6.8}$$

Note that the choice of the control parameters K and μ will set the steady state output voltage level, provided the system is stable. The stability of the system is yet to be studied for different sets of parameters. Furthermore, assuming the existence of a stable steady state, the value of the duty cycle can be found by putting $V_1 = I_2 R$ in (6.6), as

$$\delta|_{\text{steady-state}} = \frac{1}{2} - \frac{E - V_1}{2V_2}. \tag{6.9}$$

Also, since $V_2 = V_1 + E$, we can write

$$\delta|_{\text{steady-state}} = \frac{V_1}{E + V_1}. \tag{6.10}$$

Since $E > 0$ and $\delta \in [0, 1]$, $V_1 < 0$ is not possible. Thus, we have $V_1 > 0$ and the only equilibrium point is given by

$$\begin{cases} V_1 &= I_2 R = -\dfrac{E(1+\mu R)}{2} + \dfrac{E}{2}\sqrt{(1+\mu R)^2 + \dfrac{4KR}{E}} \\ V_2 &= \dfrac{E(1-\mu R)}{2} + \dfrac{E}{2}\sqrt{(1+\mu R)^2 + \dfrac{4KR}{E}}. \end{cases} \tag{6.11}$$

6.2.3 Dimensionless Equations

The afore-derived state equations can be put in a dimensionless form. Define the dimensionless state variables as follows:

$$x_1 = \frac{Ri_2}{E}, \quad x_2 = \frac{v_1}{E}, \quad x_3 = \frac{v_2}{E}. \tag{6.12}$$

Also, define the dimensionless time and parameters as follows:

$$\tau = \frac{Rt}{2L}, \quad \xi = \frac{L/R}{CR}, \quad \kappa_1 = \mu R, \quad \kappa_o = \frac{KR}{E}. \tag{6.13}$$

Direct substitution of these new dimensionless variables, time, and parameters in the autonomous equations (6.7) yields the following dimensionless autonomous equations:

$$\begin{cases} \dfrac{dx_1}{d\tau} &= -\xi\kappa_1 x_1 - (1-\kappa_1\xi)x_2 + x_3 - 1 \\ \dfrac{dx_2}{d\tau} &= 2\xi(x_1 - x_2) \\ \dfrac{dx_3}{d\tau} &= -2\xi x_1 + \xi(\kappa_o - \kappa_1 x_2)\left(1 + \dfrac{\kappa_1\xi x_1 - (1+\kappa_1\xi)x_2 + 1}{x_3}\right). \end{cases} \tag{6.14}$$

To complete the model, saturation must be included. Now, δ may be written as

$$\delta = 0.5 - \frac{\kappa_1\xi x_1 - (1+\kappa_1\xi)x_2 + 1}{2x_3}. \tag{6.15}$$

The condition for saturation is

$$\delta > 1 \quad \Leftrightarrow \quad \kappa_1\xi x_1 - (1+\kappa_1\xi)x_2 + x_3 + 1 < 0, \tag{6.16}$$

$$\text{or} \quad \delta < 0 \quad \Leftrightarrow \quad \kappa_1\xi x_1 - (1+\kappa_1\xi)x_2 - x_3 + 1 > 0. \tag{6.17}$$

By putting $\delta = 1$ or 0 in (6.5) and performing dimensionless substitution, the state equations for saturation are

$$\begin{cases} \dfrac{dx_1}{d\tau} &= 2(x_3 - x_2) \\ \dfrac{dx_2}{d\tau} &= 2\xi(x_1 - x_2) \\ \dfrac{dx_3}{d\tau} &= -2\xi x_1 \end{cases} \quad \text{for } \delta > 1 \tag{6.18}$$

$$\text{and} \quad \begin{cases} \dfrac{dx_1}{d\tau} &= -2x_2 \\ \dfrac{dx_2}{d\tau} &= 2\xi(x_1 - x_2) \\ \dfrac{dx_3}{d\tau} &= -2\xi x_1 + 2\xi(\kappa_0 - \kappa_1 x_2) \end{cases} \quad \text{for } \delta < 0. \tag{6.19}$$

The equilibrium point can be calculated by putting $dx_1/d\tau = dx_2/d\tau = dx_3/d\tau = 0$ in (6.14) and considering the restricted sign of X_2. This gives

$$X = \begin{bmatrix} X_1 \\ X_2 \\ X_3 \end{bmatrix} = \begin{bmatrix} X_s \\ X_s \\ X_s + 1 \end{bmatrix}, \tag{6.20}$$

where

$$X_s = \frac{-(1+\kappa_1) + \sqrt{(1+\kappa_1)^2 + 4\kappa_o}}{2}. \tag{6.21}$$

6.3 Stability of Equilibrium Point and Hopf Bifurcation

The Jacobian, $J(X)$, for the dimensionless system evaluated at the equilibrium point is given by

$$J(X) = \begin{bmatrix} -\kappa_1\xi & -(1-\kappa_1\xi) & 1 \\ 2\xi & -2\xi & 0 \\ J_{31} & J_{32} & J_{33} \end{bmatrix},$$

where

$$J_{31} = -2\xi + \frac{\kappa_1\xi^2(\kappa_o - \kappa_1 X_s)}{1+X_s} \tag{6.22}$$

$$J_{32} = \frac{-2\kappa_1\xi - \xi(1+\kappa_1\xi)(\kappa_o - \kappa_1 X_s)}{1+X_s} \tag{6.23}$$

$$J_{33} = \frac{\xi(\kappa_o - \kappa_1 X_s)(X_s - 1)}{(1+X_s)^2}. \tag{6.24}$$

From (6.21), $X_s(X_s+1) = \kappa_o - \kappa_1 X_s$. The Jacobian can hence be simplified to

$$J(X) = \begin{bmatrix} -\kappa_1\xi & -(1-\kappa_1\xi) & 1 \\ 2\xi & -2\xi & 0 \\ -2\xi + \kappa_1\xi^2 X_s & \frac{-2\kappa_1\xi}{1+X_s} - \xi(1+\kappa_1\xi)X_s & \frac{-\xi X_s(1-X_s)}{1+X_s} \end{bmatrix}. \tag{6.25}$$

	$\kappa_1 = 1$	Remarks
$\kappa_0 = 1$	$-0.0078725 \pm j0.232363$, -0.0274423	Stable equilibrium point
$\kappa_0 = 3$	$-0.00666899 \pm j0.232102$, -0.0275472	Stable equilibrium point
$\kappa_0 = 5$	$-0.00482465 \pm j0.231866$, -0.0275798	Stable equilibrium point
$\kappa_0 = 7$	$-0.0029592 \pm j0.231535$, -0.0276402	Stable equilibrium point
$\kappa_0 = 9$	$-0.0011668 \pm j0.231428$, -0.0276955	Stable equilibrium point
$\kappa_0 = 11$	$0.000538546 \pm j0.231217$, -0.0277466	Unstable equilibrium point

Table 6.1: Eigenvalues at $\xi = 0.0136$ showing dependence on κ_0

We attempt to study the stability of the equilibrium point and the trajectory around the equilibrium point by deriving the eigenvalues of the system at the equilibrium point. The usual procedure is to solve the following equation for λ:

$$\det\left[\lambda \mathbf{1} - J(X)\right] = 0. \tag{6.26}$$

Upon expanding, we get

$$\lambda^3 + \frac{\xi[(\kappa_1+2)+(\kappa_1+3)X_s - X_s^2]}{1+X_s}\lambda^2 + \frac{2\xi[2+(\xi+2)X_s - \xi(\kappa_1+1)X_s^2]}{1+X_s}\lambda + \frac{4\xi^2[\kappa_1+1+2X_s]}{1+X_s} = 0. \tag{6.27}$$

Using this equation, the following conditions are easily verified:

$$\lim_{\lambda \to -\infty} \det\left[\lambda \mathbf{1} - J(X)\right] \to -\infty \tag{6.28}$$

and

$$\det[-J(X)] > 0. \tag{6.29}$$

Hence, there exists at least one $\lambda \in (-\infty, 0)$ such that $\det\left[\lambda \mathbf{1} - J(X)\right] = 0$, i.e., the system has at least one negative real eigenvalue. Also, numerical calculations of eigenvalues for the practical range of parameters, $0 < \kappa_0 < 100$, $0 < \kappa_1 < 10$ and $0.01 < \xi < 10$, reveal that the other two eigenvalues are a complex conjugate pair which have either a positive or negative real part depending upon values of κ_0 and κ_1. In particular, the following observations are made:

1. For small values of κ_0, the pair of complex eigenvalues has a negative real part.

2. As κ_0 increases, the real part of the complex eigenvalues gets less negative, and at a critical value of κ_0, the real part changes from negative to positive. Table 6.1 shows a typical scenario of the variation of the eigenvalues. The locus is plotted in Fig. 6.2 for ease of reference.

3. The critical value of κ_0 depends on the values of κ_1 and ξ. Figure 6.3 shows the boundary curves where the sign of the real part of the complex eigenvalues changes. On these curves, the system loses stability via a *supercritical Hopf Bifurcation* [109], [113, 114].

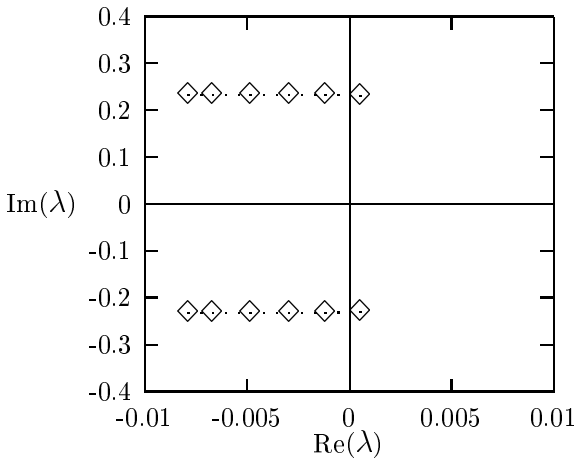

Figure 6.2: Locus of the complex eigenvalue pair corresponding to Table 6.1.

Remarks — To formally establish a supercritical Hopf Bifurcation, one needs to show that, for given ξ and κ_1, there exists κ_0 for which the following conditions are satisfied by the complex eigenvalue pair [109]:

$$\mathrm{Re}(\lambda)\big|_{\kappa_0=\kappa_{0c}} = 0 \tag{6.30}$$

$$\mathrm{Im}(\lambda)\big|_{\kappa_0=\kappa_{0c}} \neq 0 \tag{6.31}$$

$$\frac{d}{d\kappa_0}\mathrm{Re}(\lambda)\bigg|_{\kappa_0=\kappa_{0c}} \neq 0, \tag{6.32}$$

where κ_{0c} is the critical value of κ_0 at which a supercritical Hopf bifurcation occurs. Note that the last condition is necessary to ensure that the complex eigenvalue pair moves from the left side to the right side of the complex plane (preventing it from "locusing" along the imaginary axis). In fact, all the above conditions can be numerically established using (6.27).

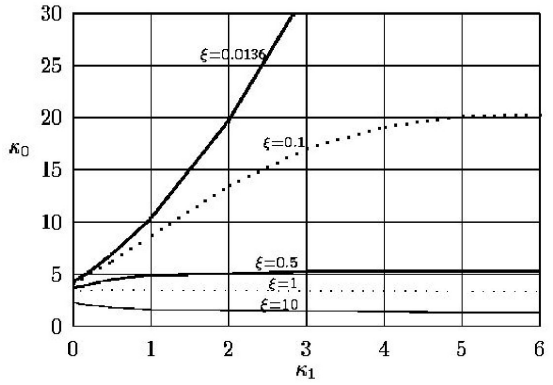

Figure 6.3: Boundary of stability. Area below the curve corresponds to stable equilibrium points, and that above to unstable equilibrium points.

6.4 Local Trajectories from Describing Equation

In this section, we re-examine the stability in terms of the local trajectories near the equilibrium point. It should be stressed that since the use of an averaged model for predicting nonlinear phenomena will become inadequate when stability is lost, our aim in this section is to observe, by plotting the local trajectories, the behaviour of the system as it goes from a stable region to an unstable region. For further investigation beyond the bifurcation point, we have to resort to the exact piecewise switched model, as will be reported in Section 6.5.

The trajectory of the system near the equilibrium point can be easily derived from the corresponding eigenvalues and eigenvectors. Suppose the eigenvalues and their corresponding eigenvectors are

$$\lambda_r, \sigma \pm j\omega \quad \text{and} \quad \bar{v}_r, \bar{v}_1 \pm j\bar{v}_2. \tag{6.33}$$

The solution in general is given by

$$\mathbf{x}(t) = c_r e^{\lambda_r t}\bar{v}_r + 2c_c e^{\sigma t}[\cos(\omega t + \phi_c)\bar{v}_1 - \sin(\omega t + \phi_c)\bar{v}_2], \tag{6.34}$$

where c_r, c_c and ϕ_c are determined by initial conditions. The geometry of the trajectory is best described in terms of the eigenline L_r, which is parallel $\bar{v}_r$, and the eigenplane E_c, which is spanned by $\bar{v}_1$ and $\bar{v}_2$, where the intersection of L_r and E_c is the equilibrium point. Essentially, since the real eigenvalue is negative, the system moves initially in the direction of L_r going towards E_c. At the same time it moves in a helical motion converging toward or diverging away from L_r, depending upon the sign of the real part of the complex eigenvalues. As it lands on E_c, it keeps spiraling along E_c towards or away from the equilibrium point.

The following examples illustrate two typical local trajectories, corresponding to a stable and an unstable equilibrium point.

We first examine the stable system with $\xi = \kappa_0 = \kappa_1 = 1$. The Jacobian evaluated at the equilibrium point is

$$J(X) = \begin{pmatrix} -1 & 0 & 1 \\ 2 & -2 & 0 \\ -1.58579 & -2.24264 & -0.171573 \end{pmatrix}. \tag{6.35}$$

The eigenvalues, λ, and their corresponding eigenvectors, $\bar{v}$, are found as

$$\begin{aligned} \lambda &= -2.74051, -0.215533 \pm j1.69491 \\ \bar{v} &= \begin{pmatrix} -0.297167 \\ 0.802604 \\ 0.517222 \end{pmatrix}, \begin{pmatrix} 0.185114 \mp j0.399955 \\ -0.114761 \mp j0.339261 \\ 0.823104 \end{pmatrix}. \end{aligned}$$

Using the INSITE program[1] [115], we can view the trajectory from different perspectives; two of which are shown in Fig. 6.4.

We next examine the unstable system with $\xi = \kappa_1 = 1$ and $\kappa_0 = 4$. As shown in Fig. 6.3, the system just loses stability. The Jacobian evaluated at the equilibrium point is

$$J(X) = \begin{pmatrix} -1 & 0 & 1 \\ 2 & -2 & 0 \\ -0.763932 & -3.36656 & 0.130495 \end{pmatrix}. \tag{6.36}$$

The eigenvalues, λ, and their corresponding eigenvectors, $\bar{v}$, are found as

$$\begin{aligned} \lambda &= -2.9757, 0.0530965 \pm j1.63879 \\ \bar{v} &= \begin{pmatrix} -0.331404 \\ 0.679316 \\ 0.654753 \end{pmatrix}, \begin{pmatrix} 0.233197 \mp j0.362892 \\ -0.033598 \mp j0.326689 \\ 0.840282 \end{pmatrix}. \end{aligned}$$

Using the INSITE program [115] again, we can view the local trajectory from different perspectives; two of which are shown in Fig. 6.5.

From the above examples, we clearly observe that the system loses stability via Hopf bifurcation as a stable spiral develops into an unstable spiral in the neighbourhood of the equilibrium point. In the next section, we re-examine the system using cycle-by-cycle computer simulations of the actual switching circuit. As we will see, the system develops into a limit cycle as it loses stability, and further develops into quasi-periodic and chaotic orbits.

[1] INSITE is a collection of software programs developed by T.S. Parker [115] for studying chaotic systems. The particular software components used in this paper are LYEXP and TRAJ for generating Lyapunov exponents and trajectories.

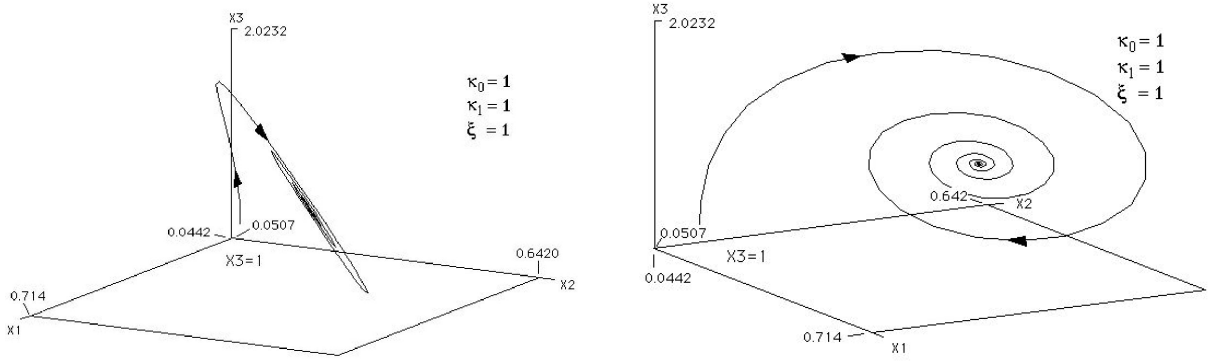

(a) (b)

Figure 6.4: Two views of the 'stable' local trajectory for $\xi = \kappa_0 = \kappa_1 = 1$ (based on averaged model).

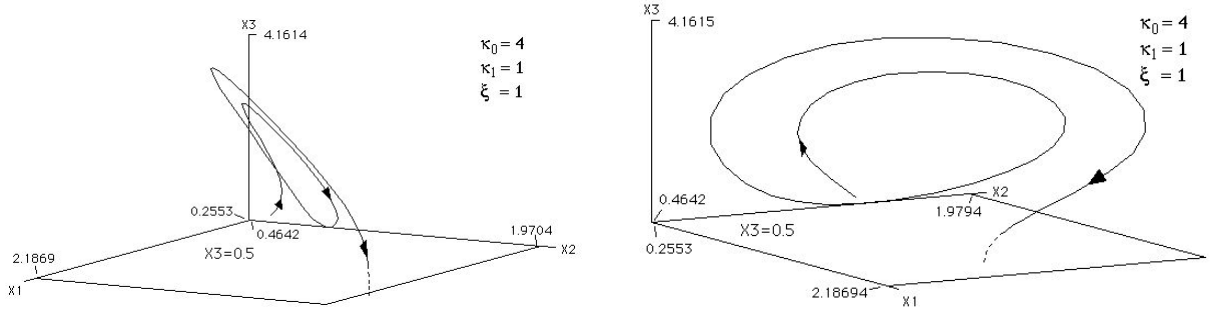

(a) (b)

Figure 6.5: Two views of the 'unstable' local trajectory for $\xi = \kappa_1 = 1$, $\kappa_0 = 4$ (based on averaged model).

6.5 Computer Simulation Study

Since the foregoing analysis is based on a nonlinear state equation which is derived from an approximate (average) continuous model, it falls short of predicting the details of the bifurcation sequence. Instead of refining the model, we examine the system using computer simulation which employs an exact piecewise-switched model. Essentially, a computer simulation program generates the cycle-by-cycle waveforms of all capacitor voltages and inductor currents by toggling between a set of linear differential equations that describe the constituent linear circuits for all possible switch states. The program also incorporates the free-running current-control algorithm for determining the switch state during simulation.

In our simulation study of the free-running Ćuk converter, we set the input voltage at 15V and the values of the components as follows:

$$L_1 = L_2 = 0.01\text{H}, \quad C_1 = C_2 = 47\mu\text{F}, \quad R = 40\Omega.$$

Note that since we are simulating the actual circuit, the parameters used will be μ and K instead of the dimensionless ones used for analysis. In particular, we focus on the qualitative change of dynamics as the parameters are varied, as hinted from the result of Section 6.3.

To see the trend, it suffices to keep μ constant at 0.01 and vary K. A summary of the observed behaviour is as follows (A complete view of the effect of ξ, μ and K on stability of the fundamental equilibrium state will be provided later in this section):

1. When K is small, the trajectory spirals into a fixed period-1 orbit, corresponding to a fixed point in the averaged system. Figure 6.6 shows the simulated trajectory and the stable period-1 orbit.

2. For a larger K, the period-1 orbit becomes unstable, and the trajectory spirals outward as shown in Fig. 6.7 (a), and settles into a limit cycle as shown in Fig. 6.7 (b).

3. For yet a larger K, a quasi-periodic orbit can be observed, as shown in Fig. 6.8 (a). A Poincaré section is shown in Fig. 6.8 (b) which is essentially the points of intersection of the trajectory and the vertical plane $i_1 = 8.2$.

4. Finally, chaos occurs when K is further increased. Figures 6.9 (a) and (b) show the measured trajectory and a Poincaré section.

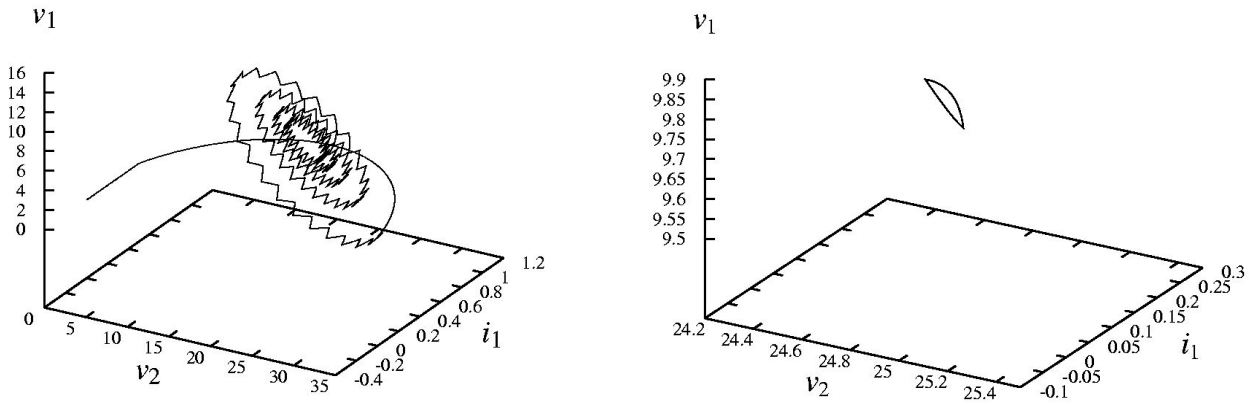

(a) (b)

Figure 6.6: (a) Trajectory spiraling into stable period-1 orbit; (b) stable period-1 orbit enlarged ($K = 0.4$).

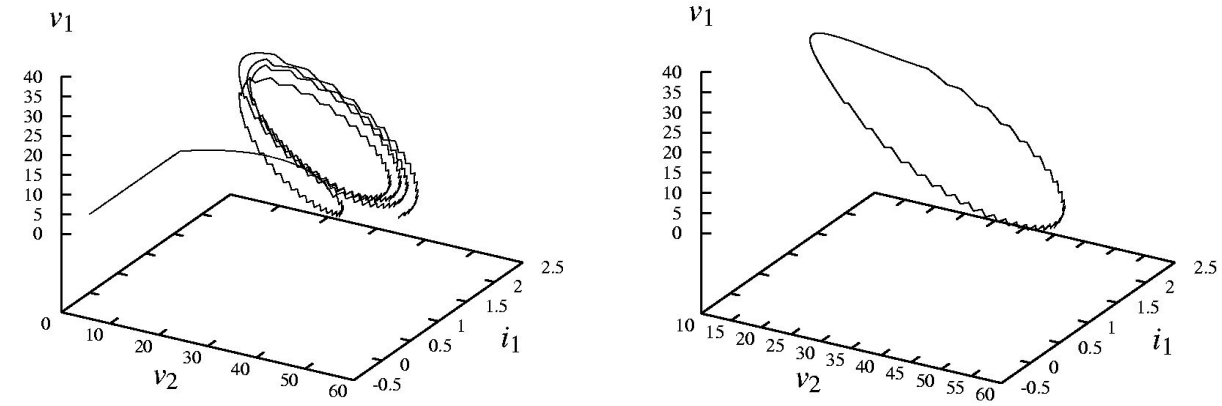

(a) (b)

Figure 6.7: (a) Trajectory spiraling away from the unstable period-1 orbit; (b) limit cycle ($K = 1.5$).

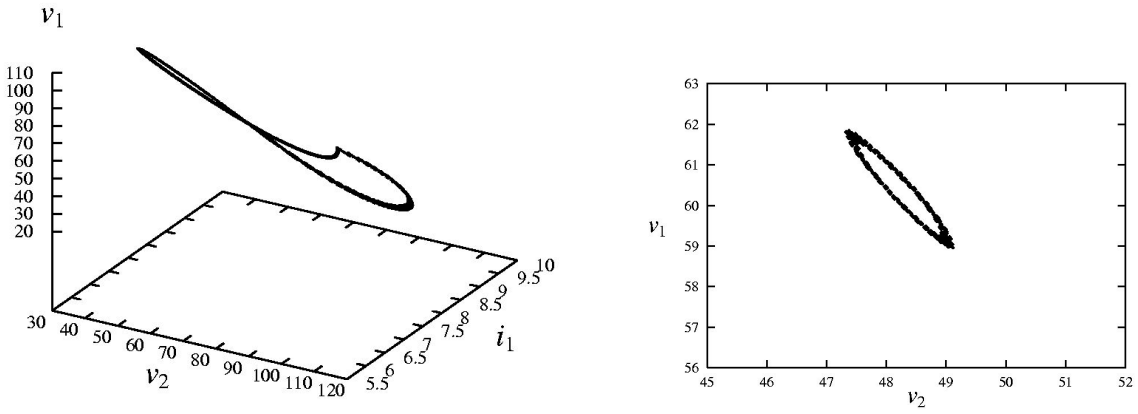

(a) (b)

Figure 6.8: (a) Quasi-periodic orbit; (b) blow-up of a Poincaré section taken at $i_1 = 8.2$ ($K = 10.5$).

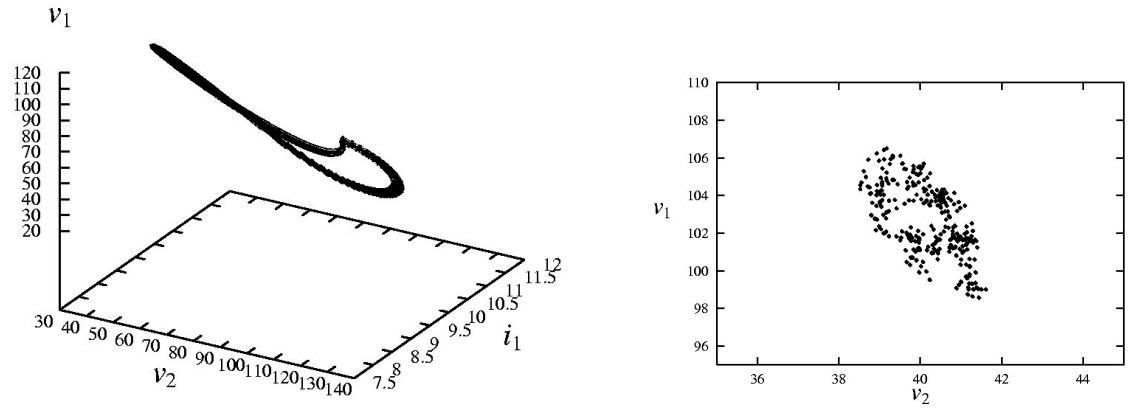

(a) (b)

Figure 6.9: (a) Chaotic orbit; (b) blow-up of a Poincaré section taken at $i_1 = 9.5$ ($K = 13$).

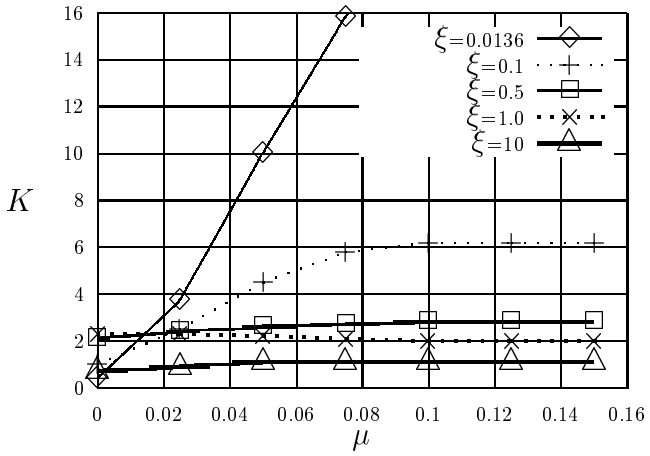

Figure 6.10: Boundary of stability from cycle-by-cycle simulation. Area below the curve corresponds to stable fundamental operation, and that above to operations other than stable fundamental operation. These curves agree with Fig. 6.3.

Furthermore, based on a number of simulation runs, we obtained the boundary of stability similar to Fig. 6.3, for different values of ξ. More precisely, the boundary curves define the values of parameters for which a trajectory changes its qualitative behaviour from one that spirals into a fixed period-1 orbit (i.e., fixed point corresponding to the case of averaged model) to one that spirals away from it. As shown in Fig. 6.10, the stability boundary curves obtained from cycle-by-cycle circuit simulations agree with those of Fig. 6.3, obtained from the averaged model.

6.6 Experimental Verification

We have constructed an experimental circuit for verifying the transition from stable equilibrium states (fixed points), through limit cycles and quasi-periodic orbits, to chaotic attractors. The circuit is shown in Fig. 6.11 (a).

The variation of μ and K is made by adjusting R_μ and R_K in the circuit. To maintain conciseness in this paper, we exemplify in Figs. 6.12 (a) through (d), the qualitative change of the behaviour of the system as K is increased. Specifically, the system goes from stable operation to chaotic operation, via limit cycles and quasi-periodic orbits.

In showing the quasi-periodic orbit and chaotic orbit, we highlight a Poincaré section on the CRO by using a simple circuit that compares the value of the y-input with a pre-set value, and generates a pulse to the z-input of the CRO

whenever the y-input is equal to the pre-set value. This simple compare circuit is shown in Fig. 6.11 (b). The CRO trace will momentarily brightens when the CRO's z-input receives a pulse. Thus, the CRO is able to highlight a Poincaré section on top of the attractor being displayed.

For the quasi-periodic orbit, we clearly see that the Poincaré section resembles a closed loop around the rim of the torus, whereas for the chaotic orbit, the Poincaré section contains some scattered points.

6.7 Conclusion

The Ćuk converter studied is a very popular design choice for DC/DC converters, but its nonlinear dynamics is seldom seriously analyzed. Previous (probably the only known) attempts in studying the nonlinear dynamics of this converter have focused on fixed-frequency current-mode control [16, 17], which permits a describing discrete-time iterative map to be used for analysis. In this chapter, we have extended the study to a different mode of control which is based on a free-running or self-oscillating loop.

Due to their simplicity, free-running switching converters are commonly used in the construction of low-cost power supplies. For simple free-running buck, boost and buck-boost types of converters, only fixed points and limit cycles are possible. However, for higher-order free-running converters, such as those employing the Ćuk, SEPIC and Zeta converters, quasi-periodicity and chaos are possible. In this chapter, we have examined in particular the nonlinear behaviour of a free-running Ćuk converter. Analysis of the describing autonomous equations reveals that the system loses stability via a Hopf bifurcation. Our study has been carried out in three phases. We first employ an analytical model to predict possible onsets of Hopf bifurcation by studying the movement of the complex eigenvalues of system's Jacobian at the equilibrium point as some chosen parameters are changed. In particular, we have observed the way the system loses stability using the INSITE software, which can be used to generate trajectories for any given dynamical system. Our second phase of study has been resorted to computer simulations of the actual system using an exact piecewise-switched model. The bifurcation from a stable equilibrium state, through limit cycles and quasi-periodic orbits, to chaos has been observed. Finally, we have confirmed the predicted Hopf bifurcation and the simulated sequence of changes in qualitative behaviour by experimental measurements of the actual circuit.

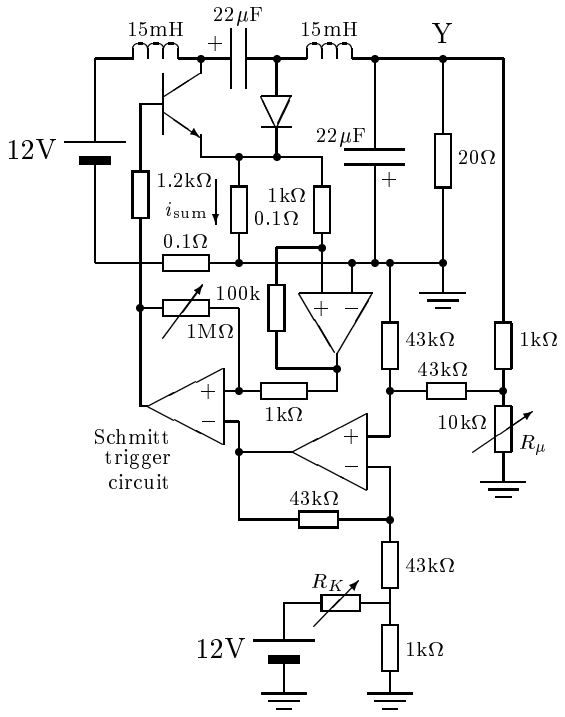

(a)

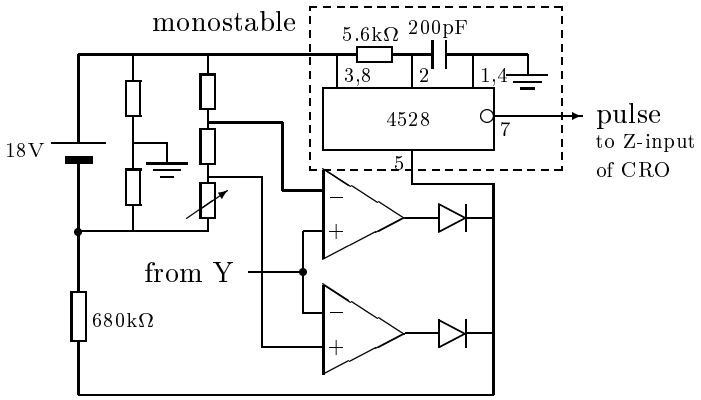

(b)

Figure 6.11: (a) Experimental free-running Ćuk converter circuit; (b) circuit for highlighting Poincaré section. The x-input of CRO is taken from voltage across the 0.1Ω that senses the input inductor current using a differential probe. The y-input of the CRO is taken from output voltage at terminal Y.

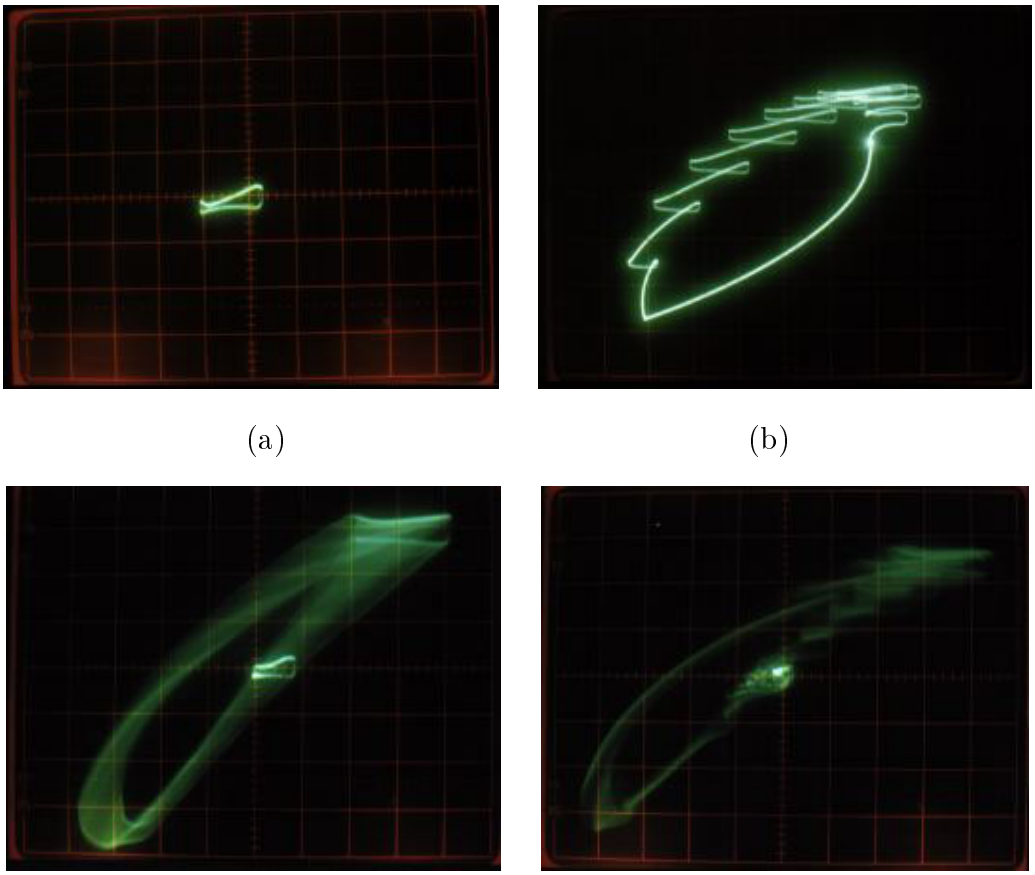

(a) (b)

(c) (d)

Figure 6.12: Phase portraits from autonomous Ćuk converter showing (a) stable period-1 orbit (equilibrium state); (b) limit cycle; (c) quasi-periodic orbit; (d) chaotic orbit. Poincaré section highlighted in (b), (c) and (d). (Horizontal scale: 0.5V/div, vertical scale: 0.2V/div.)

Chapter 7

Synchronization of Autonomous DC/DC Ćuk Converters

7.1 Introduction

Since Pecora and Carroll [116, 117] demonstrated the possibility of synchronizing two chaotic systems, many investigations have been carried out to explore the properties and applications of chaos synchronization in a range of nonlinear circuits and systems [118]–[125]. For power electronics systems, although chaos and bifurcation have been identified in a number of practical converter configurations, e.g., DC/DC converters [10]–[29], not much has been reported on the possibility of chaos synchronization. Furthermore, recent success in applying chaos to communications may suggest possible use of chaotic power converters for such applications. If power converters could be used to transmit messages, then we may speculate, however immature at this stage, that future distributed power systems may be designed to serve the dual function of a power supply system and a medium of communication. Of course, a prerequisite is a well informed operation of power converters in chaotic regimes for which further investigation is still needed.

In this chapter, we consider a very common converter circuit, namely, the Ćuk converter, and in particular its synchronization property when operating chaotically under a very simple free-running current-programmed scheme [30, 112]. The circuit configured as such can be modelled as a third-order autonomous system. Our purpose is to show that two such autonomous systems, connected in a drive-response configuration similar to that considered by Pecora and Carroll [116, 117], can synchronize. We first show, both mathematically and numerically,

that the conditional Lyapunov exponents (CLE's) of the coupled system under study are negative, and hence synchronization is possible. Finally, computer simulations of the actual system confirm the predicted synchronization phenomenon.

7.2 Review of Drive-Response Configuration

One essential property of a chaotic system is that trajectories starting from nearby initial conditions diverge exponentially with time and quickly become uncorrelated. It is therefore non-trivial to show that two chaotic systems coupled through a chaotic signal can be in perfect synchronization. In Pecora and Carroll [116, 117], such a possibility was demonstrated. The basic idea of Pecora and Carroll can be briefly described as follows.

Consider an n-dimensional dynamical system which is described by a state equation of the form

$$\dot{\bar{x}} = f(\bar{x}(t)), \tag{7.1}$$

where $\bar{x} = [x_1\ x_2\ \cdots\ x_n]^T$. The system is divided into two sub-systems ($n = m + k$) in an arbitrary way. Accordingly the state vector $\bar{x}$ is partitioned as $\bar{x} = [\bar{x}_D\ \bar{x}_R]^T$, where $\bar{x}_D$ is an m-dim vector and $\bar{x}_R$ is a k-dim vector corresponding to a drive sub-system and a response sub-system respectively, i.e., $\bar{x}_D = [x_1\ x_2\ \cdots\ x_m]^T$ and $\bar{x}_R = [x_{m+1}\ x_{m+2}\ \cdots\ x_n]^T$. Then, equation (7.1) can be rewritten as

$$\begin{cases} \dot{\bar{x}}_D &= g(\bar{x}_D, \bar{x}_R) \\ \dot{\bar{x}}_R &= h(\bar{x}_D, \bar{x}_R), \end{cases} \tag{7.2}$$

where $g(\bar{x}) = [f_1(\bar{x})\ ...\ f_m(\bar{x})]^T$ and $h(\bar{x}) = [f_{m+1}(\bar{x})\ ...\ f_n(\bar{x})]^T$.

An identical copy of the system is constructed and driven by $\bar{x}_D$ taken from the above original system. We let the state variables of this new system be $\bar{x}'$, which is likewise partitioned, i.e., $\bar{x}' = [\bar{x}'_D\ \bar{x}'_R]^T$. The dynamics of this second system is thus described by

$$\begin{cases} \dot{\bar{x}}'_D &= g(\bar{x}_D, \bar{x}'_R) \\ \dot{\bar{x}}'_R &= h(\bar{x}_D, \bar{x}'_R). \end{cases} \tag{7.3}$$

Since $\bar{x}'_D = \bar{x}_D$, we may ignore the dynamics of $\bar{x}'_D$, and hence describe the second system by only its response sub-system equation, i.e.,

$$\dot{\bar{x}}'_R = h(\bar{x}_D, \bar{x}'_R). \tag{7.4}$$

Now, the original system (7.2) and the second response sub-system (7.4) constitute a complete "coupled" system.

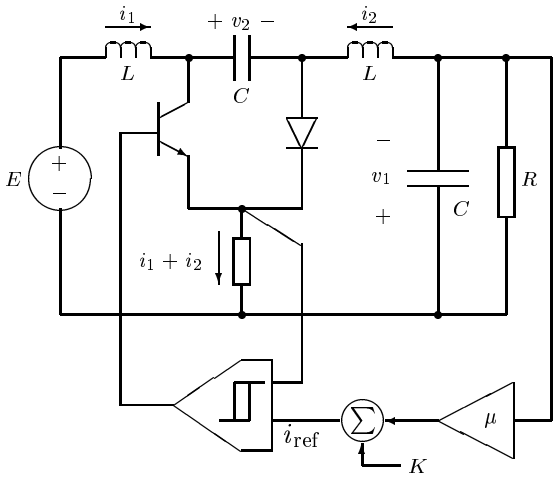

Figure 7.1: Ćuk converter under hysteretic current-mode control.

It is readily shown that if all the Lyapunov exponents of the second response sub-system (7.4), also called conditional Lyapunov exponents (CLE's), are negative, then after the decay of the initial transient, $\bar{x}'_R$ will be exactly in step with $\bar{x}_R$. More precisely, under perfect synchronization, the difference between $\bar{x}'_R$ and $\bar{x}_R$ will tend to zero asymptotically, i.e., $\lim_{t\to\infty} |\bar{x}'_R - \bar{x}_R| = 0$. Alternatively, one may examine the error system that describes the dynamics of $(\bar{x}'_R - \bar{x}_R)$. Letting $\bar{e}_R$ be $(\bar{x}'_R - \bar{x}_R)$, we can write $\dot{\bar{e}}_R(t) = h(\bar{x}_D, \bar{x}'_R) - h(\bar{x}_D, \bar{x}_R)$, or

$$\dot{\bar{e}}_R(t) = h_e(\bar{x}_D, \bar{x}_R, \bar{x}'_R). \tag{7.5}$$

The Lyapunov exponents of this system are also the CLE's. If h_e is linear, we can examine its eigenvalues and conclude that synchronization occurs if the real parts of all these eigenvalues are negative. Note that the real parts of these eigenvalues are also the CLE's. When h_e is nonlinear, we must resort to numerical procedure in order to calculate the CLE's.

For brevity, we refer to the original system as the "drive" system (with state vector $\bar{x}$), and to the second system as the "response" system (with state vector $\bar{x}'$).

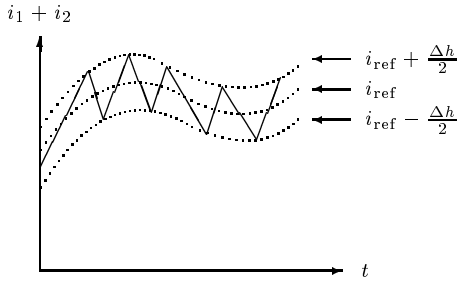

Figure 7.2: Hysteretic current-programming scheme.

7.3 Free-running Current-programmed Ćuk Converter

7.3.1 Piecewise Switched Model

The free-running current-programmed Ćuk converter under study is shown in Fig. 7.1 [30, 112]. The circuit operation can be described as follows. The sum of the inductance currents, i.e., $i_1 + i_2$, is compared with a reference current i_{ref} in a hysteretic fashion. When $i_1 + i_2$ rises above $i_{\text{ref}} + \frac{\Delta h}{2}$, where Δh is the width of a hysteretic band, the switch is turned off. When $i_1 + i_2$ falls below $i_{\text{ref}} - \frac{\Delta h}{2}$, the switch is turned on. The reference current i_{ref} is related to the output voltage v_1 by a feedback equation of the form

$$i_{\text{ref}} = K - \mu v_1, \tag{7.6}$$

where K and μ are the control parameters. Figure 7.2 illustrates this current-programming scheme.

The converter itself can be represented by the following set of state-space equations, where s=1 when the switch is closed and s=0 when the switch is open:

$$\begin{cases} \dfrac{di_1}{dt} &= -\dfrac{(1-s)v_2}{L} + \dfrac{E}{L} \\ \dfrac{di_2}{dt} &= \dfrac{v_2 s}{L} - \dfrac{v_1}{L} \\ \dfrac{dv_1}{dt} &= \dfrac{i_2}{C} - \dfrac{v_1}{CR} \\ \dfrac{dv_2}{dt} &= \dfrac{(1-s)i_1}{C} - \dfrac{i_2 s}{C}. \end{cases} \tag{7.7}$$

The above equations constitute an "exact" piecewise switched model for the Ćuk converter, which will be used for computer simulations of the actual system to be reported in a later section.

7.3.2 State-space Averaged Model

The state-space averaging approach has been widely used for modelling DC/DC converters [3]. For the Ćuk converter, the state-space averaged model has the same form as (7.7), with s replaced by the duty cycle δ, which is the fraction of the switching period, for which the switch is closed. From (7.6), we see that the current-programming scheme essentially forces $i_1 + i_2$ to be linearly related to v_2. If Δh is sufficiently small, we can write

$$i_1 + i_2 = K - \mu v_1. \tag{7.8}$$

The closed-loop system is thus reduced to third order, and the state-space averaged model becomes

$$\begin{cases} \dfrac{di_2}{dt} &= \dfrac{v_2\delta}{L} - \dfrac{v_1}{L} \\ \dfrac{dv_1}{dt} &= \dfrac{i_2}{C} - \dfrac{v_1}{CR} \\ \dfrac{dv_2}{dt} &= \dfrac{(1-\delta)(K-\mu v_1)}{C} - \dfrac{i_2}{C}, \end{cases} \tag{7.9}$$

where δ is the duty cycle. From (7.8), we get $d(i_1 + i_2)/dt = -\mu dv_1/dt$. Substitution of the involving derivatives gives

$$\delta = \frac{1}{2} - \frac{\dfrac{\mu L}{C} i_2 - \left(1 + \dfrac{\mu L}{CR}\right) v_1 + E}{2v_2}, \tag{7.10}$$

which must satisfy $0 < \delta < 1$. Finally, putting (7.10) into (7.9) results in the following set of autonomous state equations that describes the dynamics of the free-running current-programmed Ćuk converter:

$$\begin{cases} \dfrac{di_2}{dt} &= -\dfrac{\mu i_2}{2C} - \left(1 - \dfrac{\mu L}{CR}\right)\dfrac{v_1}{2L} + \dfrac{v_2}{2L} - \dfrac{E}{2L} \\ \dfrac{dv_1}{dt} &= \dfrac{i_2}{C} - \dfrac{v_1}{CR} \\ \dfrac{dv_2}{dt} &= -\dfrac{i_2}{C} + \left(\dfrac{K-\mu v_1}{2C}\right)\left(1 + \dfrac{\dfrac{\mu L}{C} i_2 - \left(1 + \dfrac{\mu L}{CR}\right) v_1 + E}{v_2}\right). \end{cases} \tag{7.11}$$

Remarks — The above representation is valid only when there is no saturation of the duty cycle δ of the converter, i.e., $0 < \delta < 1$. However, in the real system, saturation does occur, especially when it is operating in a chaotic regime. Thus, when we use (7.11) to calculate the corresponding CLE's, we must take into account the saturation of the duty cycle δ.

7.3.3 Dimensionless Equation

Equation (7.11) can be put in a dimensionless form for the sake of simplicity. Define the dimensionless state variables as follows:

$$x_1 = \frac{Ri_2}{E},\ x_2 = \frac{v_1}{E},\ x_3 = \frac{v_2}{E}. \tag{7.12}$$

Also, define the dimensionless time and other parameters as follows:

$$\tau = \frac{Rt}{2L},\ \xi = \frac{L/R}{CR},\ \kappa_1 = \mu R,\ \kappa_0 = \frac{KR}{E}. \tag{7.13}$$

Direct substitution of these new dimensionless variables, time, and parameters in the autonomous equation (7.11) gives the following dimensionless autonomous equations:

$$\begin{cases} \dfrac{dx_1}{d\tau} &= -\xi\kappa_1 x_1 - (1-\kappa_1\xi)x_2 + x_3 - 1 \\ \dfrac{dx_2}{d\tau} &= 2\xi(x_1 - x_2) \\ \dfrac{dx_3}{d\tau} &= -2\xi x_1 + \xi(\kappa_0 - \kappa_1 x_2)\left(1 + \dfrac{\kappa_1\xi x_1 - (1+\kappa_1\xi)x_2 + 1}{x_3}\right). \end{cases} \tag{7.14}$$

In the next section, we will use this set of dimensionless equations to predict the synchronization property of chaotic Ćuk converters under free-running current-mode control.

7.4 Chaos Synchronization in Free-running Current-programmed Ćuk Converters

7.4.1 Construction of Drive-Response System

We consider now two identical Ćuk converters, arranged in the drive-response configuration described in Section 7.2. Let x_1, x_2 and x_3 be the state variables of the drive converter, and x_{1r}, x_{2r} and x_{3r} be those of the response converter. In particular, we use x_3, i.e., the dimensionless equivalence of capacitor voltage v_2, as the driving signal.

The fifth-order coupled system is thus completely described by the set of drive converter equations, i.e., (7.14), and the set of response converter equations which is

$$\begin{cases} \dfrac{dx_{r1}}{d\tau} &= -\xi\kappa_1 x_{r1} - (1-\kappa_1\xi)x_{r2} + x_3 - 1 \\ \dfrac{dx_{r2}}{d\tau} &= 2\xi(x_{r1} - x_{r2}), \end{cases} \tag{7.15}$$

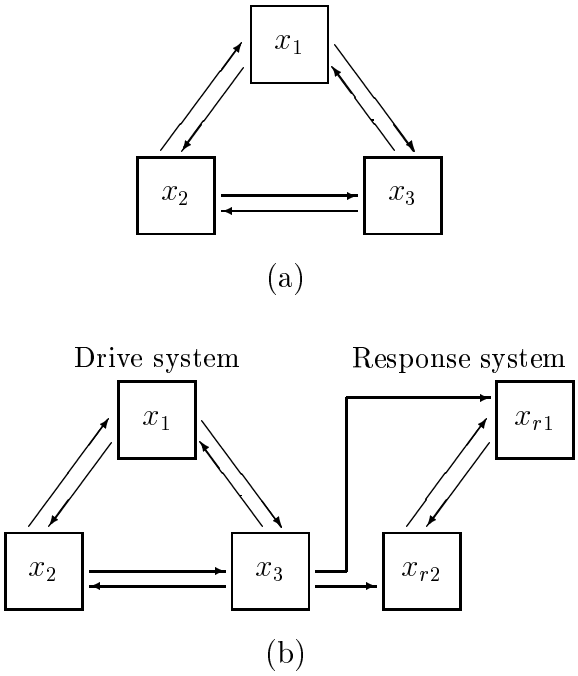

Figure 7.3: Interaction of state variables in (a) isolated converter; (b) coupled converters in drive-response configuration.

where subscript r denotes the response system variables. Figure 7.3 (a) describes the interaction of the variables for the case of an isolated converter, and Fig. 7.3 (b) describes that for the case of the two converters being connected in the drive-response configuration.

7.4.2 Derivation of the Conditional Lyapunov Exponents

As mentioned in Section 7.2, synchronization may be examined in terms of the error system, i.e., equation (7.5). For the system under study, the error system is linear. Letting $e_1 = x_1 - x_{r1}$ and $e_2 = x_2 - x_{r2}$, we can describe the error dynamics by

$$\begin{bmatrix} \frac{de_1}{d\tau} \\ \frac{de_2}{d\tau} \end{bmatrix} = \begin{bmatrix} -\xi\kappa_1 & -(1-\kappa_1\xi) \\ 2\xi & -2\xi \end{bmatrix} \begin{bmatrix} e_1 \\ e_2 \end{bmatrix}. \tag{7.16}$$

For brevity, we let $e = [e_1\ e_2]^T$ and put (7.16) as

$$\dot{e}(\tau) = Ae(\tau), \tag{7.17}$$

where A is shown in (7.16). Our objective is to find the CLE's in order to determine if synchronization is possible. As mentioned in Section 7.2, the real parts of the eigenvalues of the error system are in fact the CLE's we need to find

[126]–[127]. Let λ_1 and λ_2 be the eigenvalues of A. For this linear system, we can readily show that

$$\lambda_{1,2} = -\frac{(2\xi + \kappa_1\xi) \pm \sqrt{(2\xi + \kappa_1\xi)^2 - 8\xi}}{2}. \tag{7.18}$$

Clearly, for $(2\xi + \kappa_1\xi)^2 \geq 8\xi$, both eignevalues are real and negative. For $(2\xi + \kappa_1\xi)^2 < 8\xi$, moreover, the real part of both eigenvalues is negative for all positive values of κ_1 and ξ, i.e.,

$$\Re(\lambda_i) < 0 \qquad \text{for all } \xi, \kappa_1 > 0. \tag{7.19}$$

Thus, by choosing suitable values of ξ, κ_1 and κ_0, the drive system can be set to operate in chaotic regime (characterized by one positive Lyapunov exponent) and the response system will also be driven to chaos when synchronization occurs.

7.4.3 Numerical Calculation of the Conditional Lyapunov Exponents

In the foregoing sub-section, we have predicted that chaos synchronization is possible in the autonomous Ćuk converter. However, since the foregoing analysis is based on an averaged model of the converter which does not take into account the saturation of the duty cycle, the values of CLE's so obtained, i.e., those from (7.18), remain to be verified.

In this sub-section, we re-calculate the CLE's numerically, taking into account the saturation effect. In other words, we consider the realistic case in which the switch can remain in the ON (or OFF) state continuously, as a result of the action of the control scheme. Specifically, the describing equation for $\delta = 1$ is

$$\begin{cases} \dfrac{dx_1}{d\tau} &= 2(x_3 - x_2) \\ \dfrac{dx_2}{d\tau} &= 2\xi(x_1 - x_2) \\ \dfrac{dx_3}{d\tau} &= -2\xi x_1 \end{cases} \tag{7.20}$$

and that for $\delta = 0$ is

$$\begin{cases} \dfrac{dx_1}{d\tau} &= -2x_2 \\ \dfrac{dx_2}{d\tau} &= 2\xi(x_1 - x_2) \\ \dfrac{dx_3}{d\tau} &= -2\xi x_1 + 2\xi(\kappa_0 - \kappa_1 x_2). \end{cases} \tag{7.21}$$

κ_1	$\Re(\lambda_i)$ from (7.18)	$\Re(\lambda_i)$ from numerical calculation
0.5	-0.125	-0.12
1.0	-0.15	-0.13
1.5	-0.175	-0.15
2.0	-0.20	-0.17

Table 7.1: Comparsion of CLE's from averaged model and by numerical calculation incorporating duty cycle saturation.

Essentially, we need to include two extra subroutines to generate the flow according to (7.20) and (7.21), when the calculated duty cycle exceeds one and falls below zero, respectively.

Actual numerical calculation has been done by using the INSITE software [115], which employs a Gram-Schmidt orthonormalization procedure for calculating Lyapunov exponents. In particular, we fix ξ at 0.1 which corresponds to a realistic practical choice, and for a range of κ_1 we have numerically calculated the corresponding CLE's using INSITE. The results are compared to those obtained from (7.18). As shown in Table 7.1, the numerical CLE's are all negative and reasonably close to those obtained from (7.18). We may thus conclude that chaos synchronization is indeed possible in the free-running current-programmed Ćuk converter under study. Verification is yet to be sought using computer simulation of the actual converter circuits.

Remarks — Up to this point, validity of the averaged model has been assumed. However, as studied in [30], averaged models are only good up to the point of losing stability. Thus, as long as synchronization is maintained, the averaged model for the error system is still valid, and in this case, synchronization should be predicted by the averaged model. The converse is not true, however, and one cannot draw any definite conclusion if the averaged model predicts failure of synchronization.

7.5 Computer Simulations

7.5.1 "Exact" Time-domain Simulations for Piecewise Switched Model

In this section, we present "exact" simulations of the system under study, which consists of two identical free-running current-programmed Ćuk converters connected in the drive-response configuration, as described previously. Specifically, the drive system is exactly the circuit shown in Fig. 7.1, and the response system is constructed with the middle capacitor (the one connecting the two inductors) replaced by a voltage-controlled voltage source which copies the value of v_2 from the drive system.

Based on the piecewise switched model developed in Section 7.3.1, we have simulated the cycle-by-cycle waveforms of the actual circuit, from which the phase portraits of the drive and response systems are obtained. The values of the parameters used are $L = 0.01$H, $C = 1000\mu$F, $R = 10\Omega$, $E = 12$V, $\Delta h = 0.5$A, $\mu = 0.2$ and $K = 40$. These values correspond to $\xi = 0.1$, $\kappa_1 = 2.0$ and $\kappa_0 = 33.3$.

For ease of reporting, we use i_1, i_2, v_1 and v_2 to denote the variables of the drive circuit, consistent with Fig. 7.1, and i_{1r}, i_{2r}, v_{1r} and v_{2r} to denote those of the response circuit. The following results are presented:

1. Figure 7.4 shows the chaotic trajectories of the drive system and the response system after discarding the points in the transient period.
2. Figure 7.5 shows the curves of i_2 versus i_{r2}, and of v_1 versus v_{r1}, which verify that chaos synchronization is achieved.
3. For comparison, we have simulated the uncoupled system. The result is shown in Fig. 7.6.

7.5.2 PSPICE Simulations

The above simulations have verified the possibility of chaos synchronization in the theoretical circuit consisting of ideal switches and zero-delay switching. For further verification, we consider real MOSFET switches and practical gate drivers, and use PSPICE to simulate the system. Moreover, a voltage-controlled voltage source is again used to establish the coupling connection. The parameters used

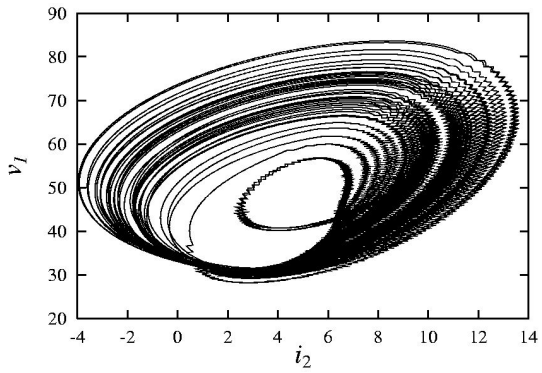

(a)

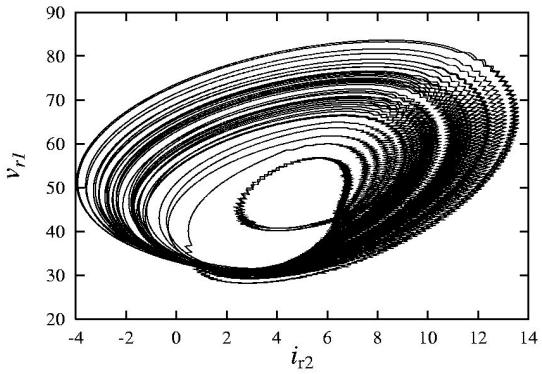

(b)

Figure 7.4: Chaotic trajectory from exact time-domain simulation of (a) drive system; and (b) response system.

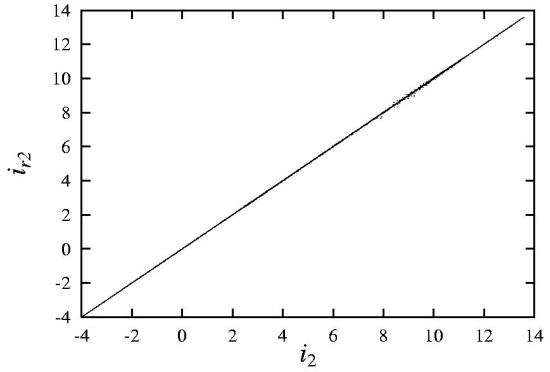

(a)

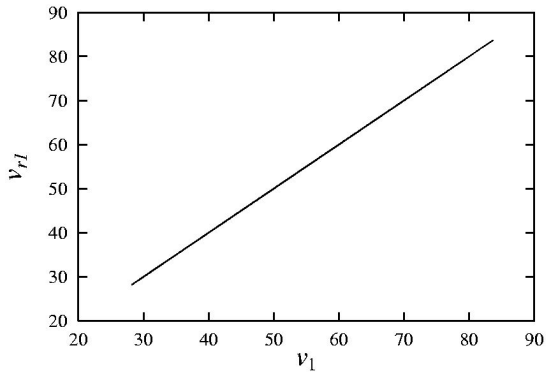

(b)

Figure 7.5: Graphical representation of synchronization from exact time-domain simulation. (a) i_{r2} versus i_2; and (b) v_{r1} versus v_1.

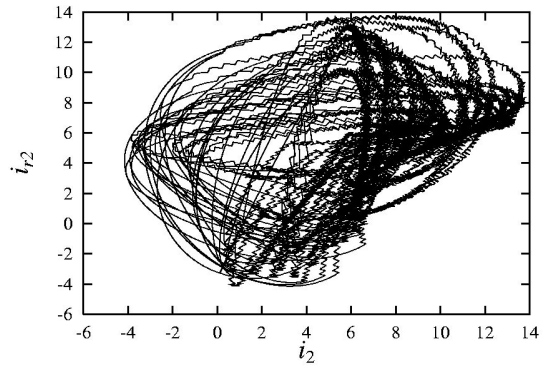

(a)

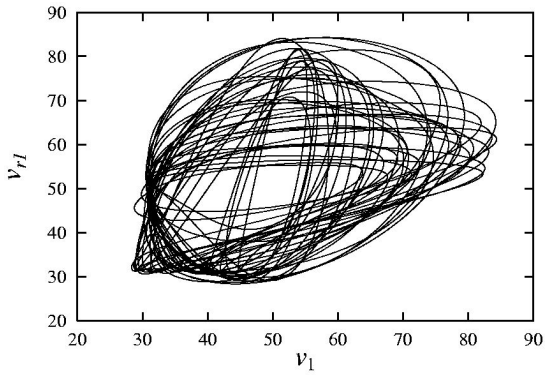

(b)

Figure 7.6: Plots of (a) i_{r2} versus i_2; and (b) v_{r1} versus v_1 for the uncoupled converters.

Component	Tolerance
L	3%
C	3%
R	5%
μ	10%

Table 7.2: Tolerance limits of circuit parameter mismatch.

here are identical to those used in Section 7.5.1. The results are shown in Figs. 7.7 and 7.8, which are in perfect agreement with those obtained in Section 7.5.1.

7.5.3 Effects of Parameter Mismatch

So far, we have assumed identical parameter values for both the drive and the response systems. In practice, parameter values in the two systems do vary, however small. It is therefore of interest to study the effects of parameter mismatch on synchronization. This mismatch problem can be translated formally to the study of two slightly different systems [128]:

$$\dot{\bar{x}} = f(\bar{x}(t), \mathbf{p}) \tag{7.22}$$

$$\dot{\bar{x}} = f(\bar{x}(t), \mathbf{p} + \delta\mathbf{p}), \tag{7.23}$$

where $\mathbf{p}$ is a vector of parameters, and $\delta\mathbf{p}$ is a vector of the differences in the values of $\mathbf{p}$ between the two systems. If we denote the variables for the response part of the two systems by $\bar{x}_R$ and $\bar{x}'_R$, $\bar{y}_R = \bar{x}'_R - \bar{x}_R = [y_{R1}\ y_{R2}\ \cdots y_{Rn}]^T$, similar to what was discussed in Section 7.2, then the condition for synchronization under a mismatch condition becomes $\lim_{t\to\infty} |y_{Ri}| \leq \epsilon\ \forall i$, where ϵ is a small number ($\epsilon_i \ll 1$).

In this chapter, instead of a formal mathematical study as outlined above, we examine the limits of parameter mismatch by computer simulations. Specifically, we keep the circuit parameters of the drive system unchanged, and vary those of the response system one at a time. Table 7.2 shows the limits of parameter mismatch, beyond which synchronization cannot be maintained. Both "exact" computer simulations and PSPICE simulations report the same findings.

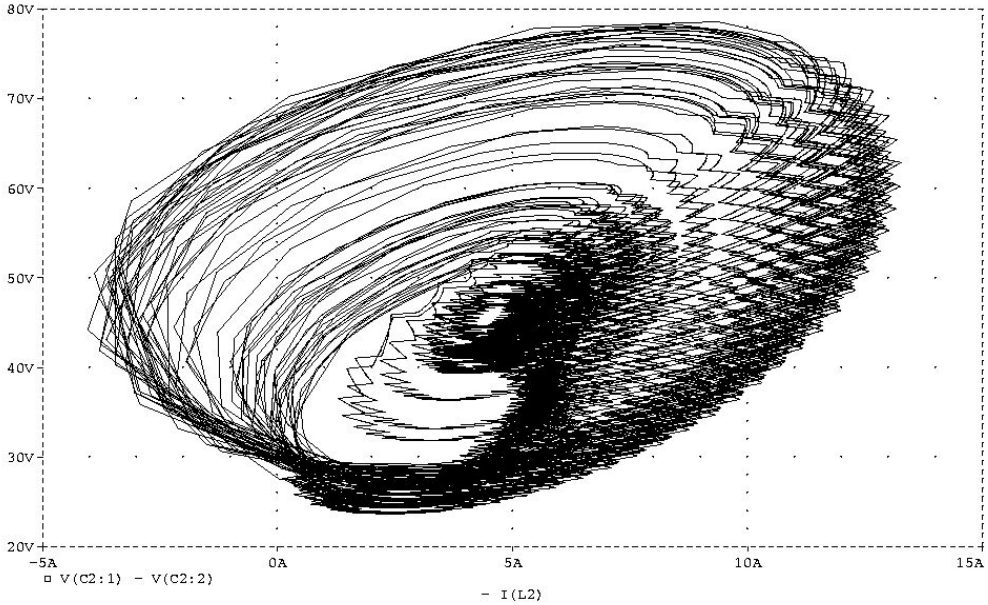

(a)

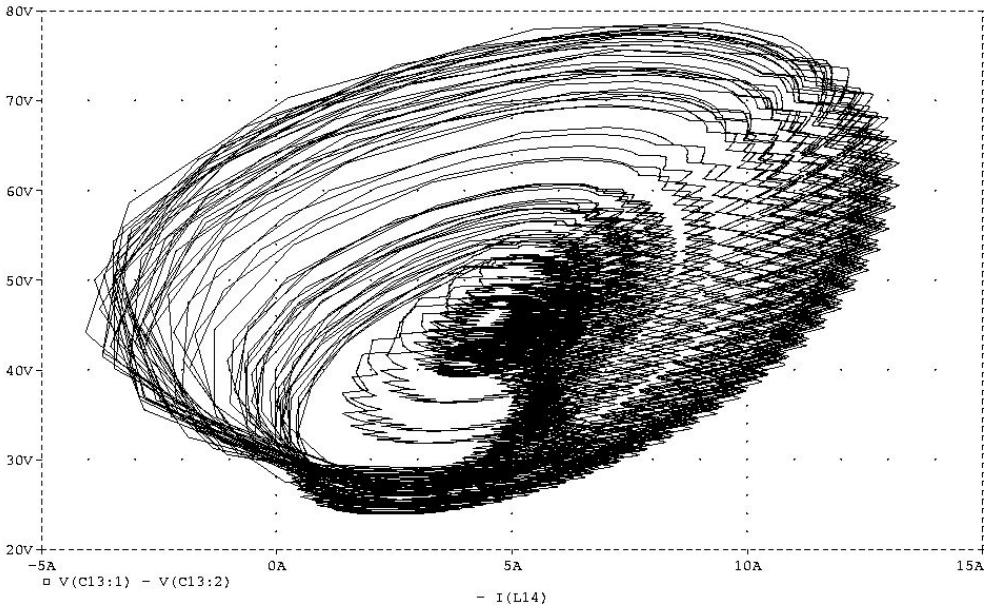

(b)

Figure 7.7: Chaotic trajectory from PSPICE simulation of (a) drive system; and (b) response system.

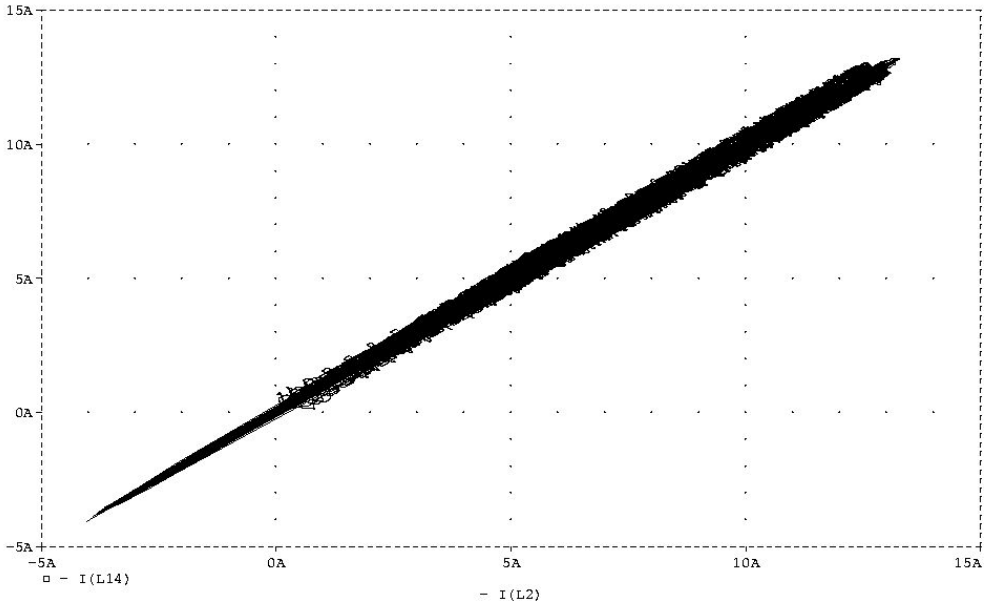

(a)

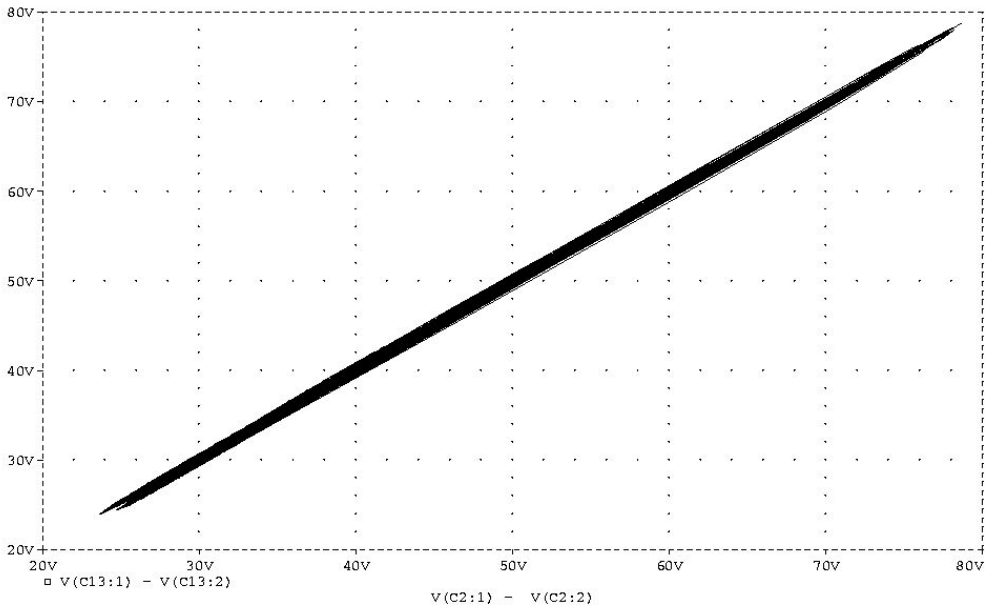

(b)

Figure 7.8: Graphical representation of synchronization from PSPICE simulation. (a) i_{r2} versus i_2; and (b) v_{r1} versus v_1.

7.6 Conclusion

Power electronics circuits, due to their switching nonlinearity, exhibit a wide range of nonlinear and chaotic behaviours. In recent years, some results concerning bifurcations and chaos have been reported in power electronics systems, and more are yet to be uncovered. In the nonlinear system literature, recent evidence of potential application in communication has arisen tremendous interest in chaos synchronization and dynamics of coupled systems. In this chapter, we have considered, for the first time, power electronics circuits within a chaos synchronization context. We have shown, in a simple drive-response connected system of chaotic power converters, the possibility of synchronization. While any potential use of chaotic power converters remains uncertain, the present study provides a first evidence of synchronizing chaotic power converters. If power converters, apart from their normal power supply function, could be used to transmit messages, then future distributed power systems may serve the dual function of a power supply system and a medium of communication.

Chapter 8

Conclusions and Suggestions for Future Research

In the past decades, chaos has been regarded as a topic of academic research. It is now becoming a topic of practical importance in various disciplines. Researchers and scientists in different disciplines are working on nonlinear dynamics and chaos. It is clear that bifurcation and chaos theory will continue to play a vital role in the development of science in the future. For instance, recent work shows that researchers have succeeded in applying chaos control in physical and biological systems [129]–[134].

In this thesis, focus is put on the identification and analysis of nonlinear phenomena in DC/DC switching converters. A number of bifurcation and chaotic phenomena have been reported in the previous chapters. In this concluding chapter, important results that have been obtained in the study are summarized, along with some suggestions for future work on nonlinear phenomena in power electronic circuits.

8.1 Contributions of the Thesis

In this section, we summarize the main contributions of this thesis under the following three main topics:

1. Bifurcation Behaviour in Parallel-connected DC/DC Converters.
2. Hopf Bifurcation and Chaos in a Free-running Current-controlled Ćuk Converter
3. Synchronization of Autonomous Chaotic Ćuk Converters

These topics are detailed in the following three subsections.

8.1.1 Bifurcation Behaviour in Parallel-connected DC/DC Converters

The bifurcation behaviour exhibited by parallel-connected DC/DC converters under a master-slave current control has been investigated. Paralleling power converter systems are becoming popular, but their nonlinear phenomena were rarely studied. Computer simulations and experiments have been performed to capture the bifurcation phenomena when some chosen parameters are varied. For parallel-connected buck converters, it is found that variation of the voltage feedback gains leads to standard period-doubling bifurcation, and variation of the current sharing ratio leads to border-collision bifurcation. For parallel-connected boost converters, it is found that variations of the voltage feedback gains and the current sharing ratio lead to standard Neimark-Sacker bifurcation. Furthermore, analysis has been performed, based on an iterative discrete-time map and its Jacobain, to explain the bifurcations observed in the simulations and experiments.

8.1.2 Hopf Bifurcation and Chaos in a Free-running Current-controlled Ćuk Converter

An autonomous free-running Ćuk converter has been used as an example of investigation to autonomous converters. Analysis of the nonlinear state equations shows that the system loses stability via a supercritical Hopf bifurcation. The boundary of stability is derived and local trajectories of motion studied. Exact computer simulations of the system reveal the typical Hopf bifurcation from a stable fixed point to chaos, via limit cycles and quasi-periodic orbits. Experimental measurements have confirmed the bifurcation scenarios.

8.1.3 Synchronization of Autonomous Chaotic Ćuk Converters

For the first time, the synchronization property of chaotic DC/DC converters has been studied. The study includes the derivation of describing differential equations and the conditional Lyapunov exponents of the synchronizing system based on the model differential equations. It is found that all the conditional Lyapunov exponents are negative for certain chosen parameters, and hence synchronization

is possible in this system. With the drive-response system connected, synchronization has been demonstrated using both exact time-domain simulations and PSPICE simulations. This work may be useful for further development in the exploitation of power converters for communication purposes.

8.2 Suggestions for Future Research

8.2.1 Applications of Chaos in Switching DC/DC Converters

Recently, chaos has found some practical applications in the field of electronic engineering [127]–[128], [135]–[137]. Researchers have attempted to explore possible practical applications of chaos in DC/DC switching converters. In 1996, Deane *et al.* suggested using chaos to improve the electromagnetic interference by "spreading" the noise spectrum [138]. In 1997, Aston *et al.* proposed an application of "targeting" orbits with fewer iterations (i.e., directing trajectories to certain orbits in as little time as possible) [139]. Meanwhile, control of chaos in DC/DC switching converters has become a hot research topic recently. In 1995, Poddar *et al.* attempted to control chaos by targeting the unstable fixed points in every cycle [31]–[32]. Batlle *et al.* made a similar study in 1996 [33], and succeeded in stabilizing unstable periodic orbits in a PWM controlled buck converter by using time-delayed feedback [34]. Further development in the area of using chaos is expected in the near future.

8.2.2 Control of Bifurcation in DC/DC Switching Converters

Power electronic circuits are designed for stable operations. In most practical situations, the required stable operation is a period-1 operation. In DC/DC converters, for instance, the design must guarantee stable operation at switching frequencies, and any subharmonic, quasi-periodic or chaotic operation is regarded as being undesirable and should be avoided. Thus, the design objective must include the prevention of any bifurcation within the intended operation range.

After a few decades of identification and analysis work on chaotic behaviour in DC/DC switching converters, researchers and engineers begin to make use of the research results in the design of practical circuits [140]. In the analysis of

nonlinear behaviour of DC/DC converters, boundaries of the stable operation region can be found. When sufficient data are collected, design curves can be constructed to provide useful information for avoiding bifurcation or instability in the circuits. Therefore, research on how to design a converter such that it is "bifurcation-free" is an important area from the practical standpoint. Furthermore, new possibilities in operating power electronics systems may be opened up.

8.2.3 Theoretical Analysis of Bifurcation and Chaos in DC/DC Converters

In the literature, numerous reports about identification and analysis of bifurcation and chaos in DC/DC converters can be found. However, establishment of rigorous mathematical proof of bifurcation behaviour such as period-doubling, Neimark-Sacker bifurcation and border-collision bifurcation in power electronic circuits is still largely insufficient [25], [141]–[142]. There is much room for further research in this aspect.

Mathematical tools for analyzing nonlinear systems, such as Shil'nikov's method, Melnikov's method, Schwarzian derivative, harmonic balance and Floquet method, may be used to analyze the bifurcation and chaotic behaviour exhibited by DC/DC converters rigorously. Of course, the main issue is the identification of suitable tools for application to the analysis of DC/DC converters.

8.2.4 Identification and Analysis of Nonlinear Phenomena in Parallel-connected Converters

In the previous chapters, bifurcation and chaos in parallel-connected DC/DC converters under a master-slave current sharing scheme were studied. When the number of converters increases, the complexity of the system escalates rapidly. The number of parameters that affects the dynamics of the system also increases. It is therefore meaningful to probe into nonlinear dynamics of parallel-connected systems with larger number of DC/DC converters.

As parallel converter systems gain popularity in power electronics applications, there is strong motivation for better understanding of their nonlinear dynamics and bifurcation behaviour [143]. Our research results will be very useful to power electronics engineers for achieving better and more reliable design.

8.2.5 Possible Applications of Chaotic Converters for Communications

In the past decade, there has been significant interest in exploiting chaotic dynamics in communications [118]–[125]. Since chaotic signals are broadband in nature, they spread the spectrum of the information signals through suitable modulation processes. The advantages of spectrum spreading are that:

- it combats the effects of jamming, multi-user interference, and multipath propagation;
- it hides a message in a noise-like carrier by transmitting it at low power; and
- it ensures message privacy in the presence of eavesdroppers.

In Chapter 7, we have demonstrated the possibility of synchronization in two chaotic autonomous DC/DC converters. If power converters could offer extra communication functions while providing their normal power conversion functions, then it would make sense to design such chaotic converters with dual purposes. However, up to now no chaotic power converters have been used in practical systems. Chaotic operation remains an unverified mode of operation which is unacceptable from the point of view of power electronics engineers. Therefore, the pre-requisite for using chaotic converters for communication is safe and reliable operation in chaotic regimes for which further investigation is still needed.

In the actual implementation, there are still some practical problems. First, the presence of channel noise and parameter mismatches will possibly cause loss of synchronization. Another problem is the inter-symbol interference that may occur when there are multiple users. We need to solve all these problems before we can use chaotic converters for communications in practice.

Publications

Journal Papers

1. C.K. Tse, Y.M. Lai and H.H.C. Iu, "Hopf Bifurcation and Chaos in a Free-running Current-controlled Ćuk Switching Regulator," *IEEE Trans. Circ. Syst. Part I,* Vol. 47, No. 4, pp. 448–457, Apr 2000.

2. H.H.C. Iu and C.K. Tse, "A Study of Synchronization in Chaotic Autonomous Ćuk DC/DC Converters," *IEEE Trans. Circ. Syst. Part I,* Vol. 47, No. 6, pp. 913–918, Jun 2000.

3. H.H.C. Iu and C.K. Tse, "Bifurcation Behaviour in Parallel-connected Buck Converters," *IEEE Trans. Circ. Syst. Part I,* to appear.

4. H.H.C. Iu, C.K. Tse, V. Pjevalica and Y.M. Lai, "Bifurcation Behaviour in Parallel-connected Boost Converters," *Int. J. Cir. Theor. Appl.,* to appear.

5. H.H.C. Iu, C.K. Tse, V. Pjevalica and Y.M. Lai, "Instability and Bifurcation in Parallel-connected Buck Converters Under a Master-slave Current Sharing Scheme," *IEEE Trans. Power Electron.,* submitted.

International Conference Papers

6. C.K. Tse, Y.M. Lai and H.H.C. Iu, "Hopf Bifurcation and Chaos in a Hysteretic Current-controlled Ćuk Regulator," *IEEE Power Electron. Specialists Conf. Rec.,* Fukuoka, Japan, pp. 1091–1097, May 1998.

7. H.H.C. Iu and C.K. Tse, "A Study of Synchronization in Chaotic Autonomous Ćuk DC/DC Converters," *Proc. of the IEEE Int'l Symp. Circ. Sys.,* Orlando, USA, pp. V266–V269, May 1999.

8. H.H.C. Iu and C.K. Tse, "Instability and Bifurcation in Current-sharing Switching Regulators," *Proc. of Int'l Symp. Nonlin. Th. Appl.,* Hawaii, USA, pp. 101–106, Nov 1999.

9. H.H.C. Iu and C.K. Tse, "Instability and Bifurcation in Parallel-connected Buck Converters Under a Master-slave Current Sharing Scheme," *IEEE Power Electron. Specialists Conf. Rec.,* Galway, Ireland, pp. 708–713, Jun 2000.

10. H.H.C. Iu and C.K. Tse, "Bifurcation in Parallel-connected Boost DC/DC Converters," *Proc. of the IEEE Int'l Symp. Circ. Sys.,* Gevena, Switzerland, pp. II473–II476, May 2000.

11. H.H.C. Iu, C.K. Tse and Y.M. Lai, "Bifurcation in Current-sharing Parallel-connected Boost DC/DC Converters," *Int'l Power Electron. and Motion Control Conf.,* Beijing, China, pp. 921–924, Aug 2000.

Bibliography

[1] B.K. Bose (Ed.), *Modern Power Electronics: Evolution, Technology and Applications,* New York: IEEE Press, 1992.

[2] D.C. Hamill, "Power Electronics: A Field Rich in Nonlinear Dynamics," in *Proc. 3rd Int. Specialists Workshop on Nonlinear Dynamics of Electronic Systems (NDES'95),* Dublin, Ireland, pp. 165-178, Jul 1995.

[3] R.D. Middlebrook and S. Ćuk, "A General Unified Approach to Modeling Switching Converter Power Stages," *IEEE Power Electronics Specialists Conf. Rec.,* pp. 18–34, 1976.

[4] S. Ćuk and R.D. Middlebrook, "A General Unified Approach to Modeling DC/DC Converters in Discontinuous Conduction Mode," *IEEE Power Electronics Specialists Conf. Rec.,* pp. 36–57, 1977.

[5] R.W. Brockett and J.R. Wood, "Understanding Power Converter Chaotic Behaviour Mechanisms in Protective and Abnormal Modes," *Eleventh Annual Int'l Power Electron. Conf. Rec.,* pp. 115–124, 1984.

[6] D.C. Hamill and D.J. Jefferies, "Subharmonics and Chaos in a Controlled Switched-Mode Power Converter," *IEEE Trans. Circ. Syst. Part I,* Vol. 35, No. 8, pp. 1059–1061, Aug 1988.

[7] J.H.B. Deane and D.C. Hamill, "Instability, Subharmonics and Chaos in Power Electronic Systems," *IEEE Power Electronics Specialists Conf. Rec.,* pp. 34–42, 1989.

[8] J.H.B. Deane and D.C. Hamill, "Analysis, Simulation and Experimental Study of Chaos in the Buck Converter," *IEEE Power Electronics Specialists Conf. Rec.,* pp. 491–498, 1990.

[9] P.T. Krein and R.M. Bass, "Types of Instabilities Encountered in Simple Power Electronics Circuits: Unboundedness, Chattering and Chaos," *IEEE Applied Power Electronics Conf. Rec.,* pp. 191–194, 1990.

[10] D.C. Hamill, J.H.B. Deane and D.J. Jefferies, "Modelling of Chaotic DC/DC Converters by Iterative Nonlinear Mappings," *IEEE Trans. Power Electron.,* Vol. 7, No. 1, pp. 25–36, Jan 1992.

[11] C.K. Tse, "Flip Bifurcation and Chaos in a Three-State Boost Switching Regulator," *IEEE Trans. Circ. Syst. Part I,* Vol. 41, No. 1, pp. 16–23, Jan 1994.

[12] C.K. Tse, "Chaos from a Buck Switching Regulator Operating in Discontinuous Mode," *Int. J. Cir. Theor. Appl.,* Vol. 22, No. 4, pp. 263–278, Jul 1994.

[13] W.C.Y. Chan and C.K. Tse, "On the Form of Control Function That Can Lead to Chaos in Discontinuous Mode DC/DC Converters," *IEEE Power Electronics Specialists Conf. Rec.,* pp. 1317–1322, 1997.

[14] K. Chakrabarty, G. Podder and S. Banerjee, "Bifurcation Behaviour of Buck Converter," *IEEE Trans. Power Electron.,* Vol. 11, No. 3, pp. 439–447, May 1995.

[15] E. Fossas and G. Olivar, "Study of Chaos in the Buck Converter," *IEEE Trans. Circ. Syst. Part I,* Vol. 43, No. 1, pp. 13–25, Jan 1996.

[16] C.K. Tse and W.C.Y. Chan, "Chaos from a Current-Programmed Ćuk Converter," *Int. J. Cir. Theor. Appl.,* Vol. 23, No. 3, pp. 217–225, May 1995.

[17] C.K. Tse, S.C. Fung and K.W. Kwan, "Experimental Confirmation of Chaos in a Current-Programmed Ćuk Converter," *IEEE Trans. Circ. Syst. Part I,* Vol. 43,, No. 7, pp. 605–608, Jul 1996

[18] J.H.B. Deane, "Chaos in a Current-Mode Controlled DC/DC Converter," *IEEE Trans. Circ. Syst. Part I,* Vol. 39, No. 8, pp. 680–683, Aug 1992.

[19] I. Zafrany and S. Ben-Yaakov, "A Chaos Model of Subharmonic Oscillations in Current Mode PWM Boost Converters," *IEEE Power Electronics Specialists Conf. Rec.,* pp. 1111–1117, 1995.

[20] W.C.Y. Chan and C.K. Tse, "Study of Routes to Chaos in Current-Programmed DC/DC Converters," *IEEE Power Electronics Specialists Conf. Rec.,* pp. 789–795, 1996.

[21] W.C.Y. Chan and C.K. Tse, "Study of Bifurcation in Current-Programmed DC/DC Boost Converters: from Quasi-periodicity to Period-doubling," *IEEE Trans. Circ. Syst. Part I,* Vol. 44, No. 12, pp. 1129–1142, Dec 1997.

[22] S. Banerjee and K. Chakrabarty, "Nonlinear Modeling and Bifurcation in the Boost Converter," *IEEE Trans. Power Electron.,* Vol. 13, No. 2, pp. 252–260, Mar 1998.

[23] S. Banerjee, E. Ott, J.A. Yorke and G.H. Yuan, "Anamalous Bifurcation in DC/DC Converters: Borderline Collisions in Piecewise Smooth Maps," *IEEE Power Electronics Specialists Conf. Rec.,* pp. 1337–1344, 1997.

[24] G.H. Yuan, S. Banerjee, E. Ott and J.A. Yorke, "Border Collision in the Buck Converter," *IEEE Trans. Circ. Syst. Part I,* Vol. 45, No. 7, pp. 707–716, Jul 1998.

[25] S. Banerjee and C. Grebogi, "Border Collision Bifurcations in Two-dimensional Piecewise Smooth Maps," *Physical Review E,* Vol. 59, pp. 4052–4061, 1999.

[26] M. di Bernardo, F. Garofalo, L. Glielmo and F. Vasca, "Quasi-Periodic Behaviours in DC/DC Converters," *IEEE Power Electronics Specialists Conf. Rec.,* pp. 1376–1381, 1996.

[27] M. di Bernardo, F. Garofalo, L. Glielmo and F. Vasca, "Switching, Bifurcations and Chaos in DC/DC Converters," *IEEE Trans. Circ. Syst. Part I,* Vol. 45, No. 2, pp. 133–141, Feb 1998.

[28] A. El Aroudi, L. Benadero, E. Toribio and G. Olivar, "Hopf Bifurcation and Chaos from Torus Breakdown in a PWM Voltage-Controlled DC-DC Boost Converter," *IEEE Trans. Circ. Syst. Part I,* Vol. 46, No. 11, pp. 1374–1382, Nov 1999.

[29] A. El Aroudi, L. Benadero, E. Toribio and S. Machiche, "Quasiperiodicity and Chaos in the DC-DC Buck-boost Converter," *Int. J. Bifur. Chaos,* Vol. 10, No. 2, pp. 359–371, 2000.

[30] C.K. Tse, Y.M. Lai and H.H.C. Iu, "Hopf Bifurcation and Chaos in a Free-running Current-Controlled Ćuk Switching Regulator," *IEEE Trans. Circ. Syst. Part I,* Vol. 47, No. 4, pp. 448–457, Apr 2000.

[31] G. Poddar, K. Chakrabarty and S. Banerjee "Control of Chaos in the Boost Converter," *Electronic Letters,* Vol. 31, No. 11, pp. 841–842, May 1995.

[32] G. Poddar, K. Chakrabarty and S. Banerjee "Experiment Control of Chaotic Behaviour of Buck Converter," *IEEE Trans. Circ. Syst. Part I,* Vol. 42, No. 8, pp. 502–504, Aug 1995.

[33] C. Batlle, E. Fossas and G. Olivar, "Stabilization of Periodic Orbits in Variable Structure Systems. Application to DC/DC Converters," *Int. J. Bifur. Chaos,* Vol. 6, No. 12B, pp. 2635–2643, 1996.

[34] C. Batlle, E. Fossas and G. Olivar, "Stabilization of Periodic Orbits of the Buck Converter by Time-Delayed Feedback," *Int. J. Cir. Theor. Appl.,* Vol. 27, No. 6, pp. 617–631, Nov 1999.

[35] R.P. Severns and G.E. Bloom, *Modern DC-to-DC Switchmode Power Converter Circuits,* Van Nostrand Reinhold, New York, 1985.

[36] S. Ćuk, "Discontinuous Inductor Current Mode in the Optimal Topology Switching Converter," *IEEE Power Electronics Specialists Conf. Rec.,* pp. 105–123, 1978.

[37] D.M. Mitchell, *DC-to-DC Switching Regulator Analysis,* McGraw-Hill, New York, 1988.

[38] N. Mohan, T.M. Undeland and W.P. Robbins, *Power Electronics: Converters, Applications, and Design,* Wiley, New York, 1995.

[39] J.G. Kassakian, M.F. Schlecht and G.C. Verghese, *Principle of Power Electronics,* Addison-Wesley, New York, 1991.

[40] G.C. Chryssis, *High Frequency Switching Power Supplies: Theory and Design,* McGraw-Hill, New York, 1989.

[41] Y.S. Lee, *Computer-Aided Analysis and Design of Switch-Mode Power Supplies,* Marcel Dekker, New York, 1993.

[42] R. Venkataramanan, A. Sababovic and S. Ćuk, "Sliding Mode Control of DC-to-DC Converters," *Int'l. Conf. Industrial Electronics, Control and Instrumentation Rec.,* Vol. 1, pp. 251–258, 1985.

[43] H. Sira-Ramirez and M. Rios-Bolivar, "Sliding Mode Control of DC-to-DC Power Converters via Extended Linearization," *IEEE Trans. Circ. Syst. Part I,* Vol. 41, No. 10, pp. 652–661, Oct 1994.

[44] W. Tang, F.C. Lee, R.B. Ridley and I. Cohen, "Charge Control: Modelling, Analysis, and Design," *IEEE Trans. Power Electron.,* Vol. 8, No. 4, pp. 396–403, Jul 1993.

[45] K.M. Smedley and S. Ćuk, "One-cycle Control of Switching Converters," *IEEE Trans. Power Electron.,* Vol. 10, No. 6, pp. 625–633, Nov 1995.

[46] Y.F. Liu and P.C. Sen, "Large-signal Modellng of Hysteretic Current-programmed Converters," *IEEE Trans. Power Electron.,* Vol. 11, No. 3, pp. 423–430, May 1996.

[47] R. Munzert and P.T. Krein, "Issues in Boundary Control," *IEEE Power Electronics Specialists Conf. Rec.,* pp. 810–816, 1996.

[48] F.H.F. Leung and P.S.K. Tam and C.K. Li, "The Control of Switching DC/DC Converters - A General LQR Problem," *IEEE Trans. Industrial Electron.,* Vol. 38, No. 1, pp. 65–71, Feb 1991.

[49] F. Garofalo, P. Marino, S, Scala and F. Vasca, "Control of DC/DC Converters with Linear Optimal Feedback and Nonlinear Feedforward," *IEEE Trans. Power Electron.,* Vol. 9, No. 6, pp. 607–615, Nov 1994.

[50] Z.Q. Wang, I. Sznaier, I. Batarseh and J. Bu, "Robust Controller Design for a Series Resonant Converter," *IEEE Trans. Aerospace and Electronic Systems,* Vol. 32, No. 1, pp. 221–233, Jan 1996.

[51] J.L. Lin and J.S. Lew, "Analysis, Modelling and Robust Controller Design for a Series Resonant Converter," *Int'l. Conf. Industrial Electronics, Control and Instrumentation Rec.,* Vol. 1, pp. 665–670, 1996.

[52] C.K. Tse and K.M. Adams, "Quasi-linear Modelling and Control of DC/DC Converters," *IEEE Trans. Power Electron.,* Vol. 7, No. 2, pp. 315–323, Mar 1992.

[53] H. Sira-Ramirez, R. Tarantino-Alvarado and O. Llanes-Santiago, "Adaptive Feedback Stabilization in PWM-controlled DC-to-DC Power Supplies," *Int. J. Control,* Vol. 57, No. 3, pp. 599–625, 1993.

[54] Y.F. Liu and P.C. Sen, "Function Control – A Novel Strategy to Achieve Improved Performance of the DC-to-DC Switching Regulators," *IEEE Trans. Industrial Electron.,* Vol. 42, No. 2, pp. 186–191, Apr 1995.

[55] Y.F. Liu and P.C. Sen, "A Novel Method to Achieve Zero-voltage Regulation in Buck Converter," *IEEE Trans. Power Electron.,* Vol. 10, No. 3, pp. 292–301, May 1995.

[56] S.R. Sanders and G.C. Verghese, "Lyapunov-based Control for Switched Power Converters," *IEEE Trans. Power Electron.,* Vol. 7, No. 1, pp. 17–24, Jan 1992.

[57] N. Kawasaki, H. Nomura and M. Masuhiro, "A New Control Law of Bilinear DC/DC Converters Developed by Direct Application of Lyapunov," *IEEE Trans. Power Electron.,* Vol. 10, No. 3, pp. 318–325, May 1995.

[58] H. Sira-Ramirez, "Nonlinear P-I Controller Design for Switchmode DC-to-DC Power Converters," *IEEE Trans. Circ. Syst. Part I,* Vol. 38, No. 4, pp. 410–417, Apr 1991.

[59] S. Hiti and D. Borojevic, "Robust Nonlinear Control for Boost Conevrter," *IEEE Trans. Power Electron.,* Vol. 10, No. 6, pp. 651–658, Nov 1995.

[60] M.E. Elbuluk, G.C. Verghese and J.G. Kassakian, "Sample-data Modelling and Digital of Resonant Converters," *IEEE Trans. Power Electron.,* Vol. 3, No. 3, pp. 344–354, Mar 1998.

[61] P.T. Tang and C.K. Tse, "Design and Implementation of Novel Quasi-linear DSP-based Control for Power Converters," *Int. J. Electronics,* Vol. 82, No. 4, pp. 415–426, 1997.

[62] G.W. Wester and R.D. Middlebrook, "Low Frequency Characterization of Switched DC/DC Converters," *IEEE Power Electronics Specialists Conf. Rec.,* pp. 9–20, 1972.

[63] V. Vorperian, "Simplified Analysis of PWM Converters Using Model of PWM Switch, Part I: Continuous Conduction Mode," *IEEE Trans. Aerospace Electronic Systems,* Vol. 26, No. 3, pp. 490–496, 1990.

[64] V. Vorperian, "Simplified Analysis of PWM Converters Using Model of PWM Switch, Part II: Discontinuous Conduction Mode," *IEEE Trans. Aerospace Electronic Systems,* Vol. 26, No. 3, pp. 497–505, 1990.

[65] A.R. Brown and R.D. Middlebrook, "Sample-data Modelling of Switching Regulators," *IEEE Power Electronics Specialists Conf. Rec.,* pp. 346–369, 1981.

[66] R.W. Erickson, S. Ćuk and R.D. Middlebrook, "Large-signals Modelling and Analysis of Switching Regulators," *IEEE Power Electronics Specialists Conf. Rec.,* pp. 240–250, 1982.

[67] D.J. Short and F.C. Lee, "Improved Switching Converter Model Using Discrete and Averaging Techniques," *IEEE Trans. Aerospace Electronic Systems,* Vol. 19, No. 2, pp. 190–202, 1983.

[68] G.C. Verghese, M.E. Elbuluk and J.G. Kassakian, "A General Approach to Sample-data Modelling for Power Electronic Circuits," *IEEE Trans. Power Electron.,* Vol. 1, No. 2, pp. 76–89, Mar 1986.

[69] S. Pavljašević and D. Maksimović, "Subharmonic Oscillations in Converters with Current-mode Programming Under Large Parameter Variations," *IEEE Power Electronics Specialists Conf. Rec.,* pp. 1323–1329, 1997.

[70] V.J. Thottuvelil and G.C. Verghese, "Analysis and Control Design of Paralleled DC/DC Converters with Current Sharing," *IEEE Trans. Power Electron.,* Vol. 13, No. 4, pp. 635–644, Jul 1998.

[71] D.J. Perreault, R.L. Selders and J.G. Kassakian, "Frequency-based Current-sharing Techniques for Paralleled Power Converters," *IEEE Trans. Power Electron.,* Vol. 13, No. 4, pp. 626–634, Jul 1998.

[72] D.J. Perreault, K. Sato, R.L Selders and J.G. Kassakian, "Switching-rippled-based Current Sharing for Paralleled Power Converters," *IEEE Trans. Circ. Syst. Part I,* Vol. 46, No. 10, pp. 1264–1274, Oct 1999.

[73] M.M. Jovanović, D.E. Crow, and F.Y. Lieu, "A Novel, Low-cost Implementation of "Democratic" Load-current Sharing of Paralleled Converter Modules," *IEEE Trans. Power Electron.,* Vol. 11, No. 4, pp. 604–611, Jul 1996.

[74] R. Giral, L. Martínez-Salamero and S. Singer, "Interleaved Converters Operation Based on CMC," *IEEE Trans. Power Electron.,* Vol. 14, No. 4, pp. 643–652, Jul 1999.

[75] C. Jamerson and C. Mullett, "Paralleling Supplies via Various Droop Methods," *High Frequency Power Conversion Conf. Proc.,* pp. 68–76, 1994.

[76] I. Batarseh, K. Siri and H. Lee, "Investigation of the Output Droop Characteristics of Parallel-connected DC-DC Converters," *IEEE Power Electronics Specialists Conf. Rec.,* pp. 1342–1351, 1994.

[77] S. Luo, Z. Ye, R.L. Lin and F.C. Lee, "A Classification and Evaluation of Paralleling Methods for Power Supply Modules," *IEEE Power Electronics Specialists Conf. Rec.,* pp. 901–908, 1999.

[78] E.N. Lorenz, "Deterministic Nonperiodic Flow," *J. Atmospheric Sciences,* Vol. 20, No. 2, pp. 130–141, Mar 1963.

[79] D. Ruelle and F. Takens, "On the Nature of Turbulence," *Commun. Math. Phys.,* Vol. 20, pp. 167-192, 1971.

[80] T.Y. Li and J.A. Yorke, "Period Three Implies Chaos," *American Mathematical Monthly,* Vol. 82, pp. 985–992, 1975.

[81] R.M. May, "Simple Mathematical Models with Very Complicated Dynamics," *Nature,* Vol. 261, No. 5560, pp. 459–467, Jun 1976.

[82] M.J. Feigenbaum, "Universal Behaviour in Nonlinear Systems," *Los Alamos Science,* Vol. 1, pp. 4–27, Nov 1980.

[83] B.B. Mandelbrot, *The Fractal Geometry of Nature,* San Francisco: Freeman, 1982.

[84] A.T. Winfree, *The Geometry of Biological Time,* New York, Springer-Verlag, 1980.

[85] B. van der Pol and J. van der Mark, "Frequency Demultiplication," *Nature,* Vol. 120, No. 3019, pp. 363–364, Sep 1927.

[86] L.O. Chua, "The Genesis of Chua's Circuit," *Archiv für Elektronik und Übertragungstechnik,* Vol. 46, No. 4, pp. 250–257, 1992.

[87] L.O. Chua, "Chua's Circuit 10 Years Later," *Int. J. Cir. Theor. Appl.,* Vol. 22, No. 4, pp. 279–305, Jul 1994.

[88] P. Cvitanović (Ed.), *Universality in Chaos,* London: The Institute of Physics Publishing, 1989.

[89] B.L. Hao (Ed.), *Chaos,* Singapore: World Scientific, 1984.

[90] M.A. van Wyk and W.H. Steeb, *Chaos in Electronics,* London: Kluwer Academic Publisher, 1997.

[91] M.J. Ogorzalek, *Chaos and Complexity in Nonlinear Electronic Circuits,* Singapore: World Scientific, 1997.

[92] T.L. Carroll and L.M. Pecora (Ed.), *Nonlinear Dynamics in Circuits,* Singapore: World Scientific, 1995.

[93] C.K. Tse, "Recent Development in the Study of Nonlinear Phenomena in Power Electronics Circuits," *IEEE Circuits and Systems Society Newsletter,* Vol. 11, No. 1, pp. 14–21, 47–48, Mar 2000.

[94] S. Banerjee and G.C. Verghese (Ed.), *Nonlinear Phenomena in Power Electronics: Attractors, Bifurcations, Chaos and Nonlinear Control,* New York: IEEE Press, to appear.

[95] M.P. Kennedy, "Basic Concepts of Nonlinear Dynamics and Chaos," in C. Toumazou (Ed.), *Circuits and Systems Tutorials,* pp. 289–313, London: IEEE Press, 1994.

[96] S. Smale, "Differentiable Dynamical Systems," *Bull. Amer. Soc.,* Vol. 73, pp. 747–817, 1967.

[97] R.L. Devaney, *An Introduction to Chaotic Dynamical Systems,* New York : Addison-Wesley, 1987.

[98] A. Wolf, "Quantify Chaos with Lyapunov Exponents," in A.V. Holden (Ed.), *Chaos,* pp. 273–290, New Jersey: Princeton University Press, 1986.

[99] B. Benettin, L. Galgani, A. Giorgilli and J. Strelcyn, "Lyapunov Characteristic Exponents for Smooth Dynamical Systems and for Hamiltonian Systems; a Method for Computing All of Them. Part I, II," *Meccanica,* Vol. 15, No. 1, pp. 9–30, 1980.

[100] A. Wolf, J.B. Swift, H.L. Swinney and J.A. Vastano, "Determining Lyapunov Exponents from a Time Series," *Physica D,* Vol. 16, pp. 285–317, 1985.

[101] J.P. Eckmann, S.O. Kamphorst, D. Ruelle and S. Ciliberto, "Lyapunov Exponents from Time Series," *Phys. Rev. A,* Vol. 34, pp. 4971–4979, 1986.

[102] M. Sano and Y. Sawada, "Measurement of the Lyapunov Spectrum from a Chaotic Time Series," *Phys. Rev. Lett.,* Vol. 55, pp. 1082–1085, 1985.

[103] H. Peitgen, H. Jürgens and D. Saupe, *Chaos and Fractals – New Frontiers of Science,* New York : Springer-Verlag, 1996.

[104] Y.A. Kuznetsov, *Elements of Applied Bifurcation Theory,* New York: Springer-Verlag, 1996.

[105] K. Siri, C.Q. Lee and T.F. Wu, "Current Distribution Control for Parallel Connected Converters: Part I," *IEEE Trans. Aerospace Electron. Syst.,* Vol. 28, No. 3, pp. 829–840, Jul 1992.

[106] K. Siri, C.Q. Lee and T.F. Wu, "Current Distribution Control for Parallel Connected Converters: Part II," *IEEE Trans. Aerospace Electron. Syst.,* Vol. 28, No. 3, pp. 841–851, Jul 1992.

[107] Y. Panov, J. Rajagopalan and F.C. Lee, "Analysis and Design of N Paralleled DC-DC Converters with Master-slave Current-sharing Control," *Appl. Power Electron. Conf. Rec.,* pp. 436–442, 1997.

[108] H.E. Nusse, E. Ott and J.A. Yorke, "Border-collision Bifurcations: an Explanation for Observed Bifurcation Phenomena," *Physical Review E,* Vol. 49, pp. 1073–1076, 1994.

[109] K.T. Alligood, T.D. Sauer and J.A. Yorke, *Chaos: An Introduction to Dynamical Systems,* New York: Springer-Verlag, 1996.

[110] S. Wiggins, *Introduction to Applied Nonlinear Dynamical Systems and Chaos,* New York: Springer-Verlag, 1990.

[111] R. Redl, "Small-signal High-frequency Analysis of the Free-running Current-mode-controlled Converter," *IEEE Power Electronics Specialists Conference,* pp. 897–906, 1991.

[112] S.C. Wong and Y.S. Lee, "SPICE Modelling and Simulation of Hysteretic Current-controlled Ćuk Converter," *IEEE Trans. on Power Electron.,* Vol. 8, No. 4, pp. 580–587, Oct 1993.

[113] J. Hale and H. Kocak, *Dynamics and Bifurcations,* New York: Springer-Verlag, 1991.

[114] S.H. Strogatz, *Nonlinear Dynamics and Chaos: with Applications to Physics, Chemistry, and Engineering,* Reading, PA: Addison-Wesley, 1994.

[115] T.S. Parker and L.O. Chua, *Practical Numerical Algorithms for Chaotic Systems,* New York: Springer-Verlag, 1989.

[116] L.M. Pecora and T.L. Carroll, "Synchronization in Chaotic Systems," *Phys. Rev. Lett.,* Vol. 64, pp. 821–824, Feb 1990.

[117] L.M. Pecora and T.L. Carroll, "Driving Systems with Chaotic Signals," *Phys. Rev. A,* Vol. 44, pp. 2374–2383, Aug 1991.

[118] L. Kocarev, K.S. Halle, K. Eckert, L.O. Chua and U. Parlitz, "Experimental Demonstration of Secure Communications via Chaotic Synchronization," *Int. J. Bifur. Chaos,* Vol. 2, No. 3, pp. 709–713, 1992.

[119] K.S. Halle, C.W. Wu, M. Itoh and L.O. Chua, "Spread Spectrum Communication through Modulation of Chaos," *Int. J. Bifur. Chaos,* Vol. 3, No. 2, pp. 469–477, 1993.

[120] C.W. Wu and L.O. Chua, "A Simple Way to Synchronize Chaotic Systems with Applications to Secure Communication Systems," *Int. J. Bifur. Chaos,* Vol. 3, No. 6, pp. 1619–1627, 1993.

[121] H. Dedieu, M.P. Kennedy and M. Hasler, "Chaos Shift Keying: Modulation and Demodulation of a Chaotic Carrier Using Self-synchronizing Chua's Circuit," *IEEE Trans. Circ. Syst. Part II,* Vol. 40, No. 10, pp. 634–642, Oct 1993.

[122] U. Parlitz and L. Kocarev, "Multichannel Communication Using Autosynchronization," *Int. J. Bifur. Chaos,* Vol. 6, No. 3, pp. 581–588, 1996.

[123] M.P. Kennedy and G. Kolumbán, "Chaos Communications: from Theory to Implementation," *Proc. of European Conf. Circ. Theo. and Design,* pp. 272-277, 1997.

[124] G. Kolumbán, M.P. Kennedy and L.O. Chua, "The Role of Synchronization in Digital Communications Using Chaos – Part I: Fundamentals of Digital Communications," *IEEE Trans. Circ. Syst. Part I,* Vol. 44, No. 10, pp. 927–936, Oct 1997.

[125] G. Kolumbán, M.P. Kennedy and L.O. Chua, "The Role of Synchronization in Digital Communications Using Chaos – Part II: Chaotic Modulation and Chaotic Synchronization," *IEEE Trans. Circ. Syst. Part I,* Vol. 45, No. 11, pp. 1129–1140, Nov 1998.

[126] L.O. Chua, M. Itoh, L. Kocarev and K. Eckert, "Chaos Synchronization in Chua's Circuit," *J. Circ. Syst. Comput.,* Vol. 3, pp. 93–108, 1993.

[127] T. Kapitaniak, *Chaos for Engineers: Theory, Applications, and Control,* New York: Springer-Verlag, 1998.

[128] T. Kapitaniak, *Controlling Chaos,* London: Academic Press, 1996.

[129] E. Ott, C. Grebogi and J.A. Yorke, "Controlling Chaos," *Phys. Rev. Lett.,* Vol. 64, pp. 1196–1199, 1990.

[130] F.J. Romeiras, C. Grebogi, E. Ott and W.P. Dayawansa, "Controlling Chaotic Dynamical Systems," *Physica D,* Vol. 56, pp. 165-192, 1992.

[131] A. Garfinkel, M.L. Spano, W.L. Ditto and J.N. Weiss, "Controlling Cardiac Chaos," *Science,* Vol. 257, pp. 1230–1235, 1992.

[132] A. Garfinkel, P.S. Chen, D.O. Walker, H.S. Karagueuzian, B. Kogan, S.J. Evans, M. Karpoukhin, C. Hwang, T. Uchida, M. Gotoh, O. Nwasokwa, P. Sager and J.N. Weiss, "Quasiperiodicity and Chaos in Cardiac Fibrillation," *J. Clinical Investigation,* Vol. 99, No. 2, pp. 305–314, 1997.

[133] S.J. Schiff, K. Jerger, D.H. Duong, T. Chang, M.L. Spano and W.L. Ditto, "Controlling Chaos in the Brain," *Nature,* Vol. 370, pp. 615–620, 1994.

[134] W.L. Ditto, M.L. Spano, V. In, J. Neff, B. Meadows, J.J. Langberg, A. Bolmann and K. McTeague, "Control of Human Atrial Fibrillation," *Int. J. Bifur. Chaos,* Vol. 10, No. 3, pp. 593–601, 2000.

[135] G. Chen (Ed.), *Controlling Chaos and Bifurcations in Engineering Systems,* Boca Raton, FL, USA: CRC Press, 1999.

[136] G. Chen and X. Dong, *From Chaos to Order: Perspectives, Methodologies, and Applications,* Singapore: World Scientific, 1998.

[137] G. Chen, J.L. Moiola and H.O. Wang, "Bifurcation Control: Theories, Methods and Applications," *Int. J. Bifur. Chaos,* Vol. 10, No. 3, pp. 511–548, 2000.

[138] J.H.B. Deane and D.C. Hamill "Improvement of Power Supply EMC by Chaos," *Electronic Letters,* Vol. 32, No. 12, pp. 1045, Jun 1996.

[139] P.J. Aston, J.H.B. Deane and D.C. Hamill, "Targeting in Systems with Discontinuities, with Applications to Power Electronics," *IEEE Trans. Circ. Syst. Part I,* Vol. 44, No. 10, pp. 1034–1039, Oct 1997

[140] C.K. Tse, Y.M. Lai and M.H.L. Chow, "Control of Bifurcation in DC/DC Converters: An Alternative Viewpoint of Ramp Compensation," *Int'l Conf. Industrial Electronics, Control and Instrumentation Rec. (IECON'2000),* Nagoya, Japan, pp. 2413–2418, Oct 2000.

[141] W.C.Y. Chan and C.K. Tse, "What Form of Control Function Can Drive a Discontinuous-mode Boost Converter to Chaos Via Period-doubling," *Int. J. Cir. Theor. Appl.,* Vol. 26, No. 3, pp. 281–286, May 1998.

[142] X.F. Wang and G. Chen, "Chaotifying a Stable Map Via Smooth Small-Amplitude High-frequency Feedback Control," *Int. J. Cir. Theor. Appl.,* Vol. 28, No. 3, pp. 305–312, May 2000.

[143] H.H.C. Iu and C.K. Tse, "Instability and Bifurcation in Parallel-connected Buck Converters Under a Master-Slave Current Sharing Scheme," *IEEE Power Electronics Specialists Conf. Rec.,* pp. 708–713, 2000.